RAPORTTEJA
RAPPORTER
REPORTS
2011:9

Probabilities of adverse weather affecting transport in Europe: climatology and scenarios up to the 2050s

Andrea Vajda[1]
Heikki Tuomenvirta[1]
Pauli Jokinen[1]
Anna Luomaranta [1]
Lasse Makkonen[2]
Maria Tikanmäki[2]
Pieter Groenemeijer[3]
Pirkko Saarikivi [4]
Silas Michaelides[5]
Matheos Papadakis[5]
Filippos Tymvios[5]
Spyros Athanasatos[5]

[1] Finnish Meteorological Institute, [2] VTT Technical Research Centre of Finland, [3] European Severe Storm Laboratory, [4] Foreca, [5] Cyprus Meteorological Service

551.583.16 (4), 551.578.45, 551.591, 551.577.37, 551.575, 551.551.553.6, 551.524.36, 551.515.3, 551.581.2

Ilmatieteen laitos
Meteorologiska Institutet
Finnish Meteorological Institute

Helsinki 2011

ISBN 978-951-697-761 (paperback)
ISBN 978-951-697-762-4 (pdf)
ISSN 0782-6079

Unigrafia Oy

Helsinki 2011

FINNISH METEOROLOGICAL INSTITUTE

Series title, number and report code of publication
Raportteja-Rapporter-Reports 2011:9

Published by Finnish Meteorological Institute
(Erik Palménin aukio 1) , P.O. Box 503
FIN-00101 Helsinki, Finland

Date 2011

Author(s)
Andrea Vajda, Heikki Tuomenvirta, Pauli Jokinen, Anna Luomaranta, Lasse Makkonen, Maria Tikanmäki, Pieter Groenemeijer, Pirkko Saarikivi, Silas Michaelides, Matheos Papadakis, Filippos Tymvios and Spyros Athanasatos

Name of project
Extreme weather impacts on European networks of transport (EWENT)

Commissioned by EU FP7

Title
Probabilities of adverse weather affecting transport in Europe: climatology and scenarios up to the 2050s

Abstract
Adverse and extreme weather events, such as heavy rain, heavy snowfall, strong winds, extreme heat and cold, drought and reduced visibility, can have a negative impact on the transport sector, causing injuries and damages as well as other economic losses. Frequency and intensity of weather and climate extremes are likely to continue to change in the future due to the projected climate change; consequences of changes will be both negative and positive for transportation.

The EWENT project (Extreme Weather impacts on European Networks of Transport) funded by the European Commission under the 7th Framework Programme (Transport, Horizontal Activities) has the objective of assessing extreme weather impacts on the European transport system. This report frames the findings of Work Package 2 (WP 2) of the EWENT project.

The study provides the first comprehensive climatology of the adverse and extreme weather events affecting the European transport system by estimating the frequency (or probability) of phenomena for the present climate (1971-2000) and an overview of projected changes in some of these adverse and extreme phenomena in the future climate until 2070.

The following phenomena are analyzed: wind, snow, blizzards, heavy precipitation, cold spells and heat waves. In addition, visibility conditions determined by fog and dust events, small-scale phenomena affecting transport systems, such as thunderstorms, lightning, large hail and tornadoes, and events that damaged the transport system infrastructure were considered. Frequency and probability analysis of past and present extremes were performed using observational and reanalysis data. Future changes in the probability of severe events were assessed based on six high-resolution regional climate model (RCM) simulations produced in the ENSEMBLES project.

There are large differences in probabilities and intensity of extremes affecting transport systems across Europe. Northern Europe and the Alpine region are impacted most by winter extremes, such as snowfall, cold spells and winter storms, while the probability of extreme heatwaves is highest in Southern Europe. Extreme winds and blizzards are most common over the Atlantic and along its shores. Although heavy rainfall may impact the whole continent on a yearly basis, the very extreme rainfall events (over 100 mm/24 h) are relative sparse. Visibility conditions indicate a pan-European improvement over the decades studied; severe fog conditions becoming almost non-existent at some of the main European airports.

The multi-model mean climate projections indicate robust changes in temperature extremes, but are less coherent with regard to extremes in precipitation and wind. Both cold extremes and snow events are likely to become rarer, especially in the north where the extreme cold might shorten by 30-40 days/year by the 2050s. On the other hand, heavy snowfalls (>10 cm/day) are not expected to decrease, instead models project a 1-5 days/year increase over Scandinavia. Extreme heat is likely to intensify over the entire continent, being more accentuated in the south (by 30-40 days/year). The analysis of the Baltic Sea ice cover indicates a decrease in the average maximum fast ice thickness of 30-40 cm by 2060. To facilitate the assessment of impacts and consequences of extreme phenomena at the continental level a regionalization of the European extreme phenomena is provided.

Publishing unit
Meteorology (MET)

Classification (UDC)
551.583.16 (4), 551.578.45, 551.591, 551.577.37, 551.575, 551.551.553.6, 551.524.36, 551.515.3, 551.581.2

Keywords
adverse weather, observations, climate change, European transport system, impact thresholds, regional climate scenarios, regionalization of extremes

ISSN and series title
0782-6079 Raportteja – Rapporter – Reports

ISBN
ISBN 978-951-697-761 (paperback)
ISBN 978-951-697-762-4 (pdf)

Language
English

Pages
85

ILMATIETEEN LAITOS

Julkaisun sarja, numero ja raporttikoodi
Raportteja-Rapporter-Reports 2011:9

Julkaisija Ilmatieteen laitos, (Erik Palménin aukio 1)
PL 503, 00101 Helsinki

Julkaisuaika 2011

Tekijä(t)
Andrea Vajda, Heikki Tuomenvirta, Pauli, Jokinen, Anna Luomaranta, Lasse Makkonen, Maria Tikanmäki, Pieter Groenemeijer, Pirkko Saarikivi, Silas Michaelides, Matheos Papadakis, Filippos Tymvios ja Spyros Athanasatos

Projektin nimi
EWENT

Toimeksiantajat EU FP7

Nimeke

Liikennettä haittaavan sään todennäköisyydet Euroopassa: klimatologia ja skenaariot 2050-luvulle

Tiivistelmä
Äärimmäisillä sääilmiöillä, kuten rankkasateilla, runsailla lumisateilla, voimakkailla tuulilla, äärilämpötiloilla, kuivuusjaksoilla sekä huonolla näkyvyydellä, voi olla haitallisia vaikutuksia liikenteelle. Nämä ilmiöt voivat aiheuttaa henkilövahinkoja sekä taloudellista menetyksiä. Sään ja ilmaston ääri-ilmiöiden esiintymistiheydet sekä voimakkuudet tulevat todennäköisesti muuttumaan tulevaisuudessa ilmastonmuutoksen myötä. Seuraukset liikennesektorille tulevat olemaan sekä positiivisia että negatiivisia.
EWENT-projekti (engl. Extreme Weather impacts on European Networks of Transport) on rahoitettu Euroopan Komission 7. puiteohjelman toimesta. Hankkeen päämääränä on arvioida äärisääilmiöiden vaikutuksia Euroopan liikennejärjestelmään. Tässä raportissa on esitetty EWENT-projektin toisen työpaketin (WP 2) tuloksia.
Tutkimuksen tuloksena on valmistunut ensimmäinen Euroopan kattava klimatologia tietyistä liikenteen kannalta haitallisista sääilmiöistä. Tuloksissa on esitetty näiden ilmiöiden esiintymistiheyksiä (tai todennäköisyyksiä) nykyilmastolle (1971–2000) sekä yleiskuva muutoksista tulevassa ilmastossa aina vuoteen 2070 asti. Tutkimuskohteena ovat olleet seuraavat sääilmiöt: tuuli, lumisade, lumipyry, rankkasateet sekä kylmät että kuumat jaksot. Lisäksi tarkasteltiin näkyvyyteen liittyviä ilmiöitä (sumut, hiekkamyrskyt), pienemmän mittakaavan ilmiöitä (ukkoset, salamointi, isot rakeet ja tornadot) sekä muita liikennejärjestelmän rakenteisiin vaikuttavia sääilmiöitä.
Esiintymistiheys- ja todennäköisyysanalyysit menneelle ja nykyilmastolle selvitettiin havaintojen ja uusanalyysien avulla. Haitallisten sääilmiöiden todennäköisyyksissä esiintyviä muutoksia tutkittiin kuuden, ENSEMBLES-projektissa kehitetyn, korkean erotuskyvyn alueellisen ilmastomallin (RCM) tulosten avulla.
Liikenteeseen vaikuttavien sääilmiöiden toistuvuuksissa ja voimakkuuksissa on suuria eroja eri puolilla Eurooppaa. Talvisista ääri-ilmiöistä kuten lumisateista, kylmistä jaksoista ja talvimyrskyistä kärsivät eniten Pohjois-Eurooppa sekä Alpit, kun taas äärimmäisten lämpöaaltojen todennäköisyys on korkein Etelä-Euroopassa. Äärimmäisiä tuulen nopeuksia sekä lumipyryjä esiintyy eniten Pohjois-Atlantilla sekä sen rannoilla. Vaikka rankkasateita voi esiintyä koko mantereen alueella vuosittain, erittäin rankkoja sateita (yli 100mm/24h) esiintyy melko harvoin. Näkyvyyden osalta on viime vuosikymmenien aikana ollut havaittavissa tilanteen paranemista. Erittäin sankat sumut ovat lähes hävinneet osasta Euroopan suurimpia lentokenttiä.
Usean ilmastomallin keskiarvot näyttävät selvää lämpenemistä äärilämpötilojen osalta, mutta heikompia muutoksia rankkasateiden ja voimakkaiden tuulien osalta. Sekä alhaiset lämpötilat että lumisateet muuttuvat harvinaisemmiksi erityisesti Pohjois-Euroopassa, jossa erittäin kylmiä päiviä saattaa esiintyä vuodessa 30–40 vuorokautta nykyistä vähemmän 2050-luvulla. Toisaalta runsaiden lumisateiden (yli 10 cm/vuorokausi) ei arvioida harvinaistuvan, vaan ilmastomallien mukaan niitä esiintyisi Skandinaviassa vuosittain 1-5 vuorokautta enemmän kuin nykyään. Tukalat helleaallot voimistuvat koko mantereella, korostetusti Etelä-Euroopassa (30–40 vrk/vuosi enemmän). Itämeren jääpeitteen analyysit näyttävät jään keskimääräisen maksimipaksuuden vähenevän 30–40 cm jo 2060-lukuun mennessä. Euroopan mantereen äärimmäisten sääilmiöiden vaikutusten ja seurausten arvioinnin helpottamiseksi on tulokset esitetty myös alueittain.

Julkaisijayksikkö
Meteorologia (MET)

Luokitus (UDK)
551.583.16 (4), 551.578.45, 551.591, 551.577.37, 551.575, 551.551.553.6, 551.524.36, 551.515.3, 551.581.2

Asiasanat
haitallinen sää, havainnot, ilmastonmuutos, Euroopan liikennejärjestelmä, vaikutusten raja-arvot, alueelliset ilmastoskenaariot, ääri-ilmiöiden alueellistaminen, ääriarvoanalyysi

ISSN ja avainnimike
0782-6079 Raportteja – Rapporter – Reports

ISBN
ISBN 978-951-697-761 (paperback)
ISBN 978-951-697-762-4 (pdf)

Kieli
Englanti

Sivumäärä
85

Table of content

1. Introduction

The EWENT project (Extreme Weather impacts on European Networks of Transport) funded by the European Commission under the 7th Framework Programme (Transport, Horizontal Activities) has the objective of assessing the impact of extreme weather on the European transport system. The goal of EWENT is to estimate and quantify in monetary terms the disruptive effect of extreme weather events and to identify strategies to make the transport system more resilient to extreme weather phenomena in a changing climate.

This report contains the main results of the Work Package 2 (WP2) of the EWENT project. The objectives of EWENT WP2 were:

(1) to develop the first comprehensive European climatology of extreme weather events relevant to the transport system to support socio-economic and technical research and decision making, and

(2) to estimate the changes in extreme weather event intensities and frequencies of occurrence relevant for the transport system.

The analyses attempt to cover the time period from the 1970s up to the 2050s; however, there are limitations in the availability of data. For some weather elements and phenomena, studies cover only the past ten to twenty years. The selection of weather events to be analyzed and their definitions are based on the results of the preceding EWENT WP1, which identified the extreme weather events relevant within the European transport system context. WP1 D1 report "Extreme Weather Impacts on Transport Systems" defines threshold values for critical weather parameters (Leviäkangas et al., 2011). A three level category for thresholds was developed for many adverse weather phenomena. The qualitative description being:

1. threshold: Adverse impacts to the transport system may start to occur. For example, if the resilience of the transport system against the phenomena in question is at low level.

2. threshold: Some adverse impacts are likely. Their severity depends on the resilience of the transport system.

3. threshold: Weather phenomena is so severe that it is virtually certain that some adverse impacts will occur.

In order to present EWENT work and receive feedback from the atmospheric sciences community, EWENT WP2 organized a "Workshop on Estimation of Probabilities of Extreme and Harmful Weather Events in a Changing Climate" at the 10th EMS Annual Meeting/8th European Conference on Applied Climatology (ECAC) on 13 – 17 September 2010 in Zürich, Switzerland. The presentations of the workshop are available at the EWENT web-site (ewent.vtt.fi). This workshop activity constitutes the deliverable D2.2 of WP2.

A parallel running ECCONET project (EU FP7 Transport, Horizontal Activities) assesses the effect of climate change on the inland waterway transport network. ECCONET project produces scenarios utilizing climate and hydrological models. Low water levels are of special concern to inland water transport and ECCONET scenarios are specifically constructed to analyze these low flows, drought-like conditions. Therefore, this EWENT does not address drought events.

This report is structured as follows. Chapter 2 describes the observational data used, development of the methodology for the analyses, and presents climatology of weather conditions affecting transport. Chapter 3 first describes the climate model simulations used in the construction of scenarios of harmful weather events before presenting scenario maps as changes in frequencies or probabilities. This chapter also depicts the changes in selected events affecting the infrastructure, synopsis of an earlier study on assessment of changes in thunderstorms in climate model simulation, projected changes in Baltic Sea ice cover, and climate scenarios for the Nordic road network. In the final chapter, the results are discussed within a broader context of related studies. A summary of results is presented for six climate regions covering Europe.

2. Climatology of adverse weather conditions affecting transport

The analysis of the relevant adverse and extreme weather phenomena takes into account the ranking and impact threshold values defined from the viewpoint of different transport modes, such as road, rail, aviation, waterways, and infrastructure within WP1 (Leviäkangas et al., 2011). Threshold indices are defined as the number of days on which a variable falls above or below a fixed threshold. In the present study three impact threshold indices were defined for each of the following phenomenon (see WP1): wind, snow, blizzard, heavy precipitation, cold spell and heat wave, in such a way that these can be applied for the entire European continent.

The estimation of the recent and past (1971-2000) adverse weather events is based on the observed data available from the meteorological services, from the E-OBS dataset and the ERA-Interim reanalysis dataset. A range of statistical methods are applied to define the features of these extremes, such as their probability, changes in the spatial extension, intensity and temporal duration.

2.1. Description of gridded observational data sets

In order to assess the spatial and temporal variation of adverse weather conditions over the European continent, two gridded datasets were used: the E-OBS dataset (Haylock et al., 2008) produced through spatial interpolation of daily station data, and the reanalysis dataset produced within the ERA project at the European Centre for Medium-range Weather Forecasting (ECMWF) through which a multi-source data assimilation system describes the state of the atmosphere, land and ocean-wave condition (Uppala et al., 2005).

The **E-OBS European high resolution land-only gridded dataset** of daily surface temperature and precipitation has been developed within the EU-funded ENSEMBLES project. The mean (TG), maximum (TX), minimum (TN) temperature and precipitation were derived through interpolation of the ECA&D (European Climate Assessment and Data) station data described by Klok and Klein Tank (2008). The full period of record used for interpolation is 1950–2009, but the period 1961–1990 has the highest station density (Hofstra et al., 2009). The E-OBS data set has been derived through a three stage process using the kriging interpolation method, computing gridded data at four resolutions: 0.25° and 0.5° regular latitude-longitude grids, and 0.22° and 0.44° latitude-longitude rotated pole grids. Details on the interpolation methods, their implementation and the calculation of uncertainties are available in Haylock et al. (2008).

E-OBS data with a 0.25° regular latitude-longitude grid was used to derive the adverse and extreme weather indices over the European continent. Since the interpolation methodology has smoothed the magnitudes of extremes in the variation of variables, we have applied correction factors for precipitation (0.66) and maximum temperature data (-1.1 °C) indicated by the cross-validation with station observations (Haylock et al., 2008).

The **ERA-40** and **ERA-Interim** datasets cover the period of 1957-2002 and from 1989 to present day, respectively. The ERA-40 (Uppala et al., 2005) dataset uses 3D-variational analysis on a spectral grid with a triangular truncation of 159 waves (corresponds approximately to a horizontal resolution of 125 km) and a hybrid vertical coordinate system with 60 levels. ERA-Interim (Simmons et

al., 2006) uses 4D-variational analysis on a spectral grid with triangular truncation of 255 waves (corresponds to approximately 80 km) and a hybrid vertical coordinate system with 60 levels.
The ERA-40 system produces four analyses per day (00, 06, 12 and 18 UTC), two forecasts per day to 6 hour ahead (06 and 18 UTC) and two forecasts per day to 36 hours ahead (00 and 12 UTC). The fields are saved on the T159 reduced Gaussian grid with spacing of 1.125°. The ERA-Interim data assimilation and forecast system produces four analyses per day (00, 06, 12 and 18 UTC) and two 10-day forecasts per day, initialized from analyses at 00 and 12 UTC. Fields from the atmospheric model are archived on the N128 reduced Gaussian grid with a spacing of about 0.7° (Berrisford et al., 2009).
Details on the ECMWF data assimilation system are available in the online documentation at http://www.ecmwf.int.

Although ERA-Interim does not cover the entire period (1971-2000) applied in our study, its enhanced data assimilation system and the improved spatial resolution justified the use of this dataset. Furthermore, a comparison between the wind gust data forecast by the two reanalysis datasets indicated a more accurate estimation of the strong wind gust frequency by ERA-Interim. Similar results were indicated in earlier studies of wind storm frequency using the two reanalysis datasets (Källberg, 2008).

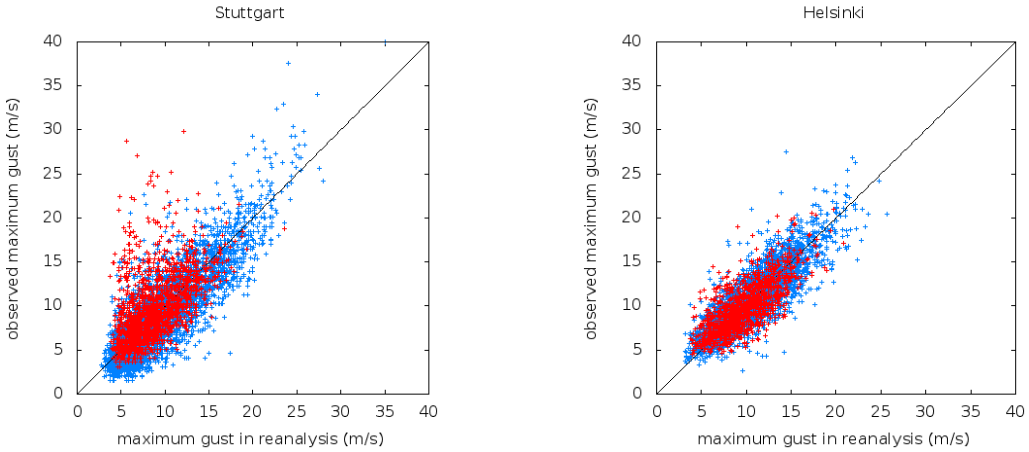

Figure 2.1. Observed gusts and gusts in ERA-INTERIM at Stuttgart and Helsinki for each day in the period 1990-2009 (Stuttgart) and 1997-2009 (Helsinki). Blue crosses occurred in the months Sep-Apr, red crosses are May-Aug.

However, the representation of some extreme wind gusts caused by convective storms is problematic in the ERA datasets. This is not surprising, because ERA six-hour gust fields are derived from a grid (N128 Gaussian truncation) that is much too coarse to resolve the thunderstorms producing them. Fig. 2.1 (left) shows that in Stuttgart (southern Germany) a sizeable fraction of the summertime gusts (in red) tend to be more intense than forecast, whereas this is much less the case in winter. Stuttgart is known for experiencing many heavy thunderstorms in summer. For Helsinki, in which thunderstorms are rarer and less intense on average, the ERA-INTERIM appears to represent summertime gusts much better, and not evidently worse than those in winter.
Figure 2.1 illustrates that neither data from ERA nor any other reanalysis or climate model with similar resolution can be used directly to estimate the occurrence of gusts that occur with convec-

tive storms. Instead, advanced methods are required to do so, but have, as far as the authors are aware, not yet been developed.

In the evaluation of probabilities and frequencies of adverse weather phenomena we utilized the parameters from the two datasets as follows:

- 2-m daily mean temperature values from E-OBS dataset for cold spell,
- 2-m daily maximum temperature values from E-OBS dataset for heat wave,
- total daily precipitation from E-OBS dataset for heavy rainfall,
- 2-m daily mean temperature ($T \leq 0$ °C) and total daily precipitation from E-OBS dataset for snowfall calculation
- 6-hour forecast of 10 m wind gust from ERA-Interim dataset for wind gust
- 6-hour forecast of 10 m wind gust and precipitation sum, 6-hour reanalysed 2-m mean temperature from ERA-Interim dataset for calculation of blizzard frequency.

The outer edge of the domain covered by the two datasets in the present study are: 32 °N, 25 °W and 72 °N, 45 °E for the E-OBS data, and 30.937 °N, 26.018 °W and 73.124 °N, 45.7 °E for the ERA-Interim reanalyses data.

In addition, to calculate the frequency of freezing precipitation, the 16-year NOAA National Climatic Data Centre database of surface observations at airports covering the period 1982-1997 was used (Lott, 2000), and additional observations were used in the evaluation of fog and dust occurrence; a full description is given in Chapter 2.10.

2.2. Description of the European Severe Weather Database

The **European Severe Weather Database** (Dotzek et al., 2009) contains an ever-growing collection of reports of individual severe weather events and is managed by the European Severe Storms Laboratory (ESSL). The events contained in the database are typically of a local and short-lived nature, and many of them are associated with severe thunderstorms. They include hail (2 cm or larger), tornadoes, severe wind gusts (25 m/s or stronger), flash floods and lesser whirlwinds (dust devils, gustnadoes). As a part of EWENT, the scope of the database was expanded to include damaging lightning, heavy snow, freezing rain and avalanches. The data in the database originates from various sources, including reports by the general public, by media, by several National Meteorological Services (NMS) and by Voluntary Observing Networks (VON). Most data is not measured by conventional measurement stations, but actually complements these networks by providing additional data that is focused on extreme events.

The nature of the dataset and its sources requires that a thorough system of quality control be in place. Indeed, this process is carried out by ESSL and its NMS and VON partners. The aim of the process is to assign any of four quality levels to each report, the lowest of which results in immediate deletion of the report. These *QC*-levels are:

- QC0: “as received” (new report, only retained if at least plausibility can be ascertained);
- QC0+: “plausibility checked” (assigned by VON, NMS or ESSL);
- QC1: “report confirmed” by reliable sources (assigned by VON, NMS or ESSL);
- QC2: “event fully verified” i.e. all information about this event is verified, consistent and comes from reliable sources (assigned by NMS or ESSL).

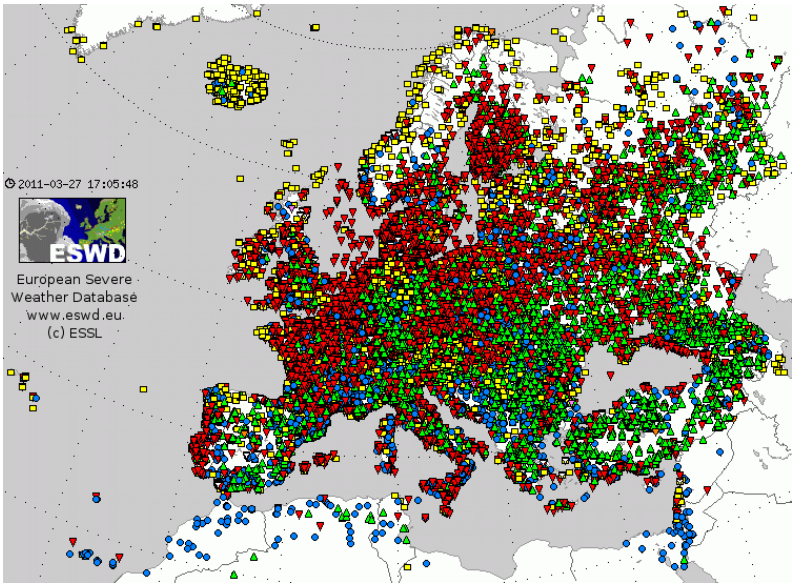

Figure 2.2. All severe weather events contained in the ESWD as of March 2011.

As of March 2011, the ESWD dataset, which is being expanded by two EWENT partners (FMI and CYMET), contains 34423 severe weather events (Fig. 2.2). The dataset is used for climate monitoring, climatological studies, development of detection algorithms using remote-sensing data, operational forecasting, and forecast verification.

2.3. The extreme value analysis method used

2.3.1. The General Extreme Value Function GEV

In most design standards and other engineering codes, as well in hydrological and meteorological literature the measure of the expected frequency of rare events is the return period R (in years). Typically, in standards such as the Eurocode, the 50-year return value x^{50} is utilized (e.g. Anon, 2001). This is the value of the variable x that is exceeded by an annual maximum once in 50 years in the mean. The return period R of an event is related to the probability P of not exceeding this event in one year by

$$R = \frac{1}{1-P} \qquad (1)$$

Hence, the 50-year return period corresponds to the annual probability of exceedance of 0.02. Determining R for some value of x or, vice versa, the return value x^{50} from measured or simulated climate data requires statistical analysis of the cumulative distribution function F(x) of the extremes. For this, the extreme value theory (Fisher and Tippett, 1928, Gumbel, 1958) has been commonly utilized. The advantage of the extreme value theory is that, ideally, the original parent distribution and its cumulative distribution function need not to be known, because the distribution of the extremes asymptotically approaches a known distribution.

In the case of annual extremes, considered here, this distribution is the generalized extreme value distribution GEV

$$F(x) = \exp\left[-\left(1+\gamma\left(x-\mu\right)/\alpha\right)^{-1/\gamma}\right] \qquad (2)$$

where $\alpha > 0$ and $1 + \gamma(x-\mu)/\alpha > 0$. GEV is a three parameter distribution, the limiting value of which at $\gamma = 0$ is the Gumbel distribution

$$F(x) = \exp\left(-\exp\left(-y\right)\right) \qquad (3)$$

where y is the reduced variate

$$y = \left(x-\mu\right)/\alpha \qquad (4)$$

Here, μ is the location parameter and α is the scale parameter. The GEV distribution has a finite upper tail for the shape parameter $\gamma < 0$ (Weibull), whereas for $\gamma > 0$ (Frechet) and $\gamma = 0$ (Gumbel) there is no upper bound.

2.3.2. Plotting positions

The cumulative distribution function of n number of annual maxima is estimated from the order statistics so that each maximum is assigned a rank m in ascending value $1 \le m \le N$. For any analysis of the order of ranked extremes one needs to associate them to some probability, the so called plotting position. We use the formula

$$P_m = m/\left(N+1\right) \qquad (5)$$

as we have shown (Makkonen 2006, 2008a,b) that this is the only correct plotting position when estimating return periods for *any* distribution of extremes.

2.3.3. Inference by GEV

The fit to estimate the parameters μ and α is traditionally performed on a Gumbel probability graph where the ordinate is the reduced variate from the estimated F(x) in Eq. (3), plotted as $y = -\ln(-\ln(F(x)))$ and the abscissa is the variate value x. This plot transforms the Gumbel distribution model in Eq. (3) into a line with a slope of $1/\alpha$ and intercept μ, as shown in eq. (4).

There are a number of ways to fit a distribution to the plotted data. In addition to the simple method of least squares, methods that weigh each extreme according to its theoretical statistical confidence have been proposed (Lieblein, 1974, Landwehr, et al., 1979, Hosking, 1985, Hosking et al., 1985, Wang, 1991, Castillo, 1988, Katz et al., 2002). In addition to the different statistical confidence of different ranks, the problem with weighing them is related to the possibility that the highest extremes may not belong to the same population as the more moderate extremes.

Once the fit is made and the parameters α and μ are determined, one can calculate x that corresponds to any probability F(x) = P from and the corresponding return period R. Often, one will need to estimate extreme values of X that are higher than those included in the data. Graphically this corresponds to extrapolation along of the fit on the graph. Here, such an extrapolation is made from the 30-year simulation data to the 50-year return value.

Commonly, the Gumbel method, eq. (3) has been the sole method used, a consequence of the background in extreme value theory, which implies that an unbounded cumulative distribution function of the annual extremes is given by eq. (3). This has often been taken too literally in spite of many words of warning (Gumbel, 1958, Cook, 1982, Galambos and Macri, 1999, Makkonen, 2008a). The theory merely states that the distribution of extremes *asymptotically approaches* the theoretical extreme value distribution when the number N of independent observations in each observation period from which the extreme is abstracted increases.
Acknowledging that the two-parameter Gumbel distribution may not always be a good model of the observed extremes, similar fitting methods may be applied to estimating the three parameters of a GEV distribution, Eq. (2). When the data display a shape parameter deviates significantly from zero, then, on a Gumbel-plot, the order ranked points form a curve that is concave or convex depending on the sign of γ. When the data show $\gamma < 0$, this has often been interpreted to indicate that the tail of the cumulative distribution function is bounded. However, as discussed above, and previously by Galambos and Macri (1998), Cook et al. (2003) and Harris (2004), this interpretation is incorrect when the number of observations per each extreme is small, and the points may thus be positioned nonlinearly within an unbounded distribution.

Accordingly, we use here GEV, but not for reasons related to the extreme value theory only. We simply use GEV to make a convenient empirical three-parameter fit to the simulated order ranked annual extremes. Additional support for this procedure comes from the finding (Furrer and Katz 2008) that GEV fits well also to extreme data that do not appear to be converging fully to an asymptotic extreme value distribution, i.e. in cases of so-called penultimate distributions.
Since our method aims at an empirical fit, all three parameters of GEV are allowed to vary freely at every grid point and for all the data analysed.

2.3.4. Selection of number of extremes included in the analysis

The selection of the number of largest extremes used in the fitting procedure is subjective and comparable to the problem of selecting the threshold in the peaks-over-threshold method that utilizes the Generalized Pareto Distribution (Brabson and Palutikof, 2000). The choice may be based on the degree of prior belief on some specific distribution or on a physical understanding on which of the highest extremes belong to the same population. In fitting the GEV to the order ranked extremes from the 30-year simulations we use the 15 largest annual extremes. This is a sufficient number to allow fitting of a three parameter GEV while limiting the analysis to those extremes that are most relevant to extrapolating to the 50-year return value.

However, in some cases the variable X may have an absolute lower limit according to the fitted GEV. This can sometimes be seen also in real data; the limiting value for snowfall is zero, for example. Since, in the extreme value analysis, we are interested in the upper tail of the distribution, values at the lower limit should not be used. Therefore, we apply a criterion on how close to the theoretical lower limit the smallest observed extremes are and reject them from the analysis accordingly. This is explained in detail at the end of the next section.

2.3.5. The fitting method

There is significant controversy related to the methods of fitting a distribution to extreme value data (Katz et al., 2002, Makkonen, 2008a). For example, the performance of the maximum likelihood method for the GEV distribution may be erratic for small sample populations (Martins and Steding-

er, 2000) and the method of probability-weighted moments is not optimal for Gumbel-distributed samples (Rasmussen and Gautam, 2003). We have developed a new method which deviates from the conventional methods and is briefly explained below.

In all conventional fitting methods applied to the extreme value analysis, the error, i.e. the differences between the observed and modelled values, is minimized with respect to the probability P. In contrast, we minimize the error between the fitted GEV and the data points with respect to the observed variable X. We do this because we have previously shown that, in order ranked data, P is not a dependent variable but *known* (Makkonen, 2008a,b, 2011).

It is noteworthy that *all* curve fitting techniques implicitly involve giving weights to the data points. In extreme value analysis the issue of the weight is particularly important and controversial. Giving larger weights to the most extreme observations may be supported by the possibility that the highest extremes do not belong to the same population with more moderate extremes. An example of this is a mixed climate where the bulk of the wind speed distribution is a result of normal low-pressure systems, but the highest extremes are results of hurricanes. Thus, putting more weight on the points with a low probability would seem to be necessary for the phenomena whose formation mechanisms are poorly understood. However, this line of thinking contradicts the commonly used approach (Harris, 1996, Landwehr et al., 1979, Hosking et al., 1985) in which the points are weighted according to their theoretical statistical confidence, thus effectively neglecting the data at the tail of the distribution.

We use the weighted least squares method in making the fit to GEV and solve the problem of the subjective weighing of the data as follows.
As mentioned above, in our fitting method, we minimize errors with respect to the random variable X, and not P.
For this purpose, from the GEV distribution we solve

$$\xi_m = \mu + \frac{\sigma}{\gamma}\left[-1-\left(-\ln F\left(\xi_m\right)\right)^{-\gamma}\right] \qquad (6)$$

where ξ_m is the value of X given by the estimate of the cumulative distribution function F at the probability corresponding to the observation x_m. In other words,

$$\xi_m = F^{-1}\left[m/(N+1)\right]. \qquad (7)$$

We give weights w_m for the data points according to the inverse of the variance of ξ_m. The variance of σ^2 can be numerically calculated when the cumulative distribution function at $F(\xi_m)$ is known.

The weights w_m are then determined by

$$w_m = \frac{1}{\sigma_m^2} \qquad (8)$$

and are normalized so that

$$\sum_{m=k}^{N} w_m = 1 \qquad (9)$$

Using these weights we minimize the sum

$$\sum_{m=k}^{N} w_m \left(x_m - \xi_m\right)^2 \qquad (10)$$

Thus, in our method the estimate of the cumulative distribution function F(ξ) needs to be applied when determining the weights. On the other hand, the weights are required in determining an estimate F(ξ). This situation is solved by considering both the weights and the fitted function simultaneously in an iteration process.

First, equal weights are given for the 15 largest extremes in order to obtain the first estimate. Then, if the fitted GEV distribution is such that $|\gamma| < 0.1$, the iteration is stopped and a Gumbel-fit is made by finding μ and α with Eqs. (3) and (4). For this case, using Eq. (2) can never result in a Gumbel distribution, eq. (3), i.e. $\gamma = 0$.

If the first iteration yields $|\gamma| > 0.1$, the iteration continues to solve for γ, while at each iteration step, the weights are adjusted according to Eqs. (8)-(10) and the three parameters of GEV are found by minimizing the sum in Eq. (10). When the estimated cumulative distribution function F(ξ) and the weights w_m do not change anymore in iteration, the CDF F(ξ) is accepted as a final result.

2.4. Wind

The impact of wind storms on transport network is considerable, with air, sea and land transportation being all affected. Wind can impede transport operation or damage vehicles and infrastructure leading to significant economic impacts and injuries. Three thresholds were considered in the wind gust analysis: 17 m/s, 25 m/s and 32 m/s.

As indicated in Figure 2.3, extreme wind gust are more frequent over the Atlantic, the most affected land areas are the British Isles, Iceland and the coastal area (40-80 days/year with wind gust over 17m/s). Most of the continent experiences 10-20 days per year with strong wind gust (17 m/s). Very extreme wind gust events (> 25 m/s) occur rarely and sporadically over Europe.

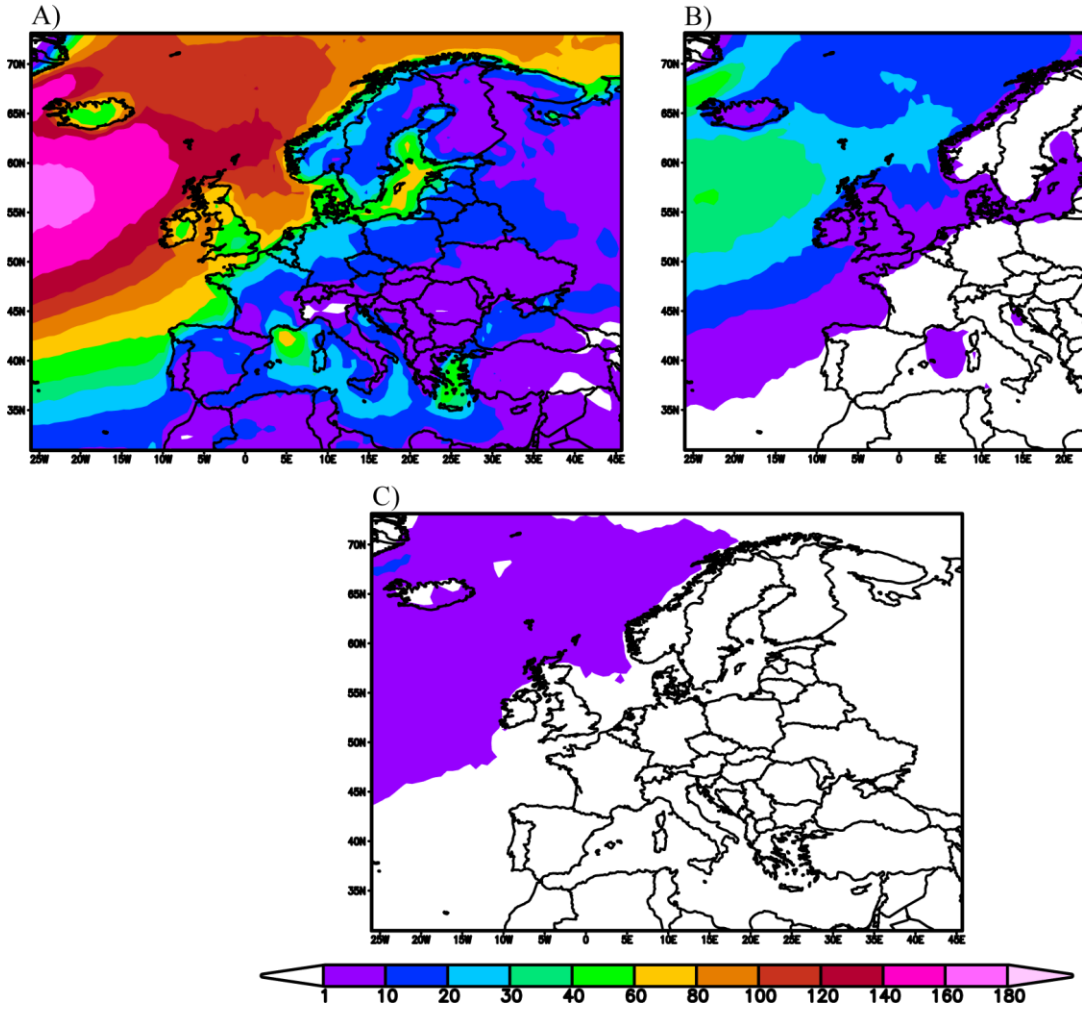

Figure 2.3. Average number of days per year with wind gust exceeding 17 m/s, 25 m/s and 32 m/s during the period 1989-2010 based on ERA-Interim data.

2.5. Snow

Snow represents a great challenge for transport system operations. Heavy snowfall results in increased travel time, delays and increased accident risk. Dense snowfall causes poor grip between the road surface and tyres and reduces the visibility, resulting in a possible reduction of road capacity by 19-27% and the traffic speed by 11-15% (Agarwal et al., 2005). Keeping roads free from snow is a major part of winter road maintenance in many European countries. Snowfall also has a strong negative impact on railway traffic and aviation, as experienced in Europe during the winters of 2009/10 and 2010/11 when many European airports were closed, generating severe economic losses.

Snow events impact almost the entire continent (Fig. 2.4) with an increase in probability toward Northern, Eastern Europe and the Alpine region, where the frequency of days with snow varies between 100-140 days/year. Although the chosen 1 cm snowfall is a relatively low threshold value,

even a thin snow cover may cause disruption, particularly in the regions where its probability is reduced.

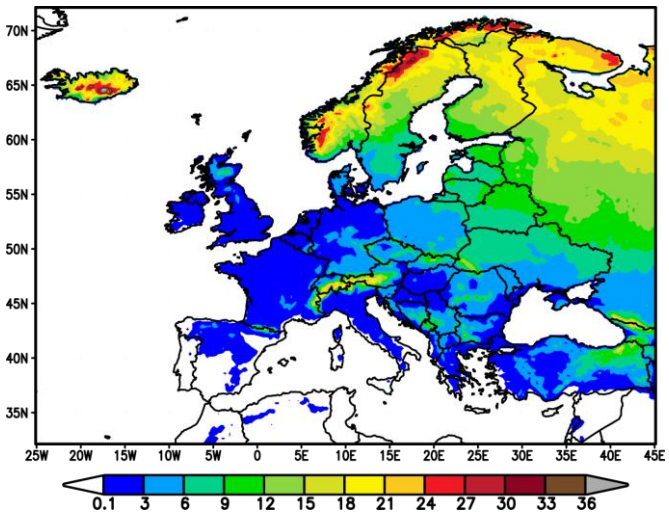

Figure 2.4. Frequency-based probability (in percent) of daily snowfall exceeding 1 cm during the period 1971-2000 based on E-OBS data.

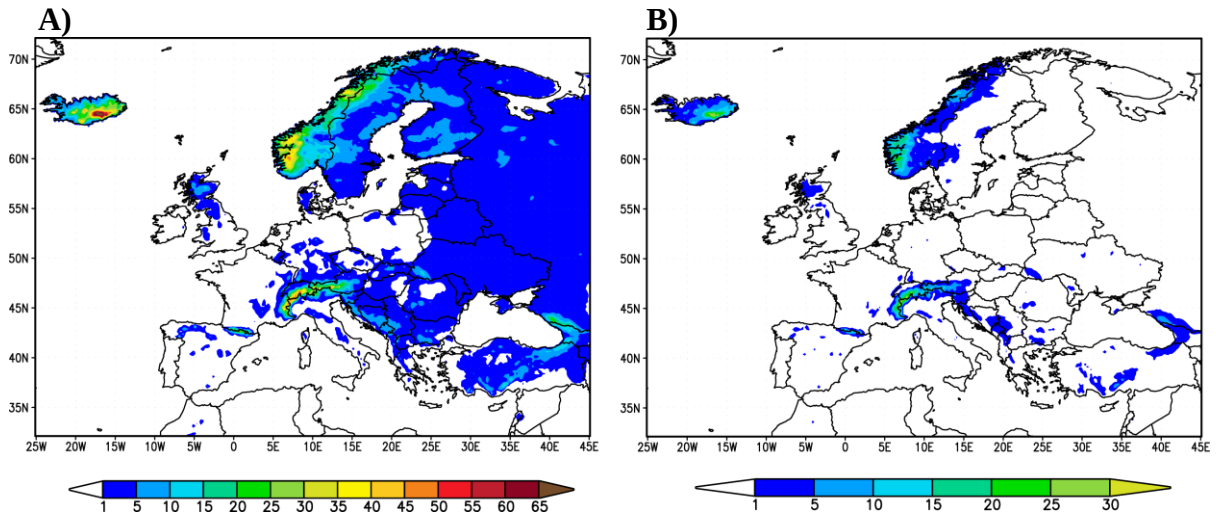

Figure 2.5. Average number of days per year with snowfall exceeding (A) 10 cm and (B) 20 cm during the period 1971-2000 based on E-OBS data.

Dense snowfall (≥10 cm/24 h) occurs only sporadically over Western, Southern and most of Central Europe (max. 5 days/year). In Scandinavia the frequency varies between 5-15 days/year, while over the eastern part of the continent and the Balkan Peninsula it rarely exceeds 5 days/year (Fig. 2.5). Heavy snowfall (≥20 cm/24 h) is frequent over Northern Europe (Norway and Iceland) and the Alps: 10-25 cases/year. Nevertheless, the analysis indicates 30-40 cases per year for the rest of Scandinavia, Eastern Europe and some parts of the Balkan Peninsula during 1971-2000.

The temporal variation of snowfall events indicates a predominant positive trend over Eastern Europe and the western part of Scandinavia, and a negative trend in central Europe, Alps and locally in Scandinavia Fig. 2.6.

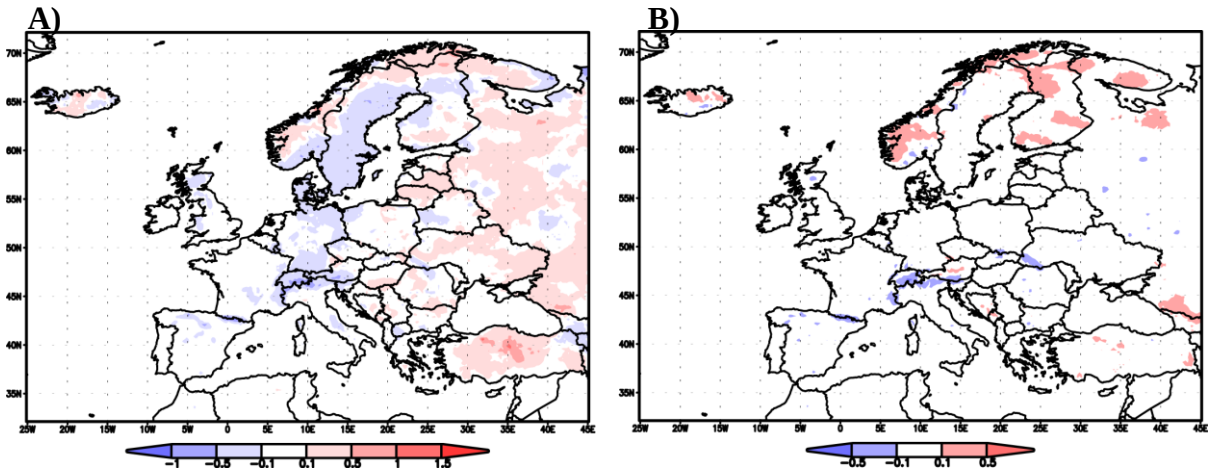

Figure 2.6. Linear trend for annual series of (A) 1 cm and (B) 10 cm of snowfall events (events/year) during the time period 1971-2000.

We also analysed the severity of very rare extreme snowfall events determined as the 50-year return period value of mm of water-equivalent precipitated in 24 hours. This was possible based on SMHIRCA-ECHAM5 simulations, discussed in Section 4.1 and the methodology presented in Section 2.2. The result is shown in Fig. 2.7 and illustrates a large range of daily extreme snowfall rate within Europe. An interesting feature that may not be very clear in observed data (Figs. 2.4 and 2.5) is that the most extreme snow storms are only weakly correlated with latitude and occur on the mountain slope areas facing typically warm and moist air flow. In these regions the extreme snow accumulation is usually 2-3 times as high as in other areas of Europe. RCM has problems in handling the eastern border of the regional climate model domain. There is an artificial maximum along the eastern border of the regional climate model domain stretching from Turkey to Russia (for RCM boundary treatment, see e.g. Rummukainen (2010)).

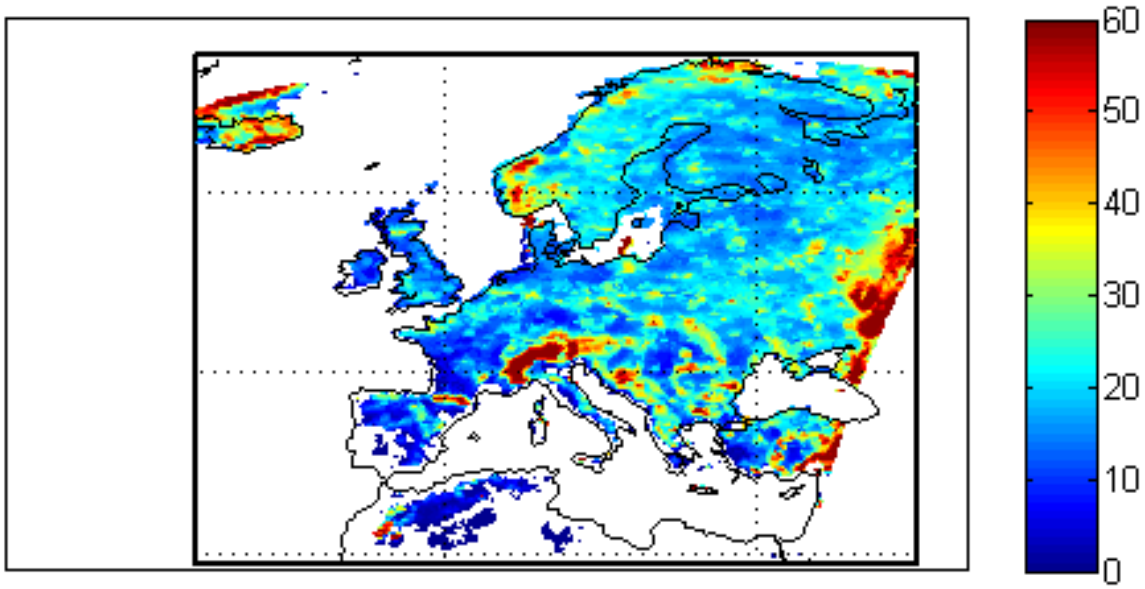

Figure 2.7. Simulated fifty-year return value of the annual maximum snow fall in 24 hours (in mm of water-equivalent) for the present climate. ***N.B.*** *Disregard the artificial maximum along the eastern border of the regional climate model domain stretching from Turkey to Russia that is due to lateral boundary condition problems (see e.g. Rummukainen (2010)).*

2.6. Blizzard

A blizzard is a severe storm condition defined by low temperature, sustained wind or frequent wind gust and considerable precipitating or blowing snow, which can cause damage to structures and, failures in transport control systems, as well as reduced road friction and visibility. A blizzard condition may generate delays and cancellations in all transport modes and increase the rate of accidents. In the present study we considered a blizzard to occur when the following criteria are met: snowfall exceeding 10 cm/24 hours, wind gust ≥ 17 m/s and daily mean temperature below 0°C.

The analysis indicated relatively low frequency of blizzards during the study period (Fig. 2.8). Blizzard conditions occur predominantly over the Alps and Northern Europe (30-40 cases in 30 years). The most affected regions are the western coast of Scandinavia and Iceland, with more than 140 cases in 1989-2010 (~10 cases/year). However, we have to take into account that, due to the difficulties in wind gust prediction and the relatively coarse resolution of ERA-Interim data, the frequency of blizzard events might be underestimated.

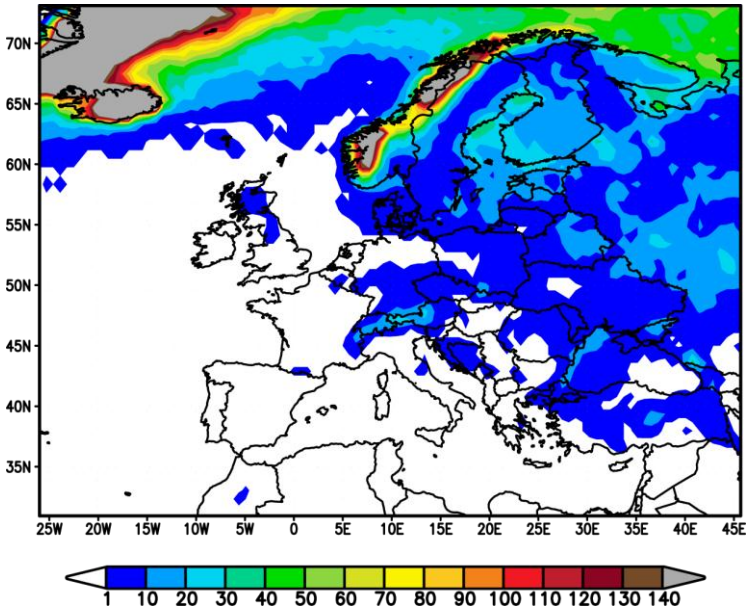

Figure 2.8. Total number of blizzard events during the period 1989-2010 based on ERA-Interim data.

2.7. Ice formed by freezing precipitation

One of the most harmful and dangerous phenomena for transport is freezing precipitation, which causes ice on the roads and consequent extreme slipperiness. Ground-based icing is hazardous for air transport as well due to ice on runways and icing of aircraft while on the ground. Even a very thin ice layer causes a slippery and aerodynamically rough surface, so that the severity of this phenomenon can be estimated by its frequency alone.

We have made an analysis of the frequency of freezing precipitation based on re-analysis data for airports in Europe. We used a 16-year NOAA National Climatic Data Centre database of surface observations at airports covering the period 1982-1997. From these data we filtered out cases where liquid precipitation was reported in the present weather code and simultaneously the wet bulb temperature was below 0 ^{o}C.

The results are shown in Figure 2.9. Although the data is limited to airports, the results provide a general view on the frequency of ice on ground. There are more than 144 hours of freezing precipitation per year in many locations in Central and Eastern Europe while the number is less than 72 hours in most of Western Europe. As one would expect the variation within areas is large, which is due to the effect of the local terrain on temperature inversions that are required for the freezing precipitation to occur. The phenomenon is most typical in isolated valley areas.

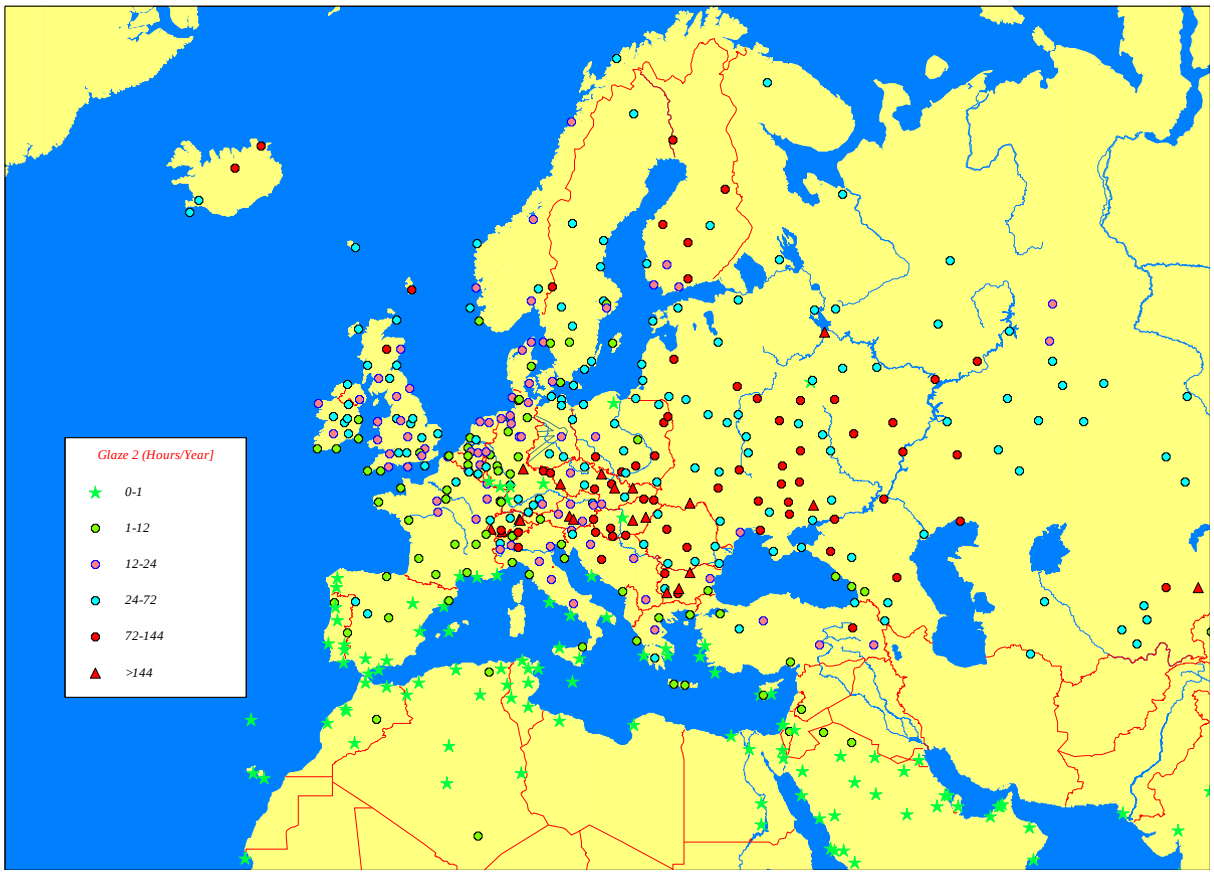

Figure 2.9. Total duration of freezing precipitation (hours/year) derived from NOAA data.

2.8. Heavy precipitation

Precipitation frequency, duration and intensity impact all transportation sectors and infrastructure. Heavy precipitation is one of the most costly weather situations, resulting in road submersion, flooding that additionally causes road washout, rail damage and destroys structures in most transportation sectors (Peterson et al., 2008). The probability of heavy precipitation was analyzed using three thresholds, e.g. 30 mm, 100 mm and 150 mm/day, defined based on their impact level and consequences. Intense precipitation events lasting only few hours or even less can cause adverse impacts to the transport system. However, due to the limited number of high frequency precipitation measurements it is difficult to perform an analysis European-wide; therefore, we focus on widely available daily precipitation data.

The probability of heavy rainfall exceeding 30 mm/24 hour over the European continent is 2% (Fig. 2.10). The frequency of days with 30 mm is higher in the Alps and on the western cost of the British Isles, the Iberian Peninsula (up to 30-35 days/year) and Scandinavia (45 days/year). The least affected European region appears to be the eastern part of Scandinavia (<5 days/year).

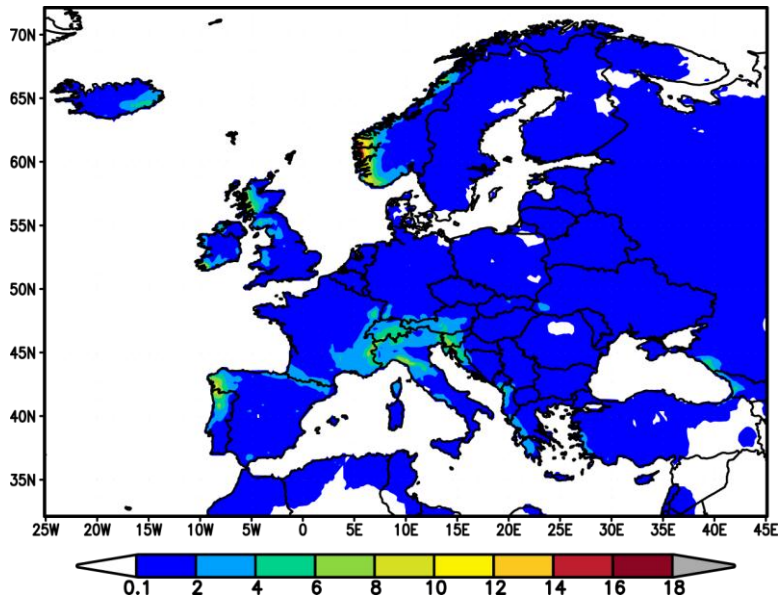

Figure 2.10. Frequency-based probability of daily rainfall exceeding 30 mm (in percent) during the period 1971-2000 based on E-OBS data.

Extreme rainfall events (≥ 100 mm/day) are rare (Fig. 2.11), in general 10-20 cases in 30 years over Western Norway, parts of the Mediterranean, Alps and sporadically over Eastern Europe. There are stations that have occasionally measured precipitation amounts exceeding 150 mm per day in practically all European countries, but these measurements may not always be part of E-OBS data archive. Nevertheless, daily precipitation amounts >150 mm are very rare; therefore, these very high values are mostly levelled off in the E-OBS gridded data (Fig. 2.11B).

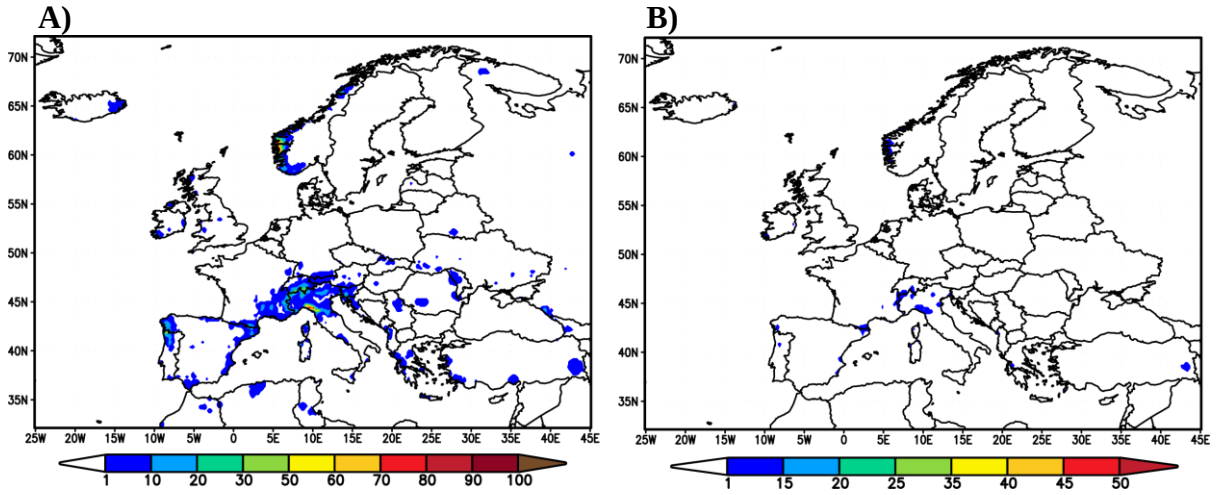

Figure 2.11. Total numbers of days with rainfall exceeding (A) 100 mm and (B) 150 mm during the period 1971-2000 based on E-OBS data.

Considering the monthly variation, heavy rainfall events (30 mm) are more frequent in the winter season, with 72% of cases occurring between October and January (Fig 2.12.).

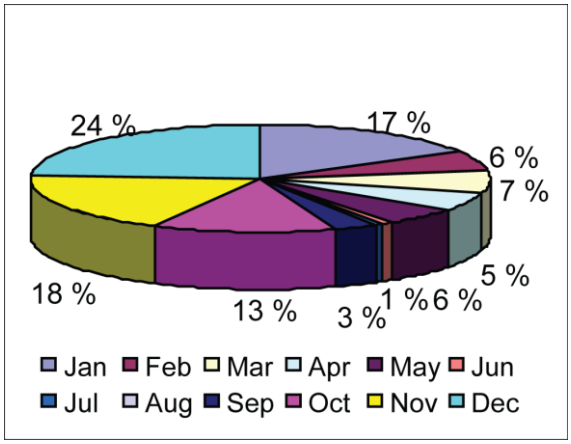

Figure 2.12. Monthly variation heavy rainfall days exceeding 30 mm.

2.9. Heat waves

Hot days and heat waves are harmful for land (road and rail), air transportation and also for infrastructure. High temperature may cause driver fatigue and road deterioration, while extreme high temperature, such as 43 °C, causes buckling in the road surface, airport runways and rail tracks, and equipment failure, thus increasing accident rates and the probability of delays or diversions. The thresholds used in the analysis of heat waves were: 25 °C, 32 °C and 43 °C.

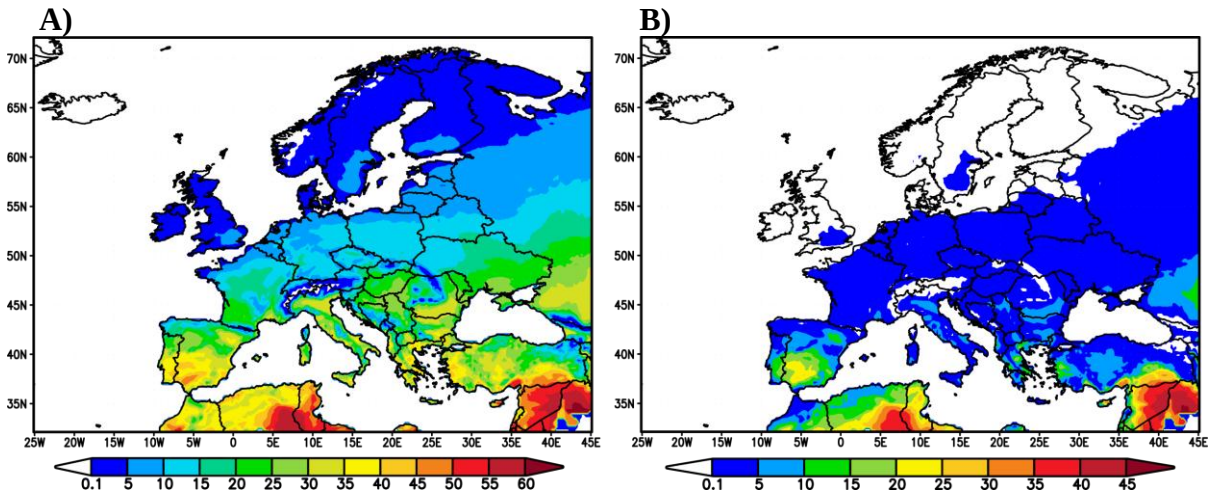

Figure 2.13. Frequency-based probability of daily maximum temperature exceeding (A) 25 °C and (B) 32 °C (in percent) during the period 1971-2000 based on E-OBS data.

There is at least a 5% probability of having high temperatures (≥ 25 °C) over the European continent (Fig 2.13). The frequency of hot days varies between the annual average of 90-150 days (for the 25 °C threshold), 30-80 days (32 °C) in southern Europe and between 15-60 days (25 °C), 10-20 days (32 °C), in the central and eastern part of the continent.

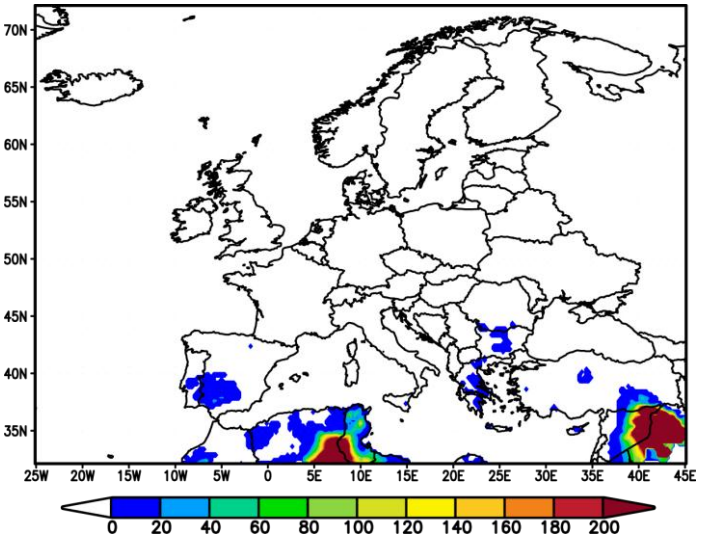

Figure 2.14. Total number of days with maximum temperature exceeding 43 °C during the period 1971-2000 based on E-OBS data.

Very hot days, with daily maximum temperature above 43 °C, are very rare with a maximum of 25 days over the Iberian and Balkan Peninsula (Fig. 2.14). However, it must be kept in mind that, although an individual station may record temperatures above 43 °C, the E-OBS data may not have a grid value above the threshold due to the gridding procedure. The trend analysis of heat waves indicates an increase of 1-2 days/year during 1970-2000 over most of the continent except Scandinavia and some parts of Russia (Fig. 2.15).

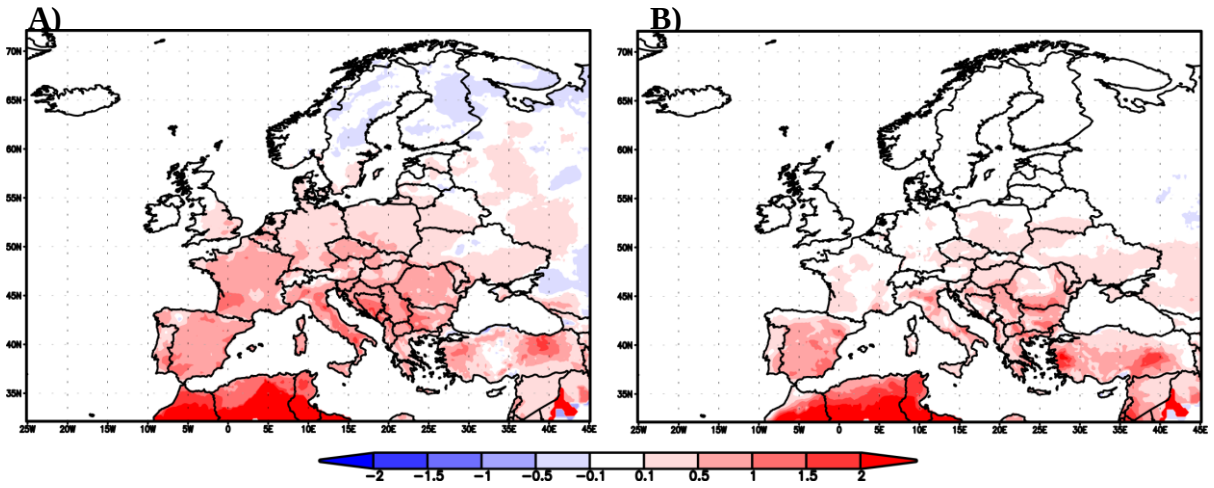

Figure 2.15. Linear trend for annual series of heat waves (events/year) above (A) 25 °C and (B) 32 °C during the time period 1971-2000.

2.10. Cold spells

Low temperature can be considered a modifier of hazardous conditions for transportation, rather than a main cause. Low temperatures contribute to the development of slippery conditions; com-

bined with precipitation and wind, this can have a disruptive effect on traffic. Extreme cold air temperature may cause disruption in the railway sector, inland waterway transport and may severely limit the work of ground crews at airports.

The spatial and temporal variation of low temperature was studied using three thresholds: 0 °C, -7 °C and -20 °C.

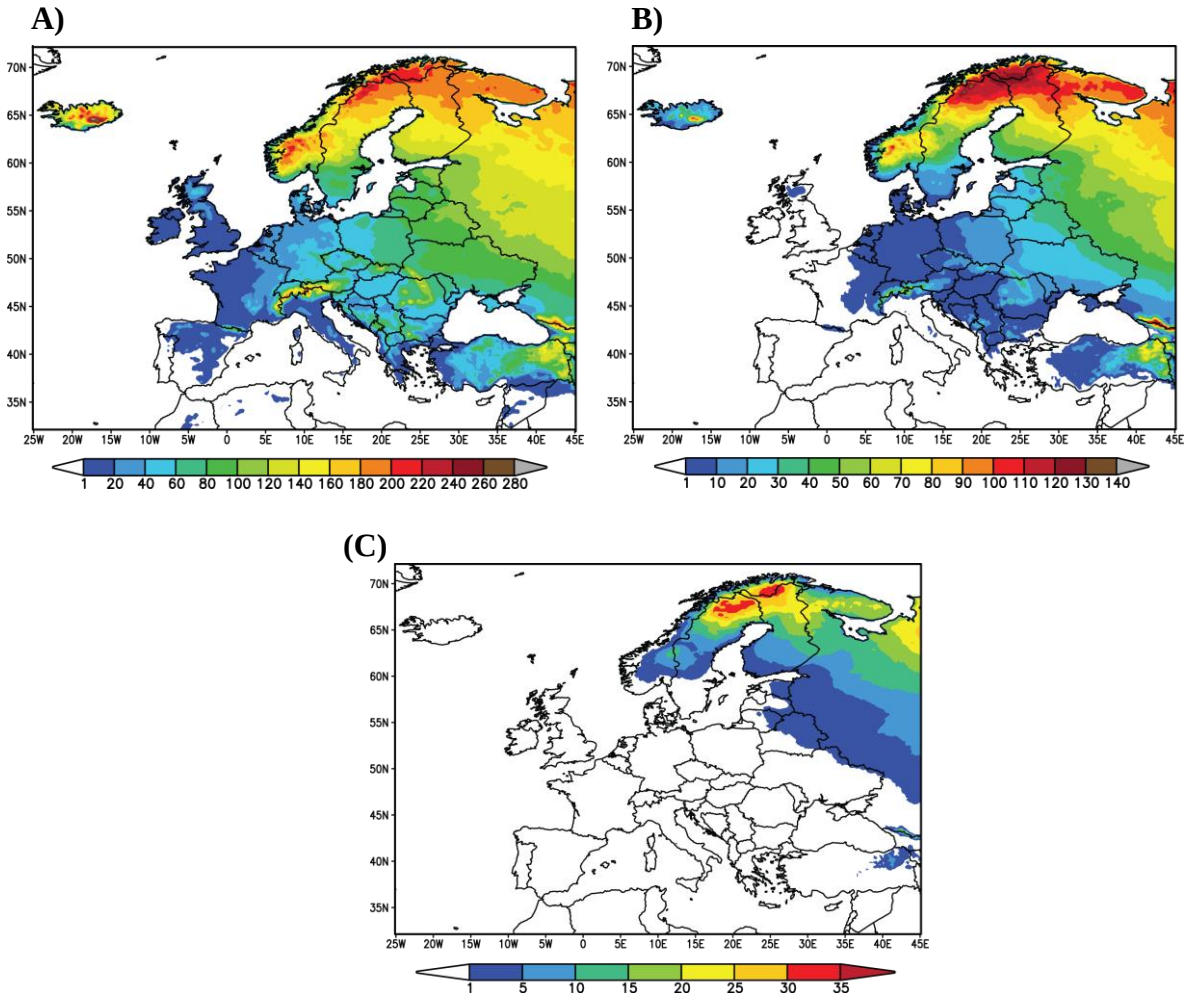

Figure 2.16. Average number of days per year with daily mean temperature below: (A) 0 °C, (B) -7 °C and (C) -20 °C, during the period 1971-2000 based on E-OBS data.

As expected, the frequency of frost days varies from 100 to 200 per year in Scandinavia, with the highest values in the Scandes (220 days), and decreases southwards, to about 20 days per year (Fig. 2.16). Most of the continent is free of very extreme cold spells (< 20 °C), except Scandinavia and the NE part of Europe (5-30 days/year). The trend analysis for the probability of cold spells (Fig. 2.17) implies predominantly a decrease during the 30 year period, especially over Northern Europe, Russia and the Alpine region.

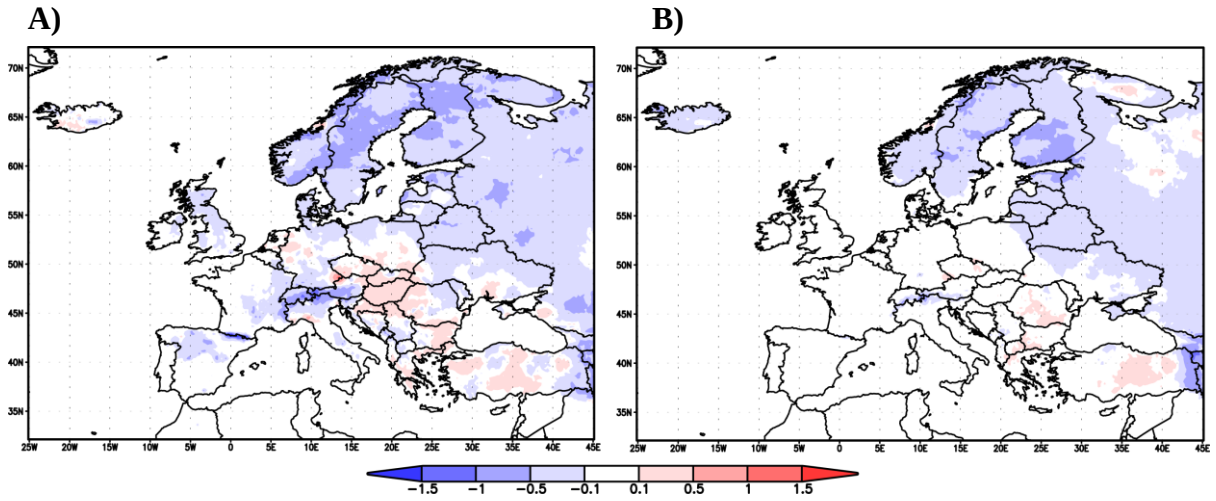

Figure 2.17. Linear trend for annual series of cold spells (events/year) with (A) 0 °C and (B) -7 °C during the period 1971-2000.

2.11. Poor visibility

Low visibility is generally caused by particles suspended in the air. These particles may be dust or sand that has been lifted up from the earth's surface in sand or dust storms. These will be discussed below. Most frequently, however, limited visibility is caused by water or ice particles. This may be the case during heavy rain- or snowfall, but it is more typical that very small suspended droplets (or ice crystals) are responsible for reduced visibility. By convention, visibility less than 1 km is termed fog.

2.11.1. Fog

Fog occurrence is a problem for many modes of transport, most importantly aviation and shipping. For shipping, it is necessary that the vessels reduce their speed to ensure safe operation. Similarly, for aviation, an increase in separation between aircrafts is required as visibility reduces. In addition to horizontal visibility, vertical visibility is another factor of importance. Vertical visibility is operationally measured by ceilometers that measure the height of the base of a cloud deck, called the *ceiling*.

The horizontal and vertical visibility conditions at airports are relevant to the requirements for the Instrument Landing System (ILS) on aircraft. These are, with increasing demands on that system, CAT I, CAT II, CAT IIIa, CATIIIb and CAT IIIc. In what follows, we will focus on the first three of these thresholds.

Table 1. List of ILS categories

	horizontal visibility	vertical visibility
CAT I	≥ 550 m	> 60 m
CAT II	≥ 300 m	≥ 30 m
CAT IIIa	≥ 200 m	
CAT IIIb/c	< 200 m	

Using hourly weather reports (known as METAR reports) originating from major European airports through the period 1975-2009, we have assessed the number of hours that these criteria are not met. Particularly, we have studied the temporal change of these hours.

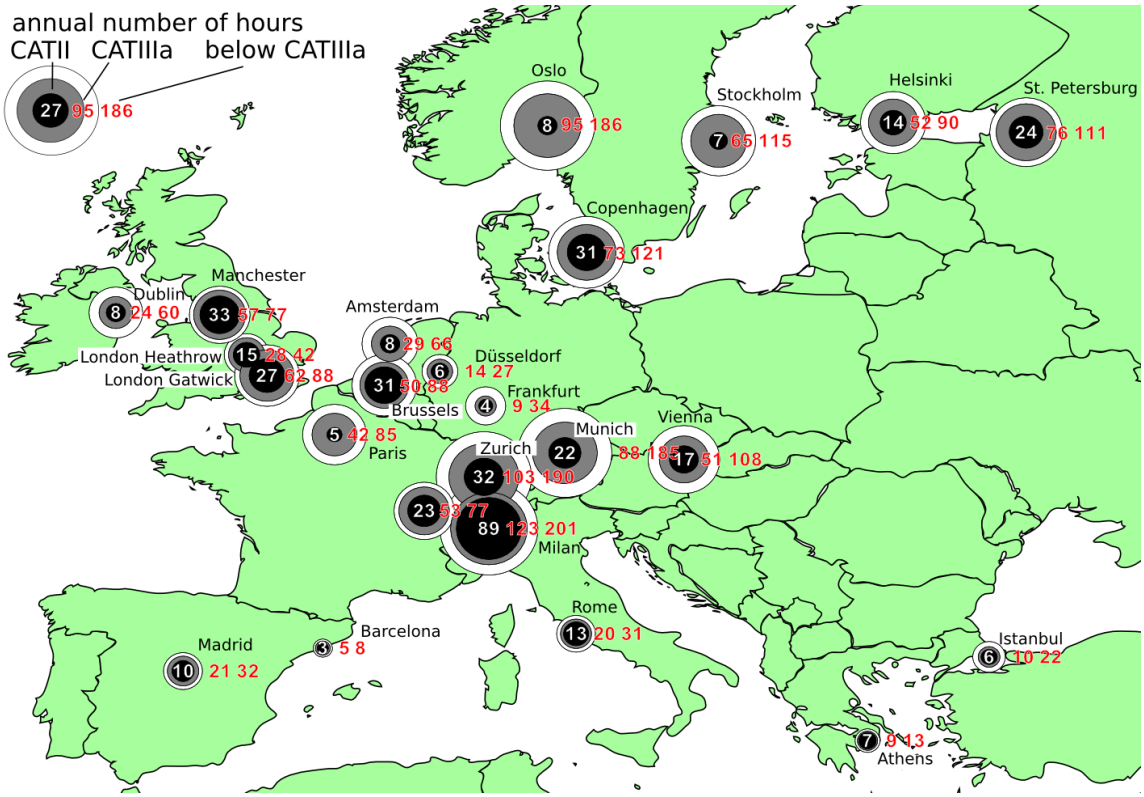

Figure 2.18. Annual number of hours that CATII (a.), CATIIIa (b.) and CATIIIb/c (c.) conditions occurred at selected major European airports during the period 2000-2009.

The occurrence of low visibility at 24 major European airports during the period 2000-2009 is depicted in Fig. 2.18. The severity of the fog problem is strongly related to the climate zone. In the Mediterranean zone, visibility problems are very rare, with the notable exception of Milan, located in the fog-prone Po-Valley. This particular airport has more than double the hours of l<200 m visibility (requiring CATIIIb/c) than any other European airport. Other airports with a notable problem (> 20 hours) with such dense fog are Manchester, London Gatwick, Copenhagen, Brussels, Geneva, Zurich, Munich and St. Petersburg. It is noted that some airports have many hours with moderate visibility problems (CATII, CATIIIa), such as Oslo and Stockholm, yet the most severe CATIIIb/c situations are rare at these locations.

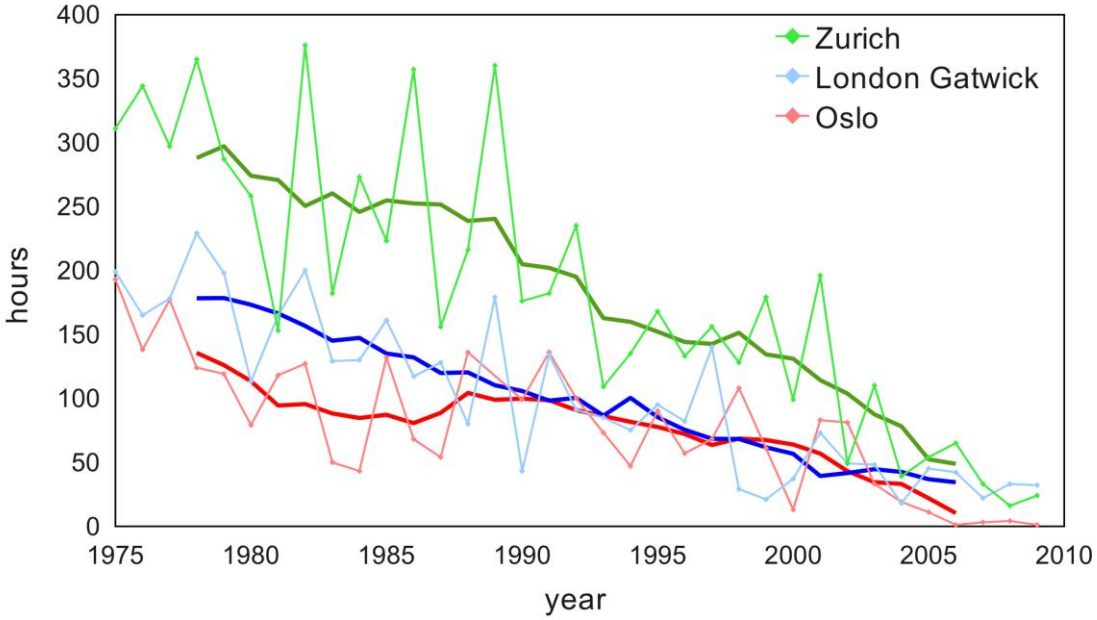

Figure 2.19. Annual numbers of hours with visibility <200 m at the airports of Zurich (green), London Gatwick (blue) and Oslo (red). Thin lines represent annual totals; thick lines are 7-year moving averages.

Recently, a number of scientists (Vautard et al., 2009; Van Oldenborgh et al., 2010) have considered the temporal trend of visibility during a number of decades across Europe and found the intriguing result that the occurrence of low visibility has strongly declined. Van Oldenborgh et al. (2010) found that this decline is due to the decrease in aerosol emissions over Europe, and not changes in flow patterns (which would show up clearly in climate model runs). For this reason, in order to predict the occurrence of visibility over the next decades, those climate models which currently do not or poorly represent aerosol emissions and chemistry, are of little help.

The METAR aviation weather report data analysed here confirm their conclusion that the low visibility problem is reducing very rapidly (Fig. 2.19). Although there are large yearly variations in hours with <200 m visibility, the overall trend is clearly and significantly downward at all 24 airports displayed in Fig. 2.13. In fact, very poor visibility conditions have diminished at some airports to the point of being almost non-existent. For example, Oslo Gardemoen airport, where, during the four years of 2006-2009, the total duration of visibility <200 m was less than 10 hours. It must be recognized, however, that, at the same airport, there were still 121 hours of visibility between 200 and 500 metres annually over the same time period. At other airports, periods of low visibility have become rarer, but do still occur.

The pan-European improvement in visibility conditions can be seen from Fig. 2.20, which shows that the average hours with conditions of CATII or worse has reduced by about a factor of four. When considering the individual categories, it can be seen that the duration of CATII has decreased much less (by a factor of 2.5) compared with that of the CATIIIb/c conditions (a factor of 5). This means that the lower aerosol content of the air is more effective at reducing the occurrence of very dense fog, compared with that of less dense fog. These CATII conditions may additionally be caused in part by heavy snowfall or very heavy rain, which are probably less sensitive to changes in aerosol content. Poor visibility caused by dust episodes are discussed in the following section 2.11.2.

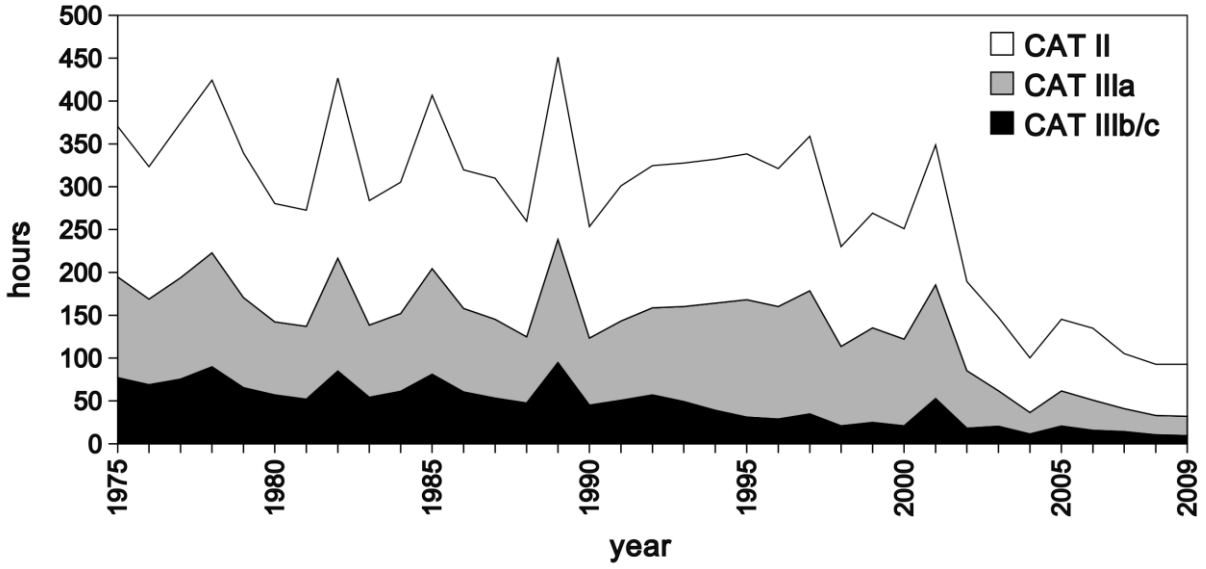

Figure 2.20. Annual numbers of hours with particular visibility conditions averaged over the 24 airports (Instrument Landing System categories, see Table 1).

For traffic, and air traffic in particular, the above results are naturally good news. We may expect that the trend of improving visibility conditions will continue in the near future, provided that actions in improving air quality continue, although the trend may level off at longer timescales. However, at particularly fog-prone airports, such as Milan Malpensa, frequent reduced visibility episodes due to fog still exist. This will be the case at other European airports, and will be for the coming decades, albeit to a lesser extent.

2.11.2. Dust transport episodes

The occurrence of high level concentrations of dust originating from deserts is quite common, even at locations quite distant from the source region. The mechanisms for lifting particulates within the source region, the conditions leading to their suspension in the atmospheric air, their transportation to great distances, and the eventual deposition (either dry or wet) on the ground, comprise a highly complex phenomenon affecting human health and several activities, including air-transportation. Below, a novel approach is presented, namely the application of Artificial Neural Networks (ANN) for diagnosing and predicting atmospheric pollutant levels over the island of Cyprus, in the eastern Mediterranean, due to the transportation of dust from the adjacent deserts.

Synoptic pattern classification

One of the major inherent problems in endeavouring to classify synoptic patterns is the *a priori* determination of the number of different classes that one can expect from such a classification. In other words, the number of distinctive synoptic patterns over any particular geographical region is by no means fixed. Traditionally, such a synoptic classification was performed by a qualitative inspection of synoptic maps. Professional meteorologists examined a series of plotted synoptic maps and picked out geometric similarities (e.g., Prezerakos et al., 1991). Nevertheless, it seems that, in an attempt to perform a classification with an unknown number of classes, experimentation with various possibilities is a practical procedure, which can lead to some useful considerations. For this reason, it was decided to run a number of experiments and build classification models with different

numbers of output nodes (i.e. classes). For the present analysis 35 output nodes are presented, as described by Michaelides et al. (2011).

The ability of ANN to group synoptic patterns into seasonally dependent clusters was noted by Michaelides et al. (2007). This seasonal discretization of classes should be an essential attribute of a classification technique.

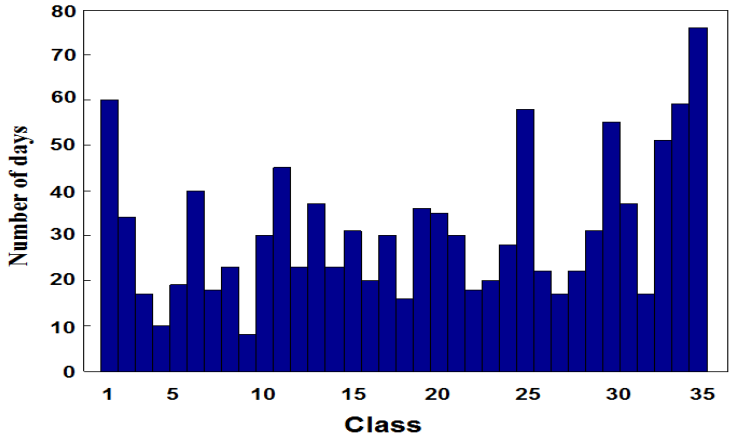

Figure 2.21. Number of days per class, for the 35 classes in the synoptic classification, during the time period 2003-2005.

Figure 2.21 shows the frequency of appearance of the synoptic patterns in the 35 classes for the three-year period 2003-2005. Apparently, class 35 is most frequently encountered, followed by classes 1 and 25. Figure 2.22 is a graphical representation of the assignment of a class to each day in the three year period. It is clear that there is a seasonal "quasi-cyclic" behavior. Certain classes occur, almost exclusively, during summer or winter; during the (Mediterranean) transitional periods of spring and autumn, both summertime and wintertime patterns can occur. This graphical representation is proposed as a practical visual tool to identify the level of seasonal discretization pursued in adopting a synoptic classification technique.

Synoptic classes and dust deposition events

During 2003-2005, 85 dust transport events were observed in Cyprus. Using the existing dust collection network, a dust transport episode is considered as a day when the average PM10 measurement exceeds the threshold of 50mg/m^3 (for more details see Michaelides et al., 2011). Figure 2.23 shows how the 85 dust transport events are distributed among the 35 classes in the synoptic classification. There appears to be a certain preference of classes associated with these events: most prone to dust events is class 1, followed by class 31; representative synoptic situations for these two classes are shown in Figure 2.23. Figure 2.24(a) refers to 1200 UTC on 1 February 2003 and Fig. 2.24(b) at 1200 UTC on 10 May 2004: in the former, a central Mediterranean upper trough extends well into the North African desert; in the latter, the trough axis extends southwards from the Iberian Peninsula. In both cases, typical patterns are identified favouring dust lofting and its transfer eastwards with the resulting south-westerly airflow over the eastern Mediterranean.

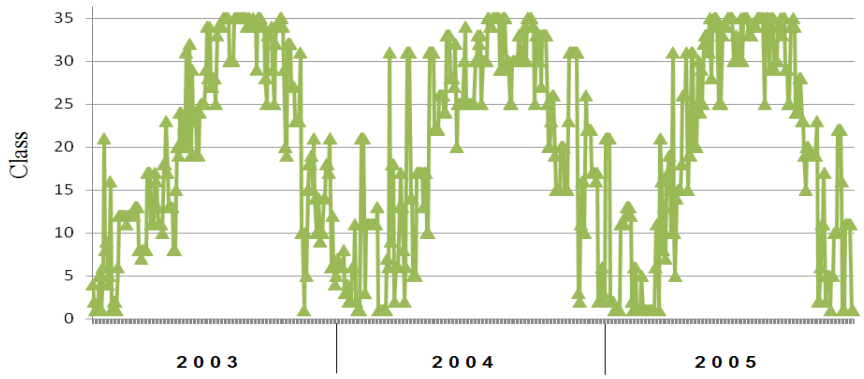

Figure 2.22. Daily distribution of 35 classes over the three-year period 2003-2005.

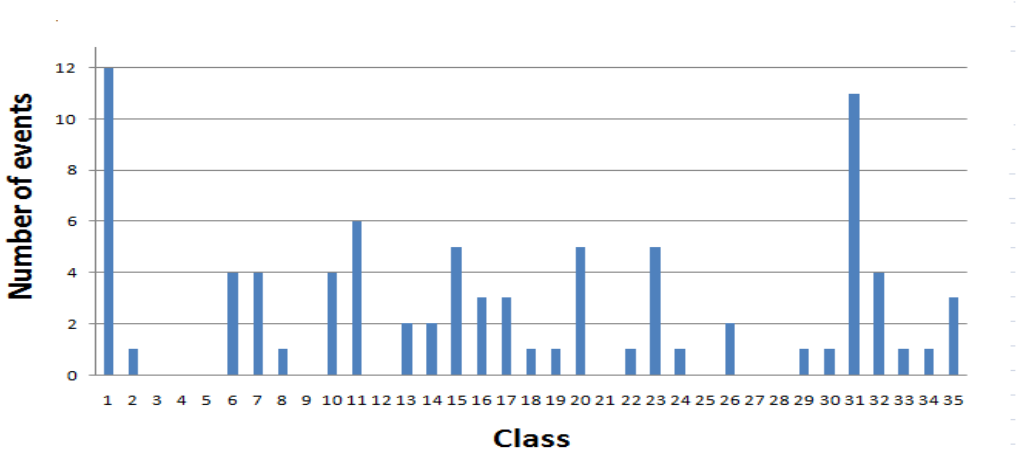

Figure 2.23. Distribution of dust deposition events per class, for the 35 classes in the synoptic classification, during 2003-2005.

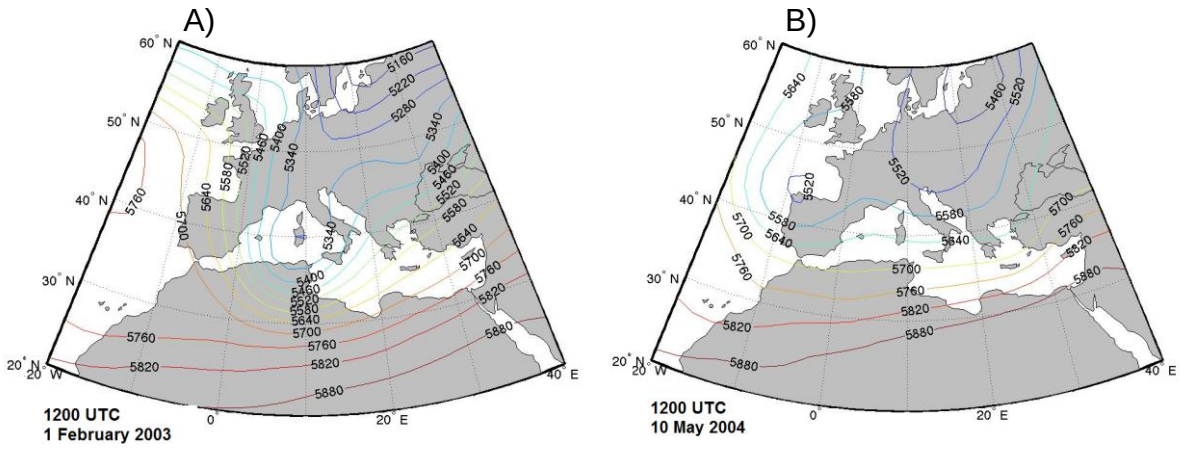

Figure 2.24. Representative synoptic situations corresponding to: (a) class 1; (b) class 31. Isolines are drawn every 60 geopotential meters.

Synoptic classes and dust deposition event trends

Since a period of 3 consecutive years (2003-2005) was examined in order to identify and classify the synoptic conditions which lead to dust transport episodes in the eastern Mediterranean, a time-line of 25 years (1980-2005) is also examined in order to identify trends of those synoptic conditions which favour dust transport episodes for this period, using the results from the 3-year period. For each year, the total number of days belonging to each of the 35 classes was counted and, using linear regression, an attempt to identify what the pattern of synoptic evolution was within the selected time frame was made. The period of three years is quite small, but we operate under the assumption that it is characteristic of a much wider period.

Figure 2.25 shows the frequency of appearance of the synoptic patterns in the 35 classification for the period 1980-2005. Again class 35 is most frequently encountered, followed by classes 30 and 25.

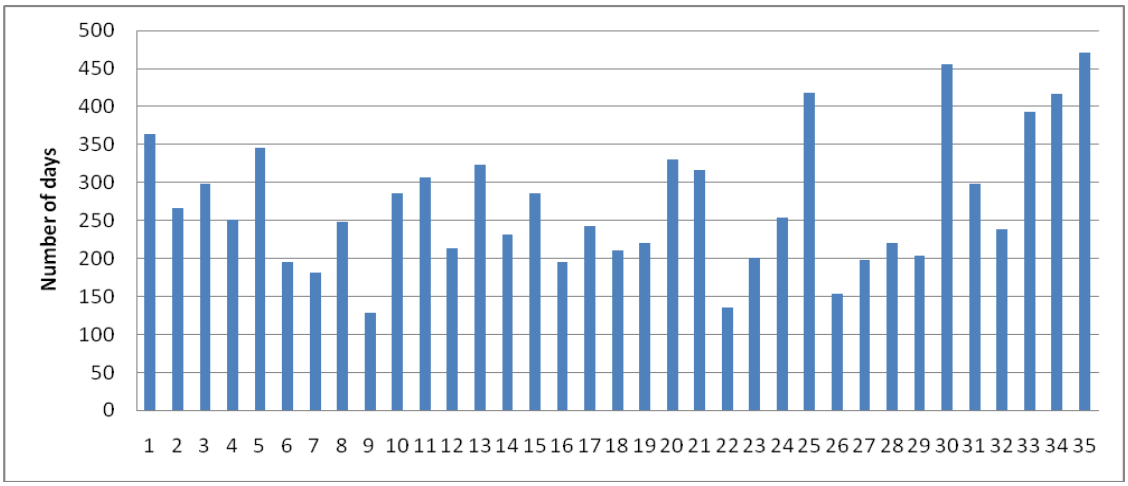

Figure 2.25. Number of days per class, for the 35 classes in the synoptic classification, during 1980-2005.

Using the results from the distribution of dust deposition events per class, for the 35 classes in the synoptic classification, during 2003-2005 (see Fig. 2.23) we were able to identify classes which favour dust deposition events and classes that present no dust events at all. Table 2 shows how the classes are distributed across the 3 distinct categories.

Table 2: Classification of Classes according to dust deposition events during the period 2003-2005

Category	Classes
Classes with dust deposit events	1,31,11,15,20,23,6,7,10,32, 16,17,35,13,14,26,2,8,18,19,22,24,29,30,33,34
Classes with no dust deposit events	3,4,5,9,12,21,25,27,28

Figure 2.26 presents the evolution of Classes 1, 31 and 11 within the 25-year period; classes which represent the synoptic conditions that favour dust deposition within the 3-year period. The first two present an overall negative trend, while the third presents a positive one.

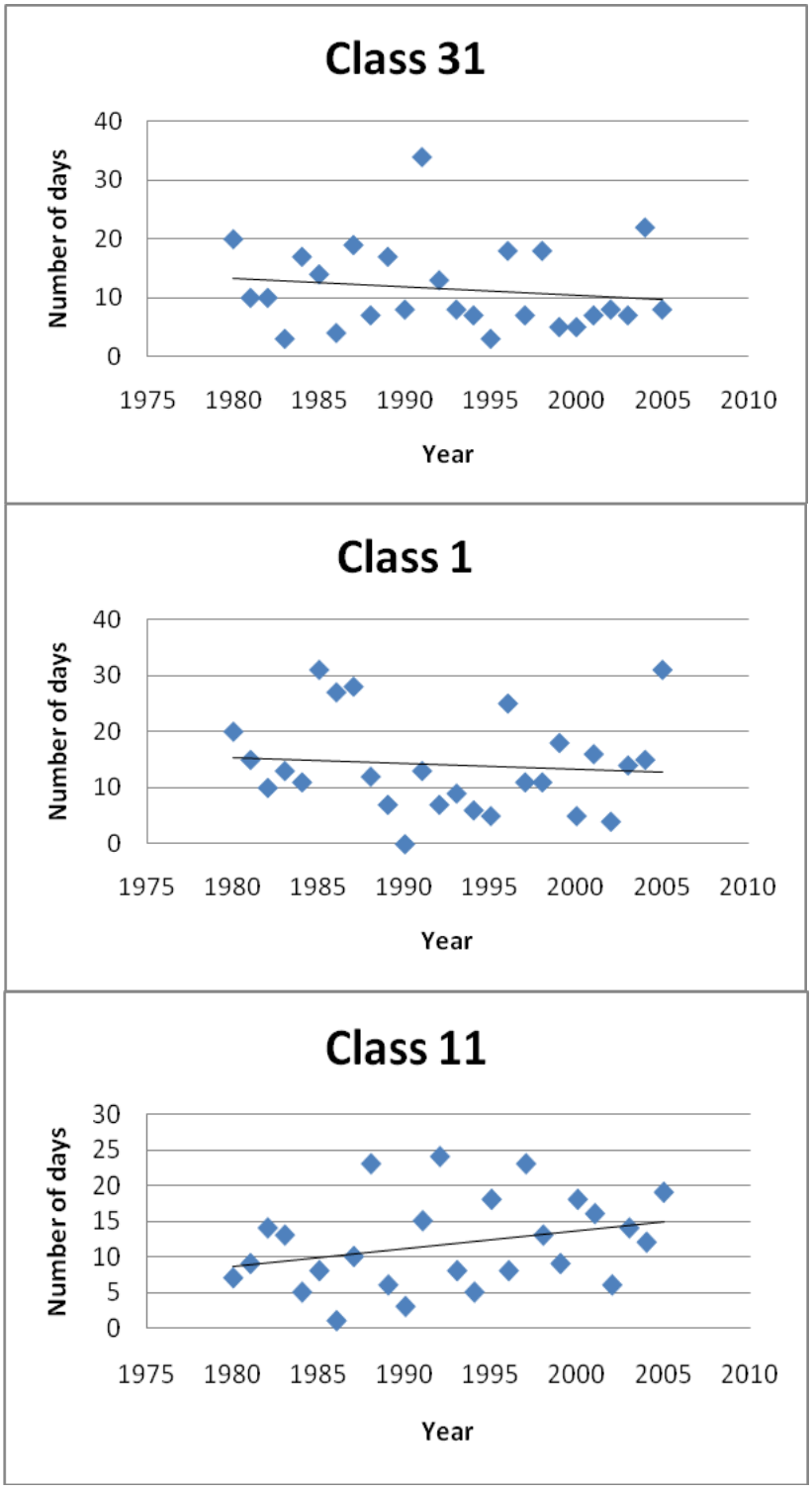

Figure 2.26. The evolution of classes 31, 1 and 11 within the 25 year period (1980-2005).

In Figure 2.27, the trends of the classes which show "no dust deposition" are presented. It is evident that for all these classes (except Class 25) the trend is negative for the 25 year period.

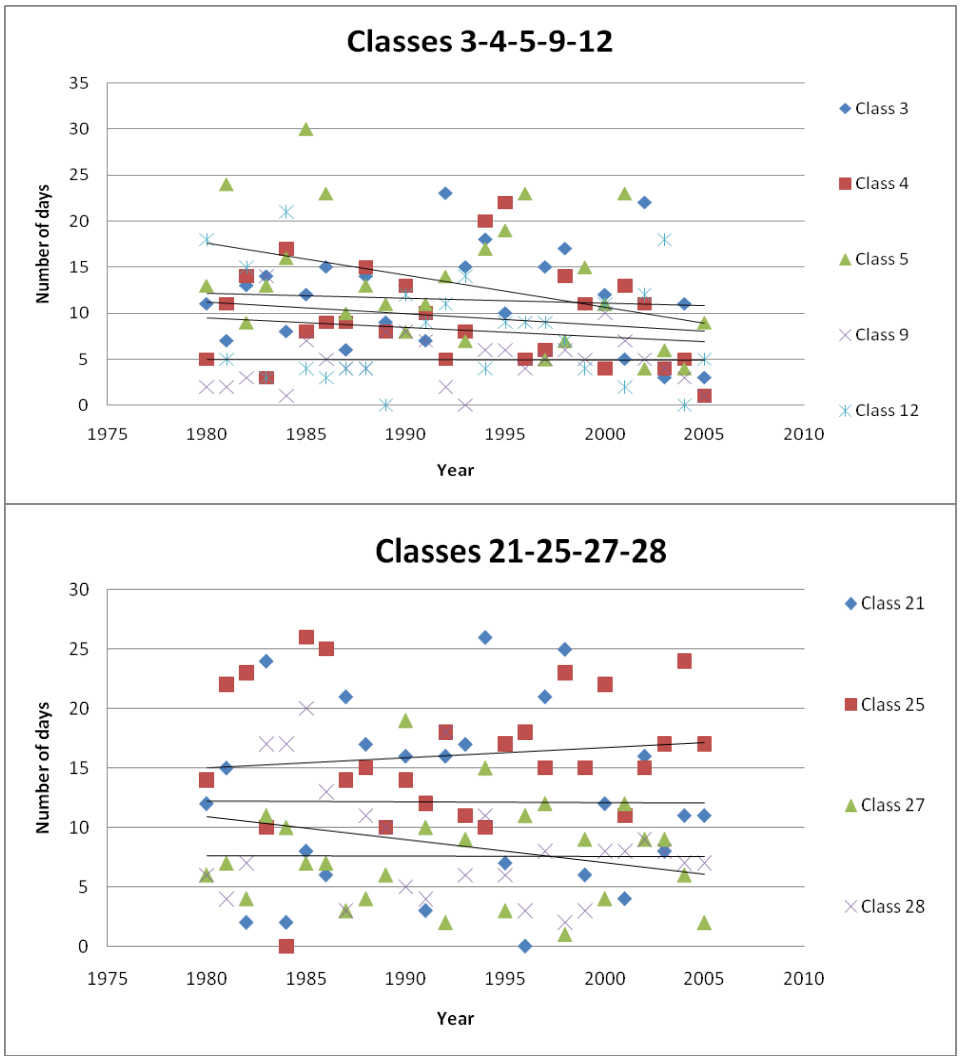

Figure 2.27. The evolution of the "no dust deposition" classes within the 25 year period (1980-2005).

The trend of each of the 35 classes is presented in the table below. From Table 3 it is evident that while in both categories there is an overall prevailing of negative trends, this is more severe in the no-dust ones; 7 out of 8 of the no-dust classes present a negative trend as opposed to 14 out of 26 classes where dust is present. Furthermore, from the last category, if we consider only classes where more than two dust events were present, then 6 out of 10 classes present positive trends. We can assume that there is an enhanced presence of classes that favour the presence of dust; however this assumption surely needs to be investigated further using a longer period that the one used for this preliminary work.

Table 3. Classes and trends for the period of 25 years (1980-2005)

Class	*Slope*	*Trend*		*Class*	*Slope*	*Trend*
1	-0,1019	NEG		19	0,0131	POS
2	-0,0588	NEG		20	0,0499	POS
3	-0,0537	NEG		21	-0,0048	NEG
4	-0,1255	NEG		22	0,012	POS
5	-0,3484	NEG		23	0,0961	POS
6	0,1036	POS		24	-0,121	NEG
7	-0,0803	NEG		25	0,0834	POS
8	0,0581	POS		26	0,0602	POS
9	-0,0058	NEG		27	-0,0048	NEG
10	0,147	POS		28	-0,1959	NEG
11	0,2574	POS		29	-0,0178	NEG
12	-0,1015	NEG		30	0,1084	POS
13	-0,0147	NEG		31	-0,1364	NEG
14	-0,0291	NEG		32	0,026	POS
15	-0,0472	NEG		33	-0,1159	NEG
16	-0,0817	NEG		34	-0,1338	NEG
17	-0,0574	NEG		35	0,6376	POS
18	-0,0229	NEG				

2.12. Small scale phenomena – thunderstorm and associated phenomena

The occurrence of thunderstorms affects transport systems in various ways, e.g. via strong winds, lightning, intense precipitation, and hail.

2.12.1. Lightning

By their definition, thunderstorms are associated with lightning, which poses a hazard for people in the open. This requires that airport aprons needing to be cleared as soon as a thunderstorm is detected. Furthermore, infrastructural damage may occur, for example to electrified railways.

Sensors have been installed on several satellites to give an impression of the lightning coverage across Europe (Fig. 2.28). Lightning-prone areas include the entire Mediterranean region, the Balkans and, to a lesser extent, parts of east-central Europe such as Poland, Ukraine and Belarus. Elsewhere, lightning is less frequent. However, except for far northern Scandinavia and parts of the northern Atlantic Ocean and Iceland, lightning does regularly occur across all of Europe. The lightning activity has a peak in early summer (June-July) across northern and central parts of Europe, and in late summer and autumn (August-Oct) across the Mediterranean Sea and adjacent coastal areas.

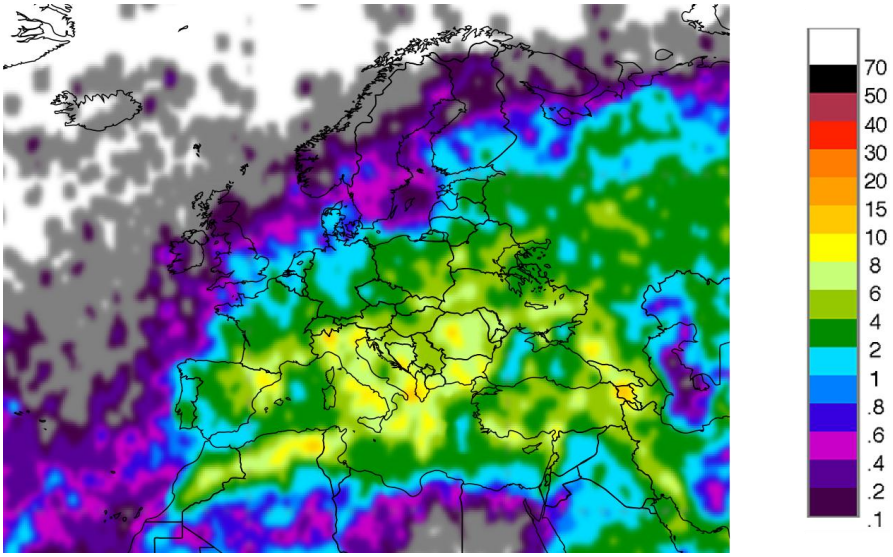

Figure 2.28. Annual lightning frequency in Europe (strikes per km^2 per year) in the period 1995-2005. Data source: NOAA Earth System Research Laboratory.

2.12.2. Thunderstorm-related gusts

In addition to lightning, some thunderstorms produce very strong wind gusts. These may be caused by the evaporation of rain and small hail (graupel) in the dry air below the bottom of the storm cloud, causing a so-called downburst, a very local phenomenon. Large thunderstorm complexes can also develop local wind systems that produce large swaths of damaging gusts.

The climatological occurrence of such thunderstorm gusts across Europe is not well known. An important reason for this is that it is often hard to reconstruct whether a recorded wind gust was associated with thunderstorms, yet it is important to treat them separately from gusts occurring with large-scale windstorms. Thunderstorm gusts occur much more locally and are generally not well represented in climate models (cf. discussion in Section 2.1).

In many regions in Europe, large-scale storm systems are responsible for the strongest gusts. These systems occur primarily in the winter season from October through March. This is the case, for example, in southern Germany (Fig. 2.29, top), where gusts stronger than 25 m/s (or about 90 km/h) are concentrated in those months. In this area however, a secondary maximum occurs in the summer season from May through August, which is attributable to gusts resulting from thunderstorms, which occur most often in this season. Many of these gusts (those in red) were more than twice as strong as indicated by the reanalysis dataset. In other areas, such as Finland (Fig. 2.29, bottom), strong gusts occurring as a result of thunderstorms are much rarer.

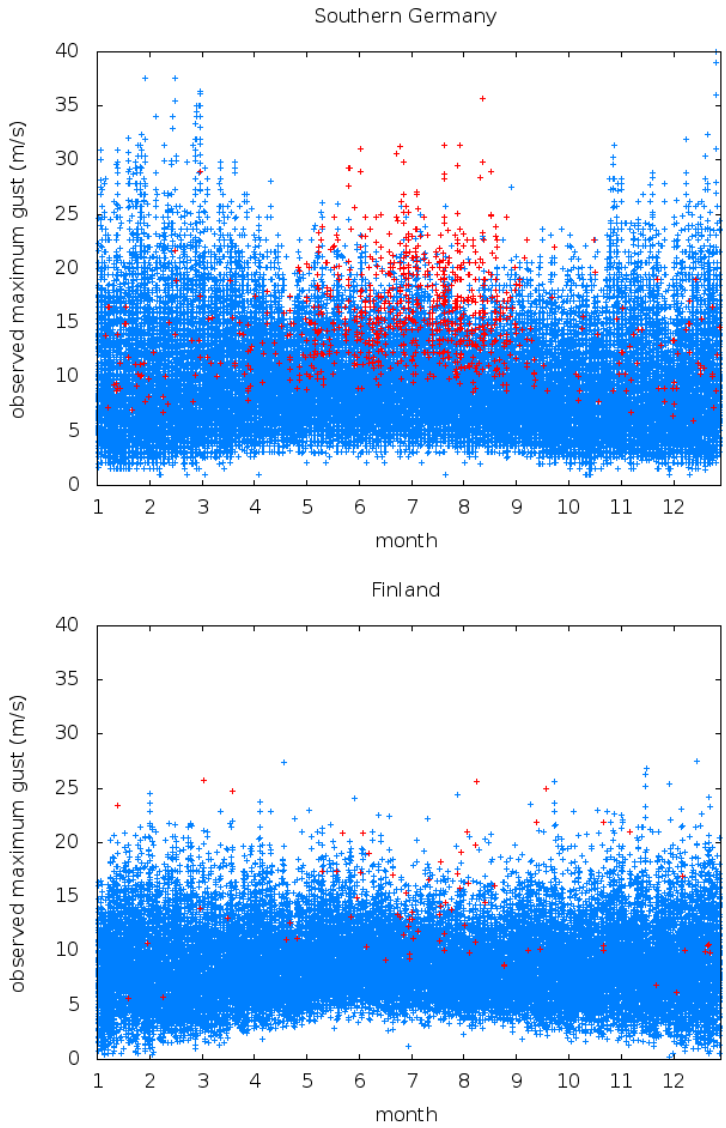

Figure 2.29. Maximum daily wind gusts at measurement stations across southern Germany (Augsburg, Bamberg, Constance, Hof, Munich, Nuremberg, Stuttgart-Echterdingen, Stuttgart-Schnarrenberg) (top) and across Finland (Helsinki, Kaarina, Maaninka, Niinisalo, Rovaniemi, Seinajoki, Siikajoki, Vihti) (bottom). German gusts are from the period 1990-2009, Finnish gusts from 2000-2009. Gusts for which the ERA values were more than 50% lower than the observed value are depicted with red crosses, all others with blue crosses.

2.12.3. Large hail and tornadoes

Large hail is a thunderstorm-related threat that occurs throughout Europe. It affects transport primarily in the sense that it is a safety concern for air traffic. Large hail is associated with the most powerful thunderstorms, which have extremely strong updraughts that can easily exceed 30 m/s (108 km/h). Moreover, the storm must have a long enough lifetime for large hailstones to form. Both conditions are given in situations when the temperature drops rapidly with height, the air close the earth's surface is humid, and strong vertical wind shear is present (i.e. the wind speed and direction changes with height).

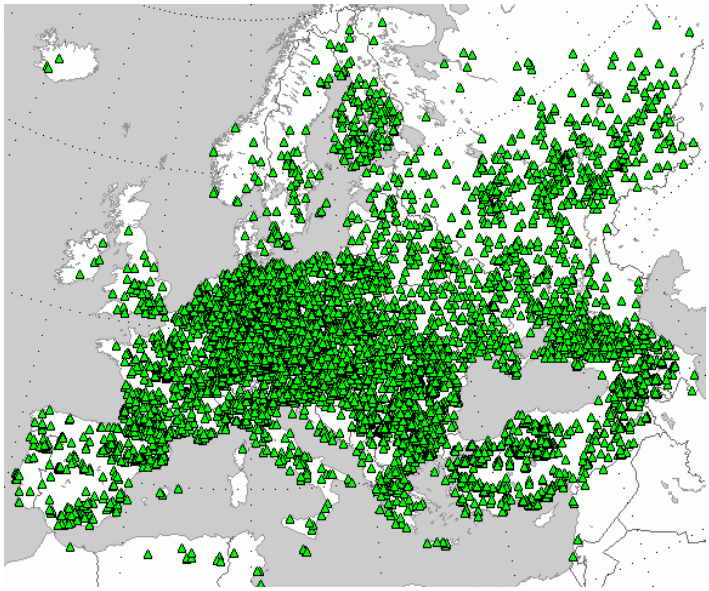

Figure 2.30. Large hail reports collected in the European Severe Weather Database. It is suspected that hail across Eastern Europe (Belarus, Baltic States, Russia, Ukraine) is strongly underreported.

Large hail is most frequent in central and eastern parts of Europe (Fig.2.30). Across western and north-western Europe its occurrence is much rarer, but all European regions that regularly experience thunderstorms are occasionally affected by large hail.

Another thunderstorm-related hazard is tornadoes. A tornado is an intense vortex typically between a few metres to a few kilometres in diameter, extending between a convective cloud and the earth's surface that may be visible by condensation of water and/or by material that is lifted from the earth's surface.

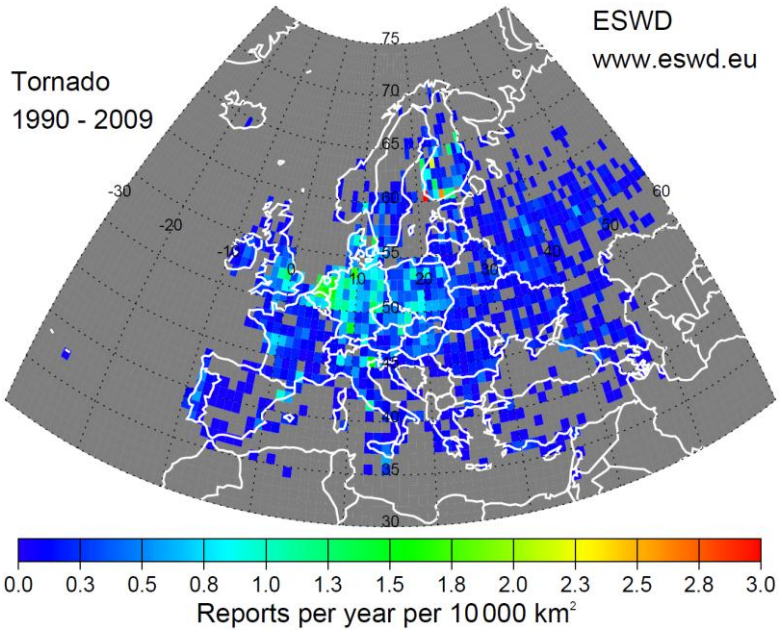

Figure 2.31. Annual frequency of tornadoes across Europe. Source: ESWD.

Tornadoes occur relatively infrequently, but do occur across all of Europe (Fig. 2.31). Tornadoes occurring over open water are often called waterspouts. Waterspouts occur more frequently than tornadoes over land, and are weaker on average. Still, many of them reach wind speeds well in excess of hurricane force (32 m/s) and cause extremely dangerous conditions for shipping. Moreover, one case is known of an aircraft encountering a tornado in the Netherlands, resulting in a serious accident in which all 16 passengers and one person on the ground died (Roach and Findlater, 1983).

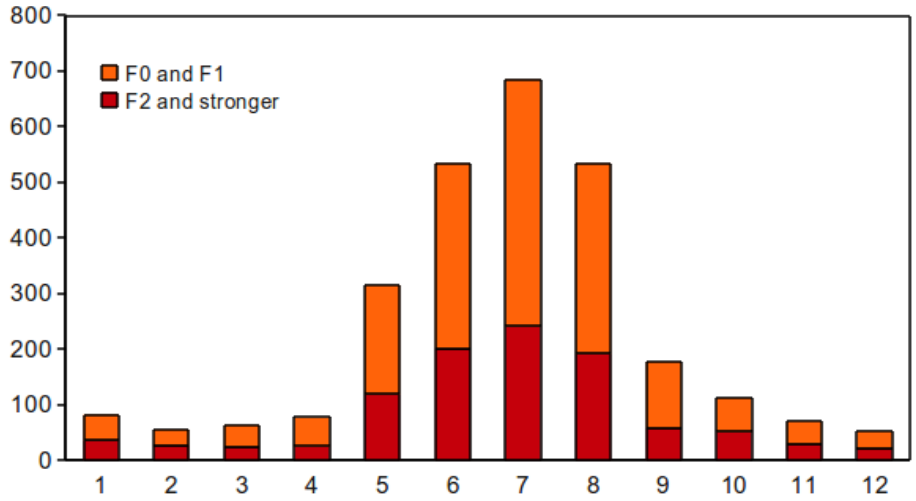

Figure 2.32. Distribution of tornadoes over the year. Source: European Severe Weather Database.

Tornadoes in Europe are most common in the summer months, although they can happen year-round. This is true as well for the most destructive tornadoes, classified as F2 or higher on the Fujita scale.

2.13. Events damaging infrastructure

Some extreme weather events, which may, or may not, disturb transport itself, can be disastrous to the infrastructure of the transport system. These events have been identified in Work Package 1 of EWENT. It was shown that of particular concern are: extreme temperatures which cause bending of railway tracks and softening of asphalt pavements, extreme long-term precipitation which causes floods, landslides and road erosion, and extreme wind speeds which may cause damage to electric power supply networks and block roads and railways by falling trees or debris. Extreme winds also prevent the use of certain large suspension bridges in Europe and operation of aircraft.

For these variables, extreme value analysis has been made for 48 000 grid points in Europe based on the E-OBS (1971-2000), ERA-Interim (1989-2009) observational data as well as SMHIRCA-ECHAM5 climate model simulations for the control period 1971-2000, with all three data sets representing present climate. Climate change projections for the extremes are based on SMHIRCA-ECHAM5 climate model simulations for the time period 2041-2070. Analysis results describing the present climate are shown below.
The fifty-year return value of air temperature (shown in Fig. 2.33) and the probabilities of it exceeding 35 ^{o}C and 40 ^{o}C (Figs. 2.34 and 2.35) show large differences across Europe and highlight that the highest extreme temperatures occur in the Mediterranean Europe.

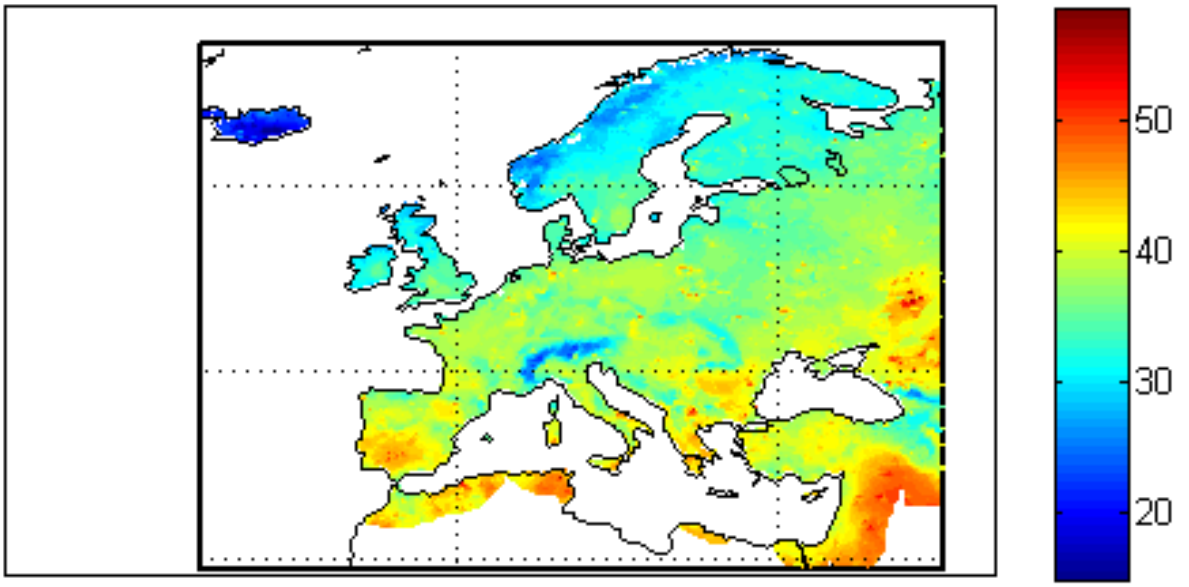

Figure 2.33. Fifty-year return value of the annual maximum air temperature (in ^{o}C) based on E-OBS data covering the time period 1971-2000.

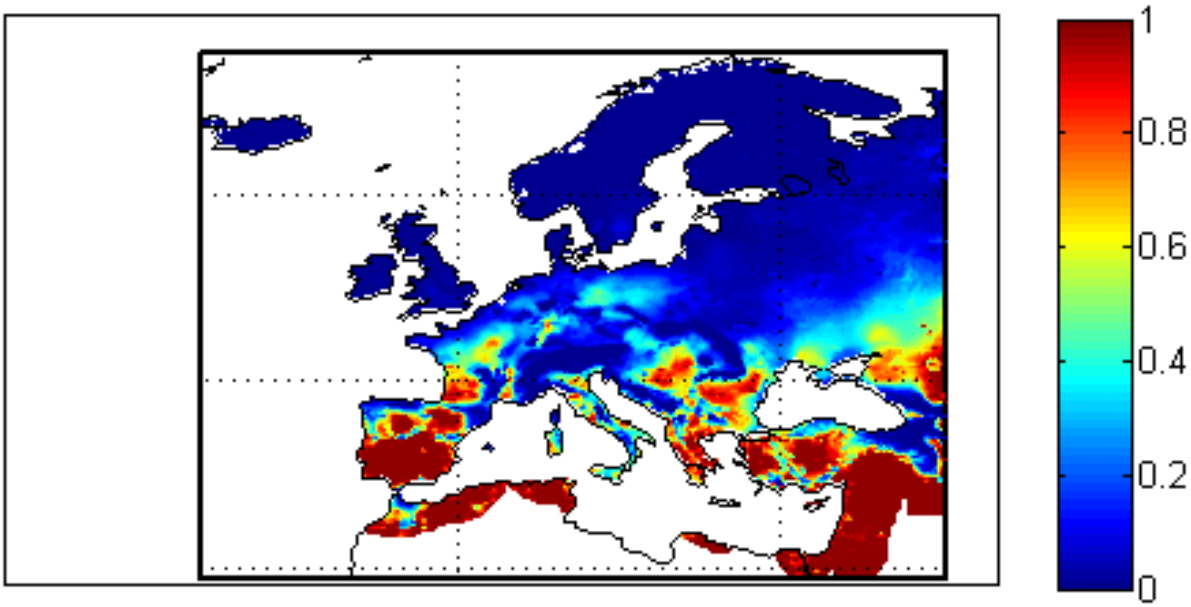

Figure 2.34. Probability of the annual maximum air temperature exceeding 35 ^{o}C during the period 1971-2000 based on E-OBS data.

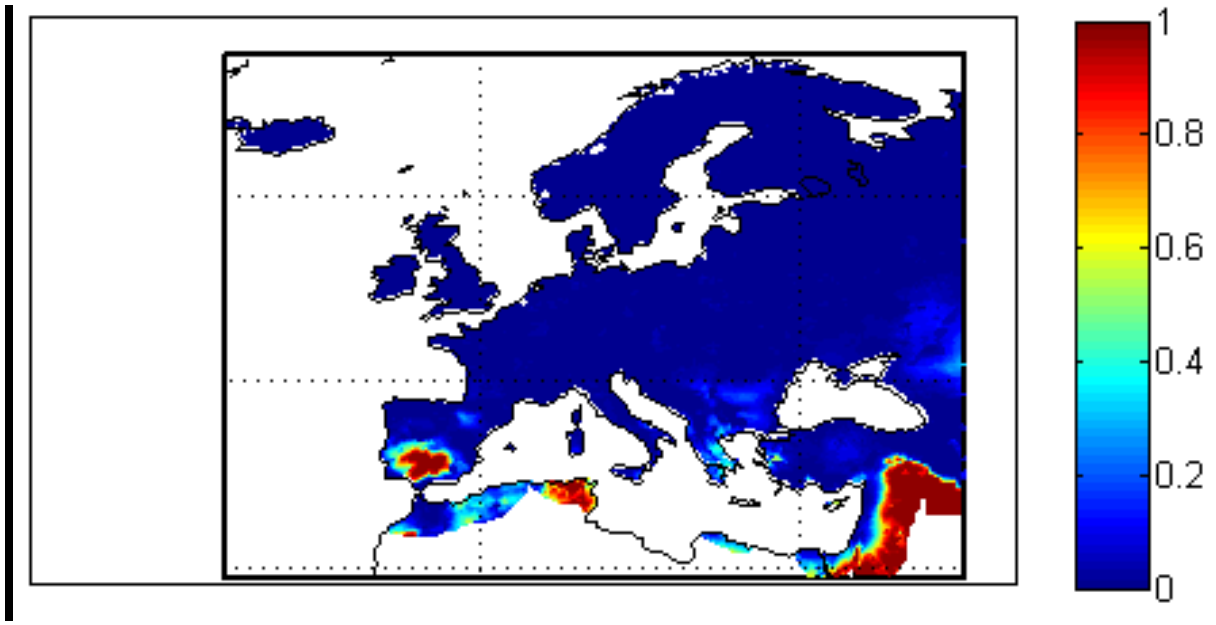

Figure 2.35. Probability of the annual maximum air temperature exceeding 40 ^{o}C during the period 1971-2000 based on E-OBS data.

The fifty-year return value of five-day precipitation is shown Fig. 2.36 and the probability of the annual maximum precipitation exceeding 100 mm in five days in Fig. 2.37. As one would expect, extreme precipitation is much more common in mountainous regions and on the West coast than elsewhere in Europe.

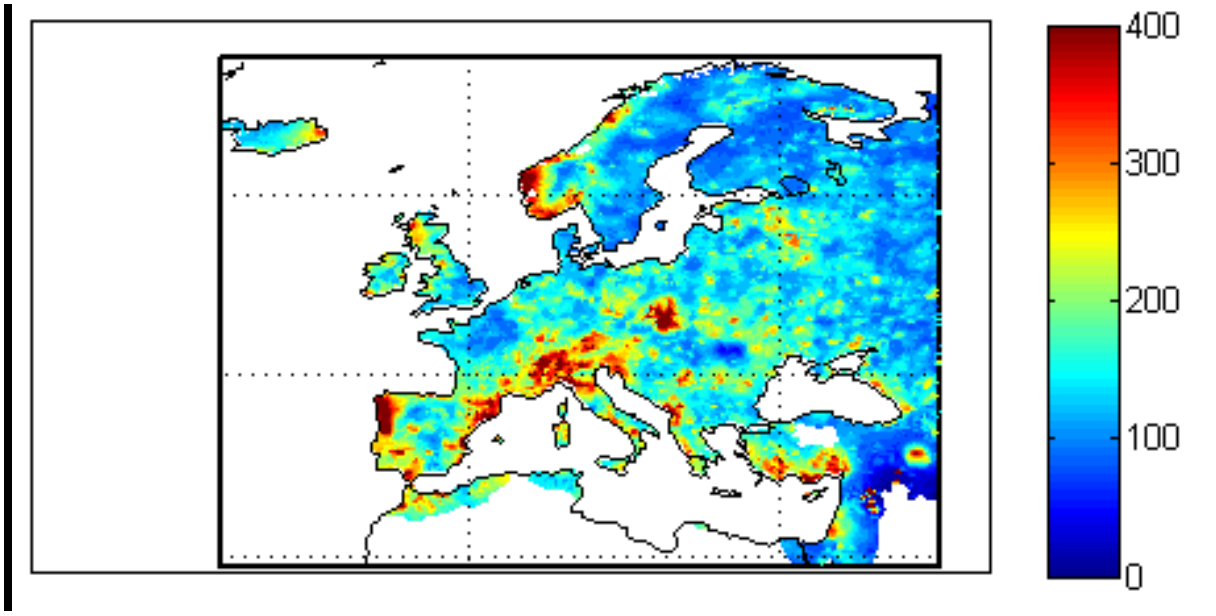

Figure 2.36. Fifty-year return value of the annual maximum of five-day precipitation totals (in mm) based on E-OBS data covering the time period 1971-2000.

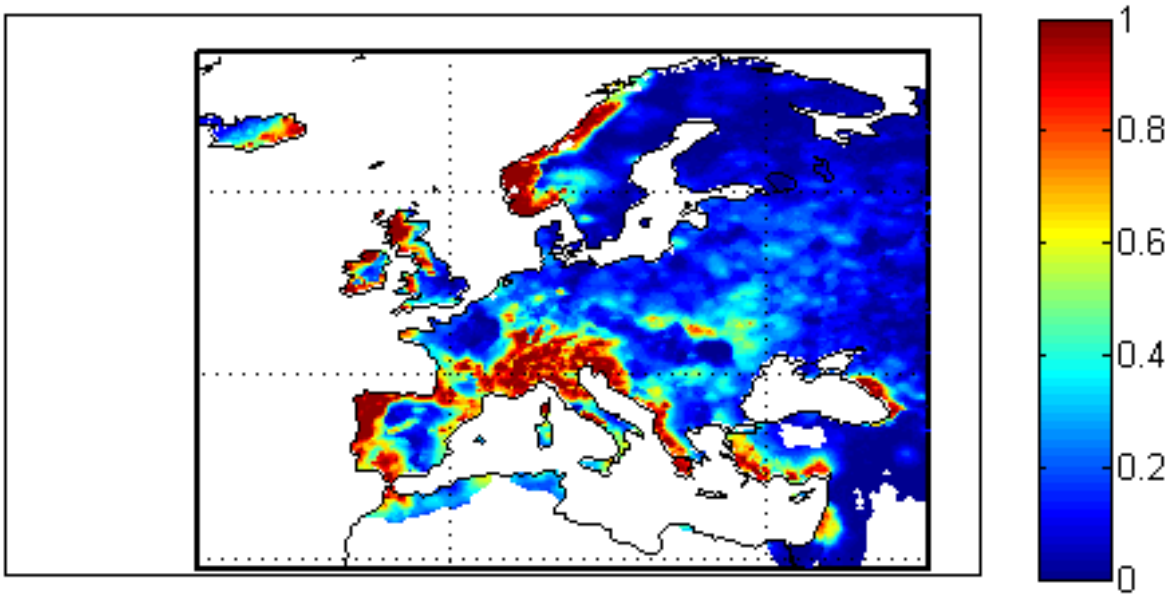

Figure 2.37. Probability of the five-day precipitation total exceeding 100 mm during the period 1971-2000 based on E-OBS data.

The fifty-year return mean wind speed is shown in Fig. 2.38 illustrating that, in general, the immediate coastline regions are much more vulnerable to extreme wind speeds than inland regions. In general, extreme wind speeds are lower in the colder regions of Europe. This is due to the fact that extreme geostrophic winds over Europe occur in winter when the boundary-layer is very stable in cold regions.

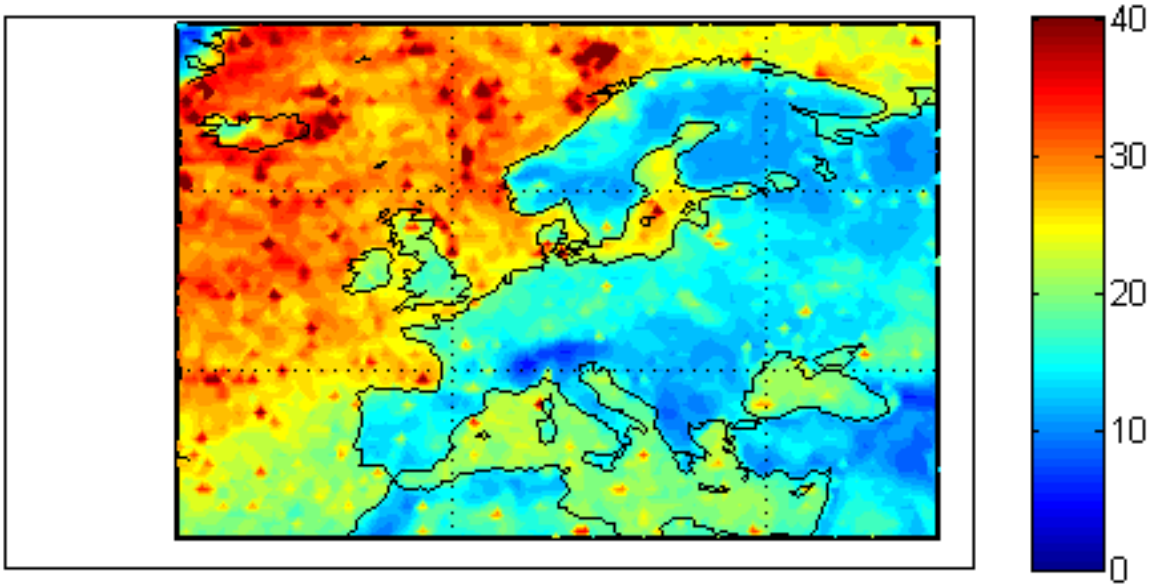

Figure 2.38. Fifty-year return value of the 10-minute mean wind speed (m/s) during the period 1989-2009 based on ERA-Interim data.

3. Scenarios of adverse weather conditions

3.1. Description of model simulations

The EWENT project Description of Work proposed the assessment of changes in the probability of magnitude and frequency of adverse or extreme weather conditions in Europe by the 2050s using the outputs of the first multi-model system of regional climate models available in the ENSEMBLE project. For this purpose we have used six high-resolution (ca. 25x25 km^2) Regional Climate Model (RCM) simulations produced in the ENSEMBLES project.

The EU-funded project ENSEMBLE is a collaborative effort between different European institutes to provide a reliable quantitative risk assessment of long term climate change and impact. In particular, dynamical downscaling of five different General Circulation Models (GCMs) was performed using different RCM runs by fifteen institutes. The RCMs were run over a common area covering the entire continental European region with a spatial resolution of 25 km and 50 km, the highest resolution currently available. All GCMs used the A1B (medium, non-mitigation) emission scenario (van der Linden and Mitchell, 2009).

Within ENSEMBLES, an initial RCM verification experiment was carried out using reanalyses from ECMWF (ERA-40) as boundary conditions for the RCMs, and running the RCMs over the common period of 1961-1990. In another experiment, regional climate change scenarios over Europe with different weighting techniques were produced by nesting the RCMs within different GCM simulations for control climate and future projections. More details of ensemble model experiments are given in the ENSEMBLE project final report (van der Linden and Mitchell, 2009).

We selected six models that provide all variables required for our analyses and covered the time horizon studied: near-future (2011 to 2040) and far-future (2041 to 2070). The regional climate change projections chosen were:

- SMHIRCA-ECHAM5-r3
- SMHIRCA-BCM
- SMHIRCA-HadCM3Q3
- KNMI-RACMO2-ECHAM5-r3
- MPI-M-REMO-ECHAM5-r3
- C4IRCA3-HadCM3Q16

Daily values of 2–m mean temperature, maximum temperature, total precipitation and wind gust were used in the computation of changes in probability of severe weather phenomena. The area covered by the models is shown in Figure 3.1.

There are three main uncertainties in climate projections: internal variability of the climate system that exists even in the absence of any external forcing; uncertainty in radiative forcing due to future emissions of greenhouse gases and aerosols; and model uncertainty (Hawkins and Sutton, 2009). We have chosen to neglect the uncertainty due to emissions and focus on the A1B emission scenario, because the uncertainty in emission scenarios rivals model uncertainty only in the latter half of the 21st century.

The use of regional climate models provides advantages in spatial and temporal resolution but also some additional sources of uncertainties: the initial and boundary conditions from the GCM used as

driving force, the downscaling method applied, parameterization and resolution of the regional climate model (Foley, 2010; Kjellström et al., 2011). Since numerical models can represent the aspects of climate in slightly different ways, using different parametrizations, the inter-model variability can be considerable. The changes can be better assessed using an ensemble mean and combining multiple predictions from six regional climate models, than by the individual simulations; still, inter-model variability is represented in the spread of the projection (Foley, 2010).

Even though regional climate models are run at high resolution, the evaluation of many extremes may be complicated, since gridded data provided by RCMs is more homogeneous in space than observations, thus attenuating extremes (Rummukainen, 2010). Internal variability is a natural characteristic of the climate system. GCMs do simulate natural variability but, for climate change experiments this is considered to be noise that obscures the signal due to external forcings. The use of three different GCMs reduces the noise due to internal variability in the multimodel mean scenarios presented in this study.

Figure 3.1. Spatial coverage of ENSEMBLE regional climate models used in this study.

During this project, a new methodology for extreme value analysis was developed (Ch. 2.3). Due to limited resources, these methods have tentatively been applied with thresholds relevant for transport infrastructure (Ch. 2.13 and 3.6.1) and some other parameters (Figs. 2.7 and 3.12) based on SMHIRCA-ECHAM5 simulations only. SMHIRCA-ECHAM5 simulations were selected mainly for the following two reasons: SMHI regional climate model simulations have been used in earlier work by Makkonen et al. (2007), and ECHAM5 simulations have also been used in the statistical downscaling (see 3.3 and 3.7).

3.2. Description of scenario construction

Regional climate models can potentially better represent local climate variability and extremes by providing more realistic climate data (Rummukainen, 2010). However, one problematic issue related to these models are systematic biases in the outputs. One of the most common approaches to handle the biases is the delta-change method, by which differences in climate variables are extracted from the control and scenario simulations of the model and transferred onto an observed dataset. Although the method has its benefits, it also has the possible drawback of being locked within a historical course of variability and extremes (Rummukainen, 2010). Another disadvantage of the delta-change method is that the use of the observed climate as a baseline implies that the number of rainy days does not change for the future climate and that the extreme values are modified by the same factor as the mean values. Another alternative is to rescale and use time series directly from the model.

In order to compare the outcome of these two approaches we have calculated the change in annual 17 m/s wind gust days using the delta-change method and the direct model simulations (Fig. 3.2). The changes in the frequency of strong wind gusts differ by a maximum of 5 days over the continent in the two analyses. Taking into account that the wind variables are among those that are difficult to model correctly, we anticipated an even stronger correlation for the other climate variables. These results confirmed the use of the direct model outputs in order to assess the changes in future adverse and extreme weather events.

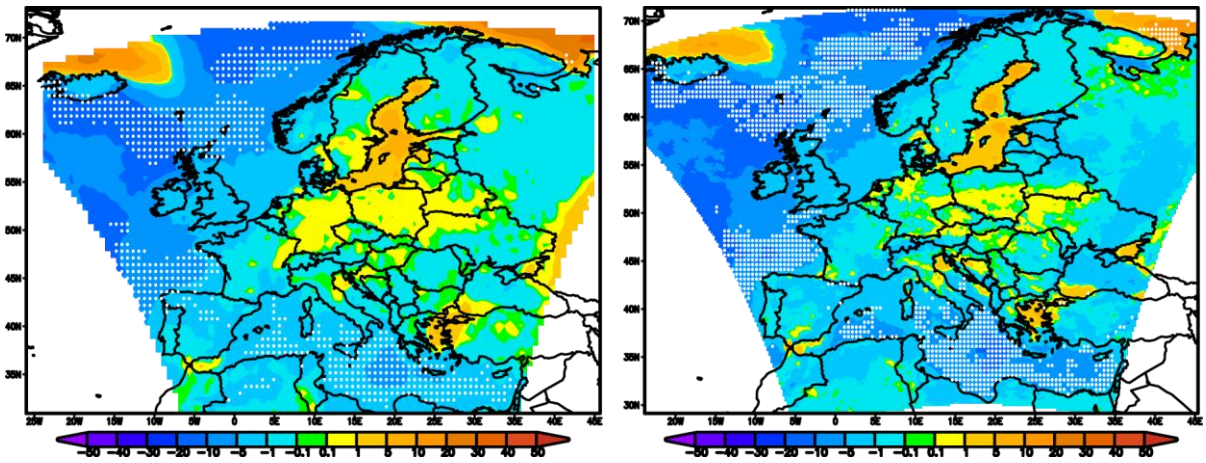

Figure 3.2. Comparison of two methods to calculate the change in annual number of days with wind gusts exceeding 17 m/s. In the left panel, the time series has undergone a bias removal by applying the delta-change approach; the right panel shows the time series taken directly from the model.

Based on the calculation of frequencies using the six RCMs, the multi-model mean of the change compared to the control period (1971-2000 for wind gusts and 1989-2009 for blizzards), furthermore the upper and lower limits of the change has been defined and presented for each threshold of the adverse and extreme phenomena. The multi-model mean is the average change indicated by the six models giving each model equal weight. The range of changes is also indicated for each grid that describes well the inter-model variability, i.e. upper and lower limit. The upper limit (maxi-

mum) shows the “most positive” change of any model, while the lower limit (minimum) indicates the “most negative” change.

3.3. Other methods of downscaling to road network

Neither global nor regional climate models are sufficiently accurate or detailed to allow road weather conditions to be simulated directly. Instead, road-weather time-series must be derived from GCM or RCM outputs using statistical relationships between large-scale atmospheric patterns (which GCMs simulate well) and the observed road weather, a process known as *empirical statistical downscaling*. The relationships between large-scale atmosphere and road weather must be determined by analyzing historical atmospheric patterns and road weather time-series. A simple statistical downscaling technique, which can be, and has been, confidently applied is the *analogue model*. This method involves iterating over each day in the GCM future scenario, and for each day finding the day in the historical record for which the large-scale atmospheric patterns match most closely. The future road-weather for each future day is taken to be the historical road-weather on the most closely matched historical day.

ERA-NET Road project IRWIN (2008-2010) used this method with the longest possible archived road weather information system (RWIS) observation time series in Finland and Sweden to assess the affect of climate change on winter road maintenance. The analogue model proved quite successful, even though the existing RWIS data archives date back only for about 10-15 years, as this was long enough to find analogues for present and future road climatology for scenarios 30-50 years onwards.

The resulting downscaled time series provided realistic climate scenarios for road networks as revealed by RWIS observations, giving estimates also for road surface temperature, which is missing from general weather observations. It is worth noting that the road climatology may, in some locations, indeed be substantially different from the general climatology if the RWIS stations have been placed directly adjacent to roads rather than with the principle of providing the best estimates of the average conditions in the area. In particular, temperature may differ by several degrees from the average, and wind directions may be blocked from some directions due to road construction.

Similar assessments to those performed in Scandinavia could be repeated relatively easily in other parts of Europe too, if enough road weather information was archived and available. Taking into account the seriousness of climate change and its implications, it is urgent to manage European-wide operational archival and quality control of all road weather observations.
Results and conclusions of the IRWIN project on downscaled climate scenarios projected on the Nordic road network are further discussed in Chapters 3.6.4.

3.4. Scenario maps (2011-2040)

3.4.1. Wind

Figure 3.3 presents the spatial variation of the projected changes in wind gusts by 2040 for the three selected wind gust thresholds: 17 m/s, 25 m/s and 32 m/s. The six RCMs indicate, on average, a decrease in severe gust events over the Atlantic and the Mediterranean Sea of 1-5 days/year. The sea areas with a projected positive change in storm events during the near future are the Baltic Sea, Barents Sea, north of Iceland and partially around the British Isles, especially in the terms of wind gusts over 25 m/s.

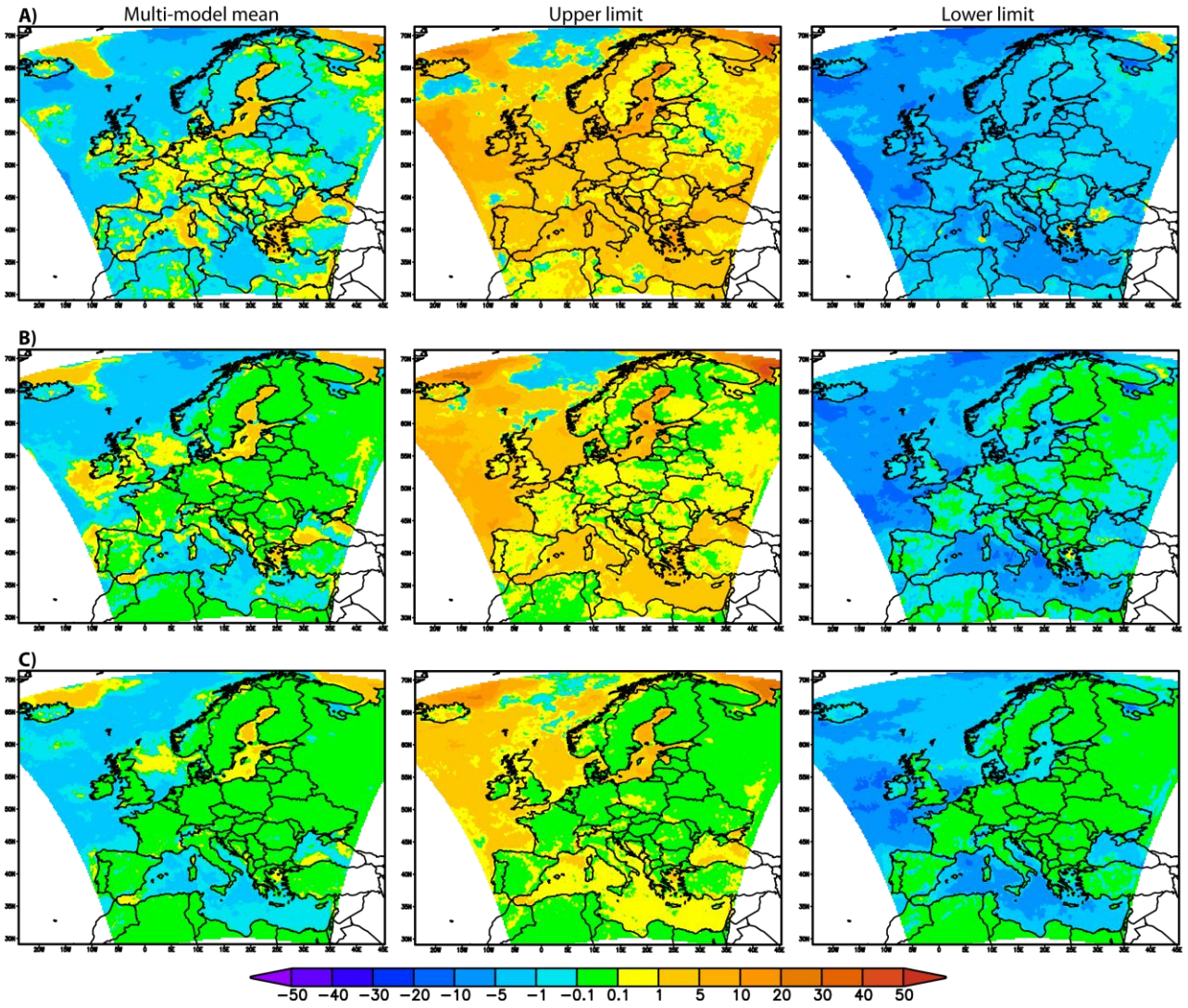

Figure 3.3. Multi-model mean, upper and lower limit of changes in annual wind gust days from 1989-2009 to 2011-2040 exceeding the (A) 17 m/s, (B) 25 m/s and (C) 32 m/s thresholds, based on six RCM simulations.

Multi-model means indicate an increase of 5 days/year for these regions, with higher values (10-20 days/year) over the Barents Sea; the most positive change indicated measures up to 30 days for all three thresholds (as shown in the upper limit maps). Over the continent, most countries situated in

Central, Western and Southern Europe experience an increase of 1-5 days/year in the frequency of wind gusts >17 m/s; however the sign of the change is not uniform. Considering the Iberian Peninsula, the change is positive over the coast for gusts exceeding 17 m/s and 25 m/s and predominantly negative over the land. In Northern and Eastern Europe, simulations generally indicate a slight decrease in wind gusts >17 m/s.

Wind gusts are one of the most difficult variables for numerical models to predict and there are large differences in how it is parameterized in each RCM. Therefore, it was anticipated that there would be a large range of outcomes predicted by the models, as shown by the opposite signs of change in the upper and lower limits.

3.4.2. Snow

As the number of freezing days decreases in the future climate, the frequency of snowfall events shows a decreasing tendency as well, with a shift from snow to liquid or mixed precipitation, as shown in Figure 3.4.

The RCM multi-model mean exhibits a decrease in the frequency of snow events (1cm) for the whole continent. The magnitude of change increases progressively northward, from 1-5 days in Southern Europe, 5 days over most of the continent, to 10 days over Northern Europe. Although winter precipitation is projected to increase in northern and central Europe in the future (Christensen and Christensen, 2007), more is expected to occur as liquid precipitation because of the reduced frequency of frost days. On the other hand, the intensity of heavy snowfall (10 cm/day and 20 cm/day) is expected to increase partially over Scandinavia, especially at high elevations (Scandes), and Eastern Europe. Over the coastal region of Northern Europe and the rest of the mainland a slight decrease in the occurrence of heavy snowfall is indicated, with the magnitude of this change higher in mountainous areas (Alps, Pyrenees and Carpathians). The models present a fairly similar outlook on the sign of the change in terms of snowfall; however some models indicated an increase of 5-10 days in the frequency of heavy snow events over most of the continent.

3.4.3. Blizzards

Due to its combined nature, the changes in the frequency and intensity of blizzards are defined by the changes in heavy snowfall, strong winds and cold days. As the storminess is projected to decrease over most of the Atlantic region by 2040, the intensity of blizzards is also expected to decrease by 1-5 days over the Northern Atlantic, Barents Sea, Gulf of Bothnia, western cost of Norway, Iceland and isolated patches over the mainland (Fig. 3.5). However, for most of the blizzard-affected regions in the current climate, no significant change is anticipated in the near future. Enhanced blizzards are expected only over the Icelandic glaciers and in Norway.

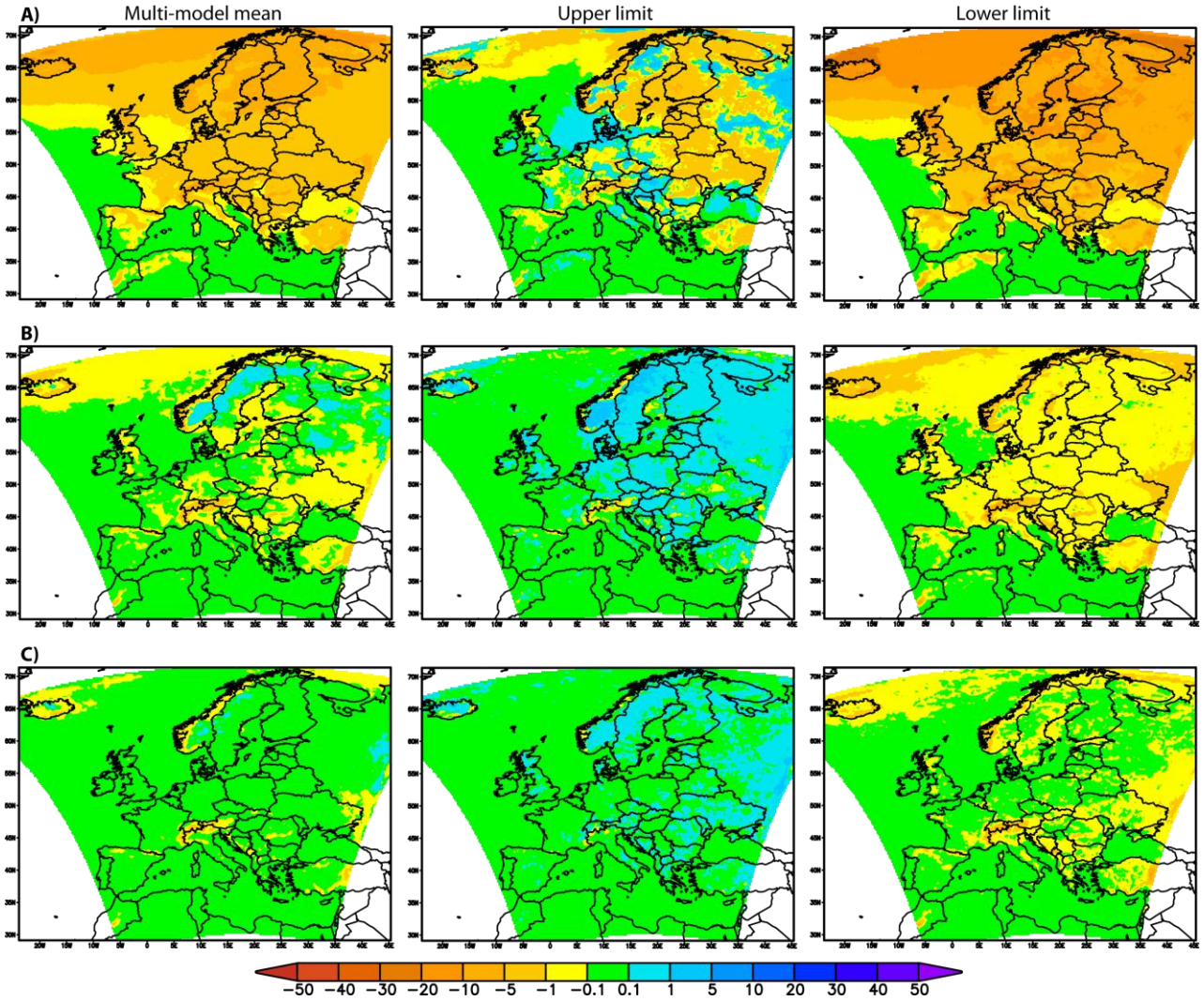

Figure 3.4. Multi-model mean, upper and lower limit of changes in annual snowfall days from 1971-2000 to 2011-2040 exceeding (A) 1 cm, (B) 10 cm and (C) 20 cm based on six RCM simulations.

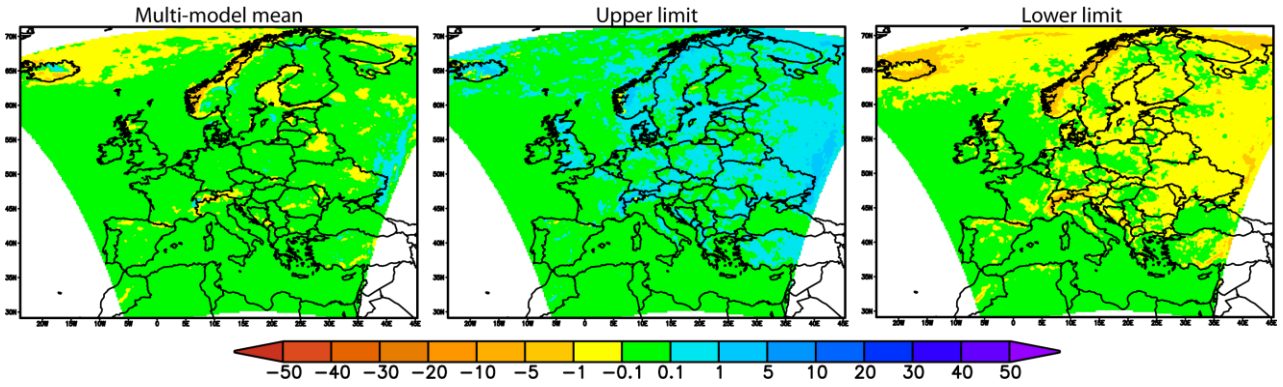

Figure 3.5. Multi-model mean, upper and lower limit of changes in annual blizzard days from 1989-2010 to 2011-2040 based on six RCM simulations.

3.4.4. Heavy rainfall

The near-future projections indicate a positive change (1 day/year) in the frequency of heavy rainfall (≥ 30 mm) compared to the control period (1971-2000) over the continent (Fig. 3.6). Heavy rainfall events are projected to become less isolated in southern Europe. The upper- and lower limit maps indicate large inter-model variation; the dominant pattern suggested by the most positive model is a 1-5 day decrease in extreme precipitation, while the lower limit maps indicate slight decrease or no change over the continent. RCMs forecast a reduced number of very heavy precipitation events (≥ 100 mm) in the present and future climate simulations. Therefore, no major changes could be detected. However, current RCMs still show problems in simulating high intensity precipitation (e.g., Boberg et al., 2009).

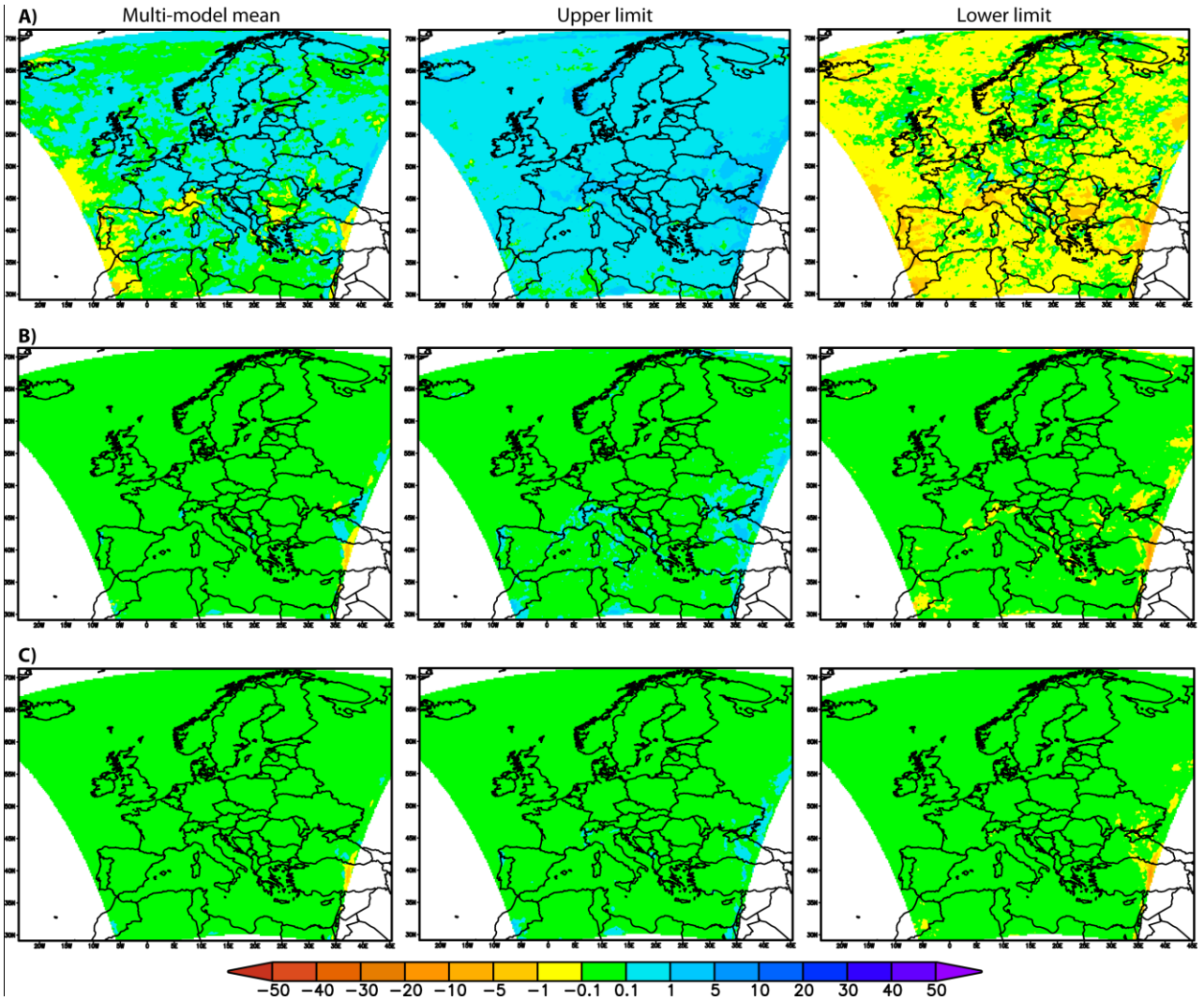

Figure 3.6. Multi-model mean, upper- and lower limit of changes in annual heavy rainfall days from 1971-2000 to 2011-2040 exceeding (A) 30 mm, (B) 100 mm and (C) 150 mm based on six RCM simulations.

3.4.5. Heat waves

The positive trend in the frequency of heat waves indicated by observations is likely to continue, inasmuch as the RCMs record an increase in the occurrence and intensity of high temperature.

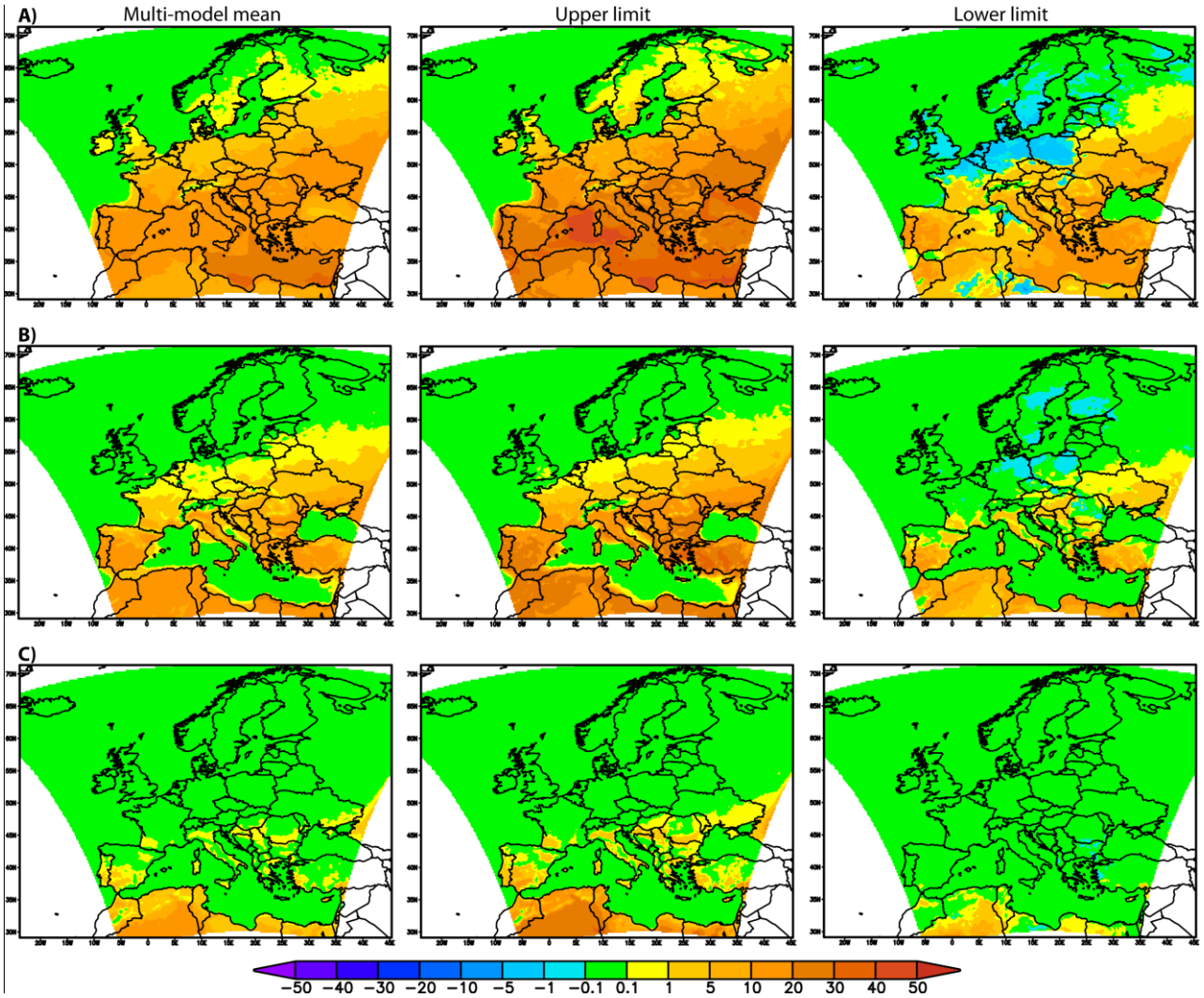

Figure 3.7. Multi-model mean, upper- and lower limit of changes in annual heat-wave days from 1971-2000 to 2011-2040 exceeding (A) 25 °C, (B) 32 °C and (C) 45 °C based on six RCM simulations.

The multi-model mean maps (Fig. 3.7) depict a significant positive change in the frequency and intensity of heat waves in the near future. The mean number of days with a maximum temperature above 25 °C will increase by 20-30 days/year in Southern Europe and by 5-20 days/year in mid-latitudes compared to the current climate. The change is less evident in Scandinavia; 1 day/year in the south, while most of Norway, Sweden and Iceland expect no increase in heat waves. The change of largest magnitude indicated by the models (shown in the upper-limit maps) varies between 40-50 days/year over the Mediterranean Sea and Black Sea, and 30-40 days/year over southern Europe.

The frequency of hot days, with daily maximum temperatures above 32 °C records the greatest change (by 10 days/year) over the Iberian Peninsula, Italy and the Balkan Peninsula, while the fre-

quency of extreme hot days (43 °C) is predicted to increase by 1-5 days locally over Portugal, Spain, Italy, the Balkans, Romania and Hungary.

3.4.6. Cold spells

Multi-model mean indicates a significant decrease in the frequency and intensity of cold spells (Fig. 3.8) for the near-future climate, the change being more intense at high latitudes. The dominant pattern suggests a decrease of 20 days/year in the frequency of frost days over Northern Europe, Russia, the Alps and the Carpathians, and by 50 days/year over the Arctic. Over the mid-latitude regions 5-10 fewer frost days/year are expected by 2040, while over the southern European countries 1-5, there will be isolated patches with 10 days fewer frost days per year.

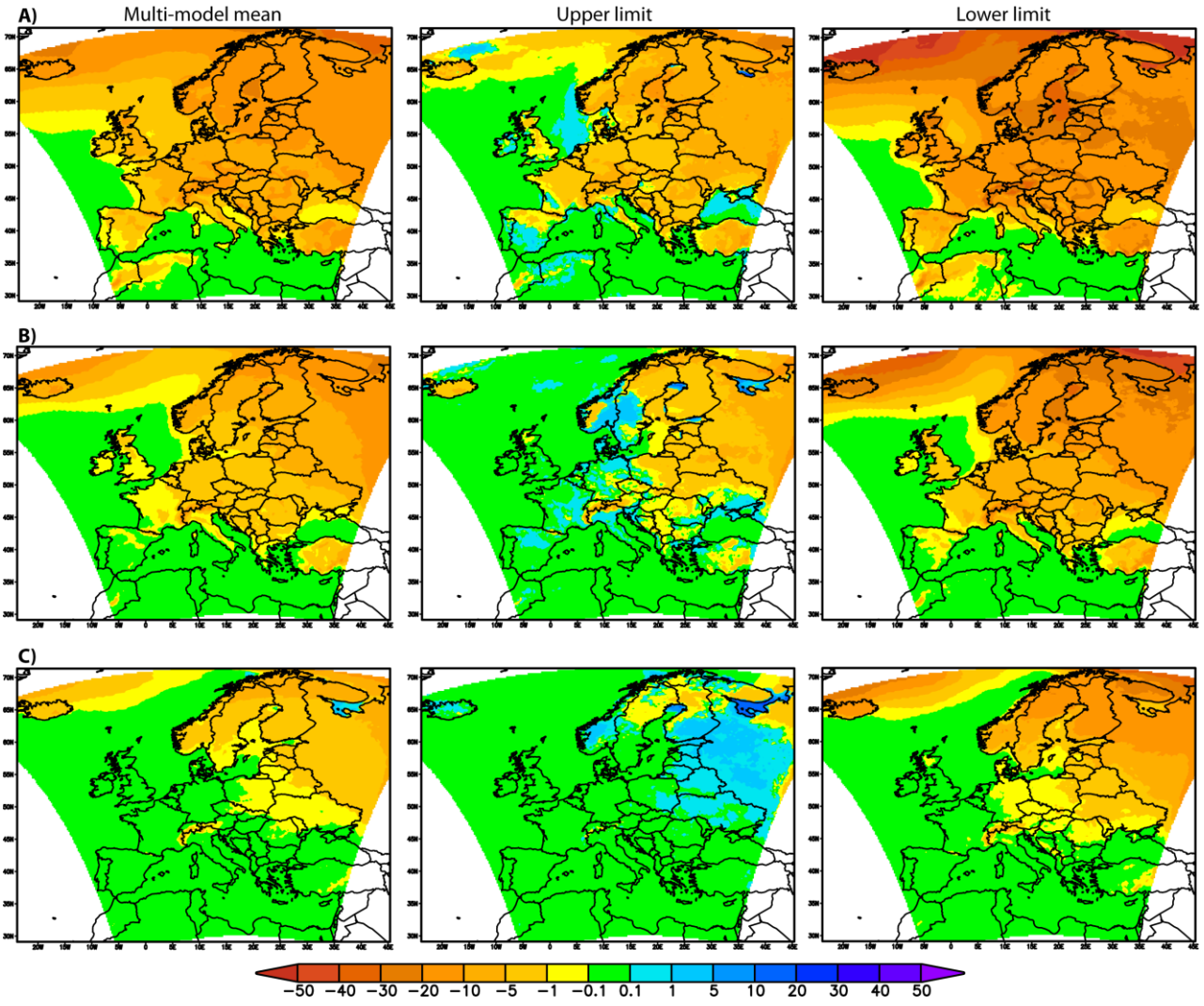

Figure 3.8. Multi-model mean, upper- and lower limit of changes in annual cold-spell days from 1971-2000 to 2011-2040 exceeding (A) 0 °C, (B) -7 °C and (C) -20 °C based on six RCM simulations.

Extreme cold events will also decrease in frequency: 10-20 fewer cold days (with daily mean temperatures below -7 °C) over Scandinavia, the Baltic, Russia, Scotland and the Alps; predominantly

5 days fewer cold days over Central, Easter Europe and the Balkan Peninsula; and by 1 day over France, Italy and the British Isles. Scandinavia, the Baltic and Eastern Europe will also experience fewer very extreme cold spells (-20 °C) compared to the current climate. However, according to the most positive projection, the frequency of these events may slightly increase in most of the affected regions (shown on the Upper limit maps). This increase likely results from the fact that the signal from climate change is still comparable in size to the natural climate variability on regional scales.

3.5. Scenario maps (2041-2070)

3.5.1. Wind

Figure 3.9 shows the expected mean changes by the 2050s for three wind gust thresholds. Over ocean and sea areas, the most notable change is the decrease in the frequency of severe wind gusts

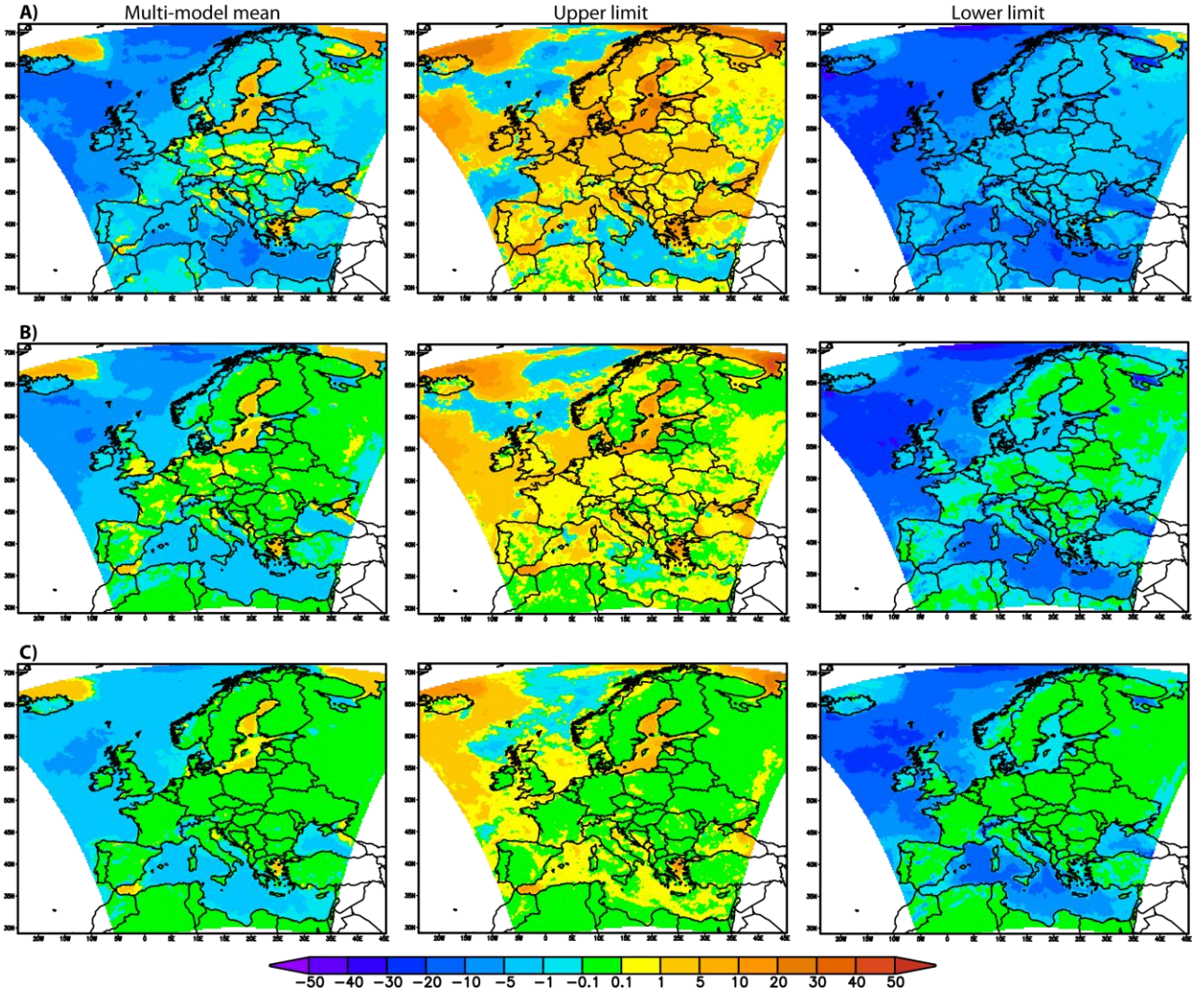

Figure 3.9. Multi-model mean, upper and lower limit of changes in annual wind gust days from 1989-2009 to 2041-2070 exceeding the (A) 17 m/s, (B) 25 m/s and (C) 32 m/s thresholds based on six RCM simulations.

over most of the Northern Atlantic and the Mediterranean Sea. The multi-model mean shows a decrease of 1-20 days per year for > 17 m/s wind gusts in these areas.

The most distinctive areas where all six used models agreed on the sign of the change (a decrease in the number of events exceeding the 17 m/s threshold) are also found in the Northern Atlantic and the Mediterranean Sea. The most significant increases over sea regions are located north of Iceland, over the Barents Sea and the Baltic Sea.

The multi-model mean indicates that the 17 m/s wind gust threshold will be exceeded 1-10 more days per year over the Baltic Sea in the 2050s, compared to the control 1989-2009 time-frame. Similarly, the increase in winds above the 25 m/s threshold is 0.1-5 days per year. Over land changes in severe wind gust days are less evident. A slight increase is shown in parts of Central and Eastern Europe for wind gusts > 17 m/s, but overall in Europe there is a tendency for a slight decrease (17 m/s) or no clear change in either direction for the higher thresholds (25 m/s and 32 m/s) .

3.5.2. Snow

The frequency of snowfall events will continue to decrease. The signal is more pronounced by the 2050s, relative to the 2020s. The multi-model means (Fig. 3.10) show 1-5 fewer days of snow in southern Europe, with changes in the frequency of snow days increasing progressively northward, to 10-20 days in Scandinavia compared to 1971-2000. The sign of change is consistent among all six RCMs, except in the Mediterranean and the western part of the continent. Contrary to the general decrease in snow days, the probability of extreme snowfall (> 10 cm) increases over large areas of Scandinavia and north-eastern Russia (1-5 days/year). This increase is partly due to the anticipated increase of total precipitation in the future but also due to warmer temperatures, since heavy snowfall tends to occur close to near-zero degrees Celsius. As shown in the upper limit maps, some models indicate a more robust increase in the frequency of 10 cm and especially 20 cm snowfall/day for several central and eastern European countries. The anticipated decrease in snowfall and frozen precipitation would have a positive impact on road, rail and air transportation reducing the cost of maintenance in many European countries; however in the Nordic countries, where heavy snowfall is already one of the most common disruption factors, it seems to become a more severe phenomenon.

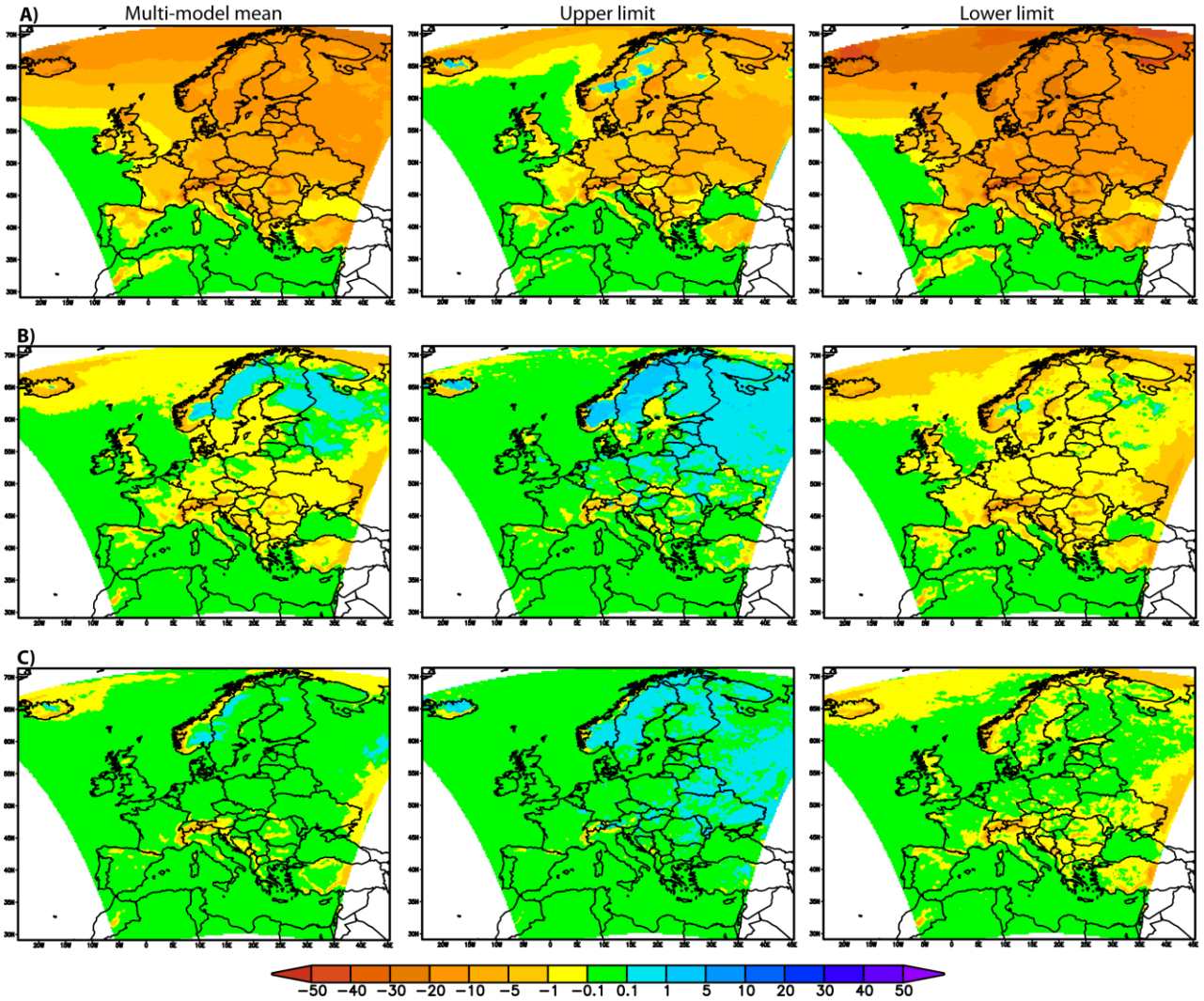

Figure 3.10. Multi-model mean, upper and lower limit of changes in annual snowfall days from 1971-2000 to 2041-2070 exceeding (A) 1 cm, (B) 10 cm and (C) 20 cm based on six RCM simulations.

We also analysed the projected change in extremely severe snow fall events by the SMHIRCA-ECHAM climate model simulation data. We chose here the 50-year return event (mm of water in 24 hours) as the parameter of interest. These changes can be compared to the present climate simulations for the same parameter, shown in Fig. 2.6. The results for the change, shown in Fig. 3.11, show that the 50-year return daily snow precipitation will increase significantly in Northern England and Southern Scotland, the coastal area of Netherlands, and in some mountainous regions, particularly in Eastern Europe. The exact geographical distribution of areas with increase and decrease partly result from random variability.

The results in Figure 3.11 are based on one simulation, but they are supported by multi-model mean results for 10 cm snowfall (Fig 3.11), thus illustrating the remarkable possibility of increasing extremely severe snow-related disturbances of the European transport system, while snow problems are clearly reducing in general.

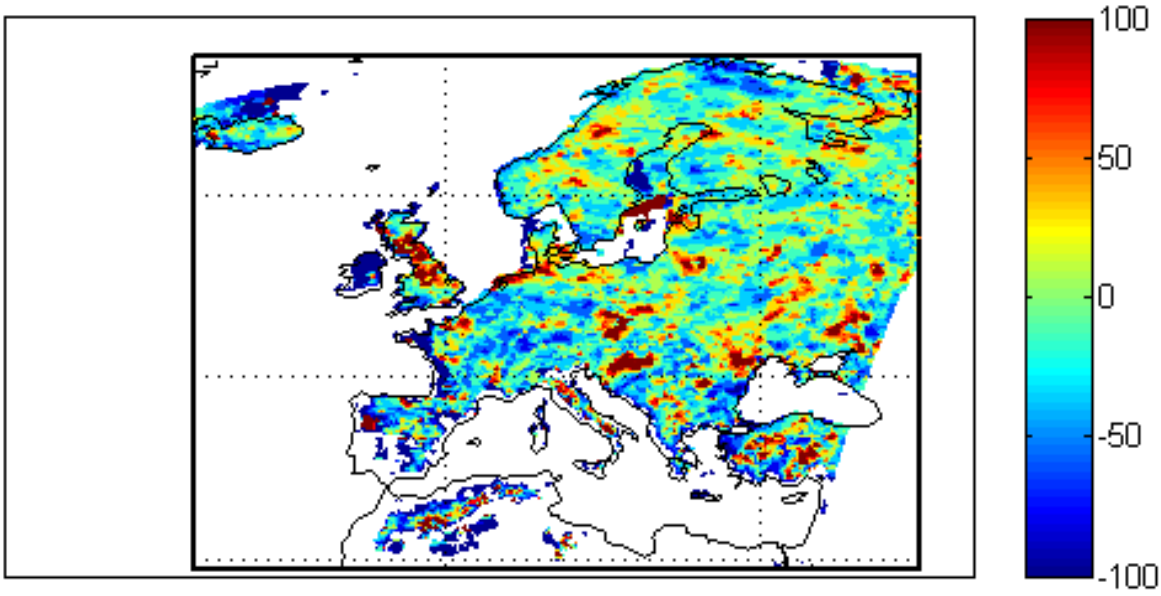

Figure 3.11. Simulated change in the fifty-year return value of the annual maximum snow fall in 24 hours (in percent of water equivalent) based on SMHIRCA-ECHAM simulations.

3.5.3. Blizzards

Blizzards are expected to become sparser (Fig. 3.12) in the 2050s with 1-5 fewer days per year compared to the present climate over the North-Atlantic, Iceland, Baltic Sea and its coastal area, the fjord coast of Norway, in the Alps and Pyrenees. Increasing tendencies (by 1 day/year) are sparse and less coherent. The sign of change is not consistence among the models, with the indicated patterns varying between an increase in the frequency of blizzards by 5 days (upper limit maps) and a decrease by 5 days (lower limit) over Northern and Eastern Europe.

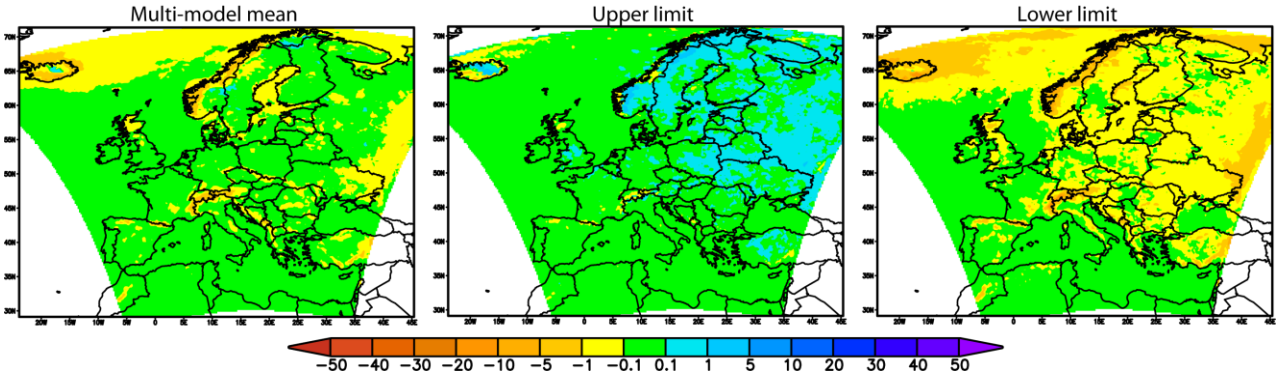

Figure 3.12. Multi-model mean, upper and lower limit of changes in annual blizzard days from 1989-2010 to 2041-2070 based on six RCM simulations.

3.5.4. Heavy precipitation

The European-scale pattern of change in precipitation extremes (> 30 mm/day) shows an increase of 1-5 days, except over the Mediterranean Sea and the coastal Mediterranean, where no or only small changes are projected to occur (Fig. 3.13.). Concerning the variation of very extreme precipitation events (> 100 mm/day), no significant change has been predicted by the selected RCMs. Furthermore, the sign of the change is not consistent among the models, indicating large intermodal differences due to the internal climate variability present in simulations, but possibly also due to model differences in the parametrization of deep convection. There is no clear signal for very extreme precipitation events (100 mm/day), presumably a result of the limitations of RCMs. Even if the climate models were to be run at high resolution, the gridded data generated is more homogeneous and the extremes are typically attenuated relative to observations (Rummukainen, 2010). Furthermore, the thresholds used in the present study were defined based on station observations and the extreme values are most probably underestimated by the models in both control and future climate runs.

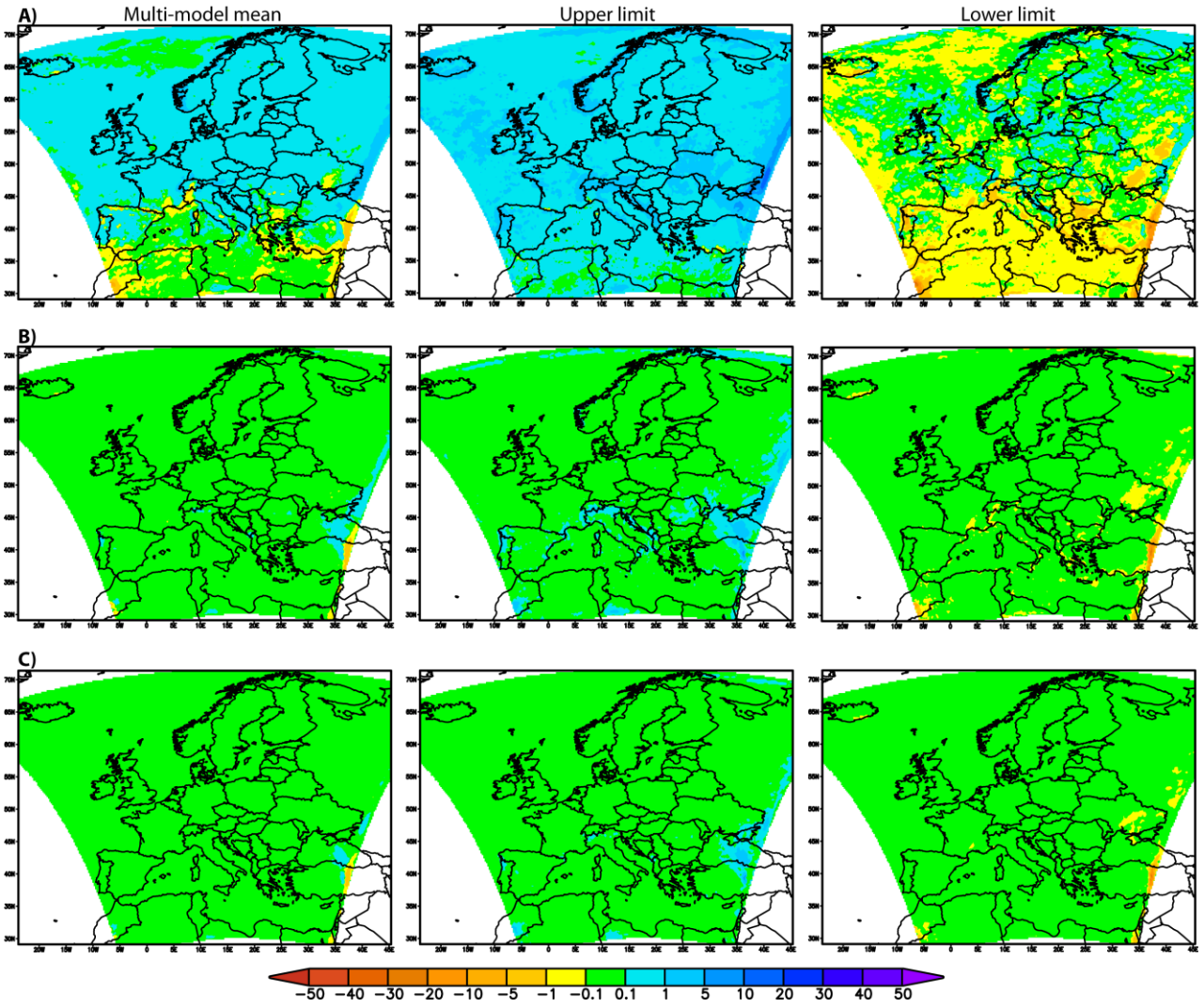

Figure 3.13. Multi-model mean, upper and lower limit of changes in annual heavy rainfall days from 1971-2000 to 2041-2070 exceeding (A) 30 mm, (B) 100 mm and (C) 150 mm based on six RCM simulations.

3.5.5. Heat waves

As Figure 3.14 shows, warm days (mean temperature above 25 °C) will become more prevalent by the 2050s. Scandinavia will experience 5 more warm days/year and Southern Europe 30-40 more days/year. In western and central parts of the continent, the projections suggest warm days will become more frequent by 20-30 days/year. The spatial variation of hot days (maximum temperature above 32 °C) suggests a substantial increase for the southern part of the continent, up to 40 days/year, and an increase of 5-20 days/year in the mid-latitudes. This change implies that mid-latitudinal regions may experience as many days with heat waves by 2070 as the Mediterranean countries do in the present climate. As for the frequency and spatial variation of days above 43 °C, more countries will be affected than nowadays, with most of S and SE Europe experiencing extreme heat waves, their number increasing by 5 days/year. Some of the climate models indicate an increase of 20 days/year for the Mediterranean countries.

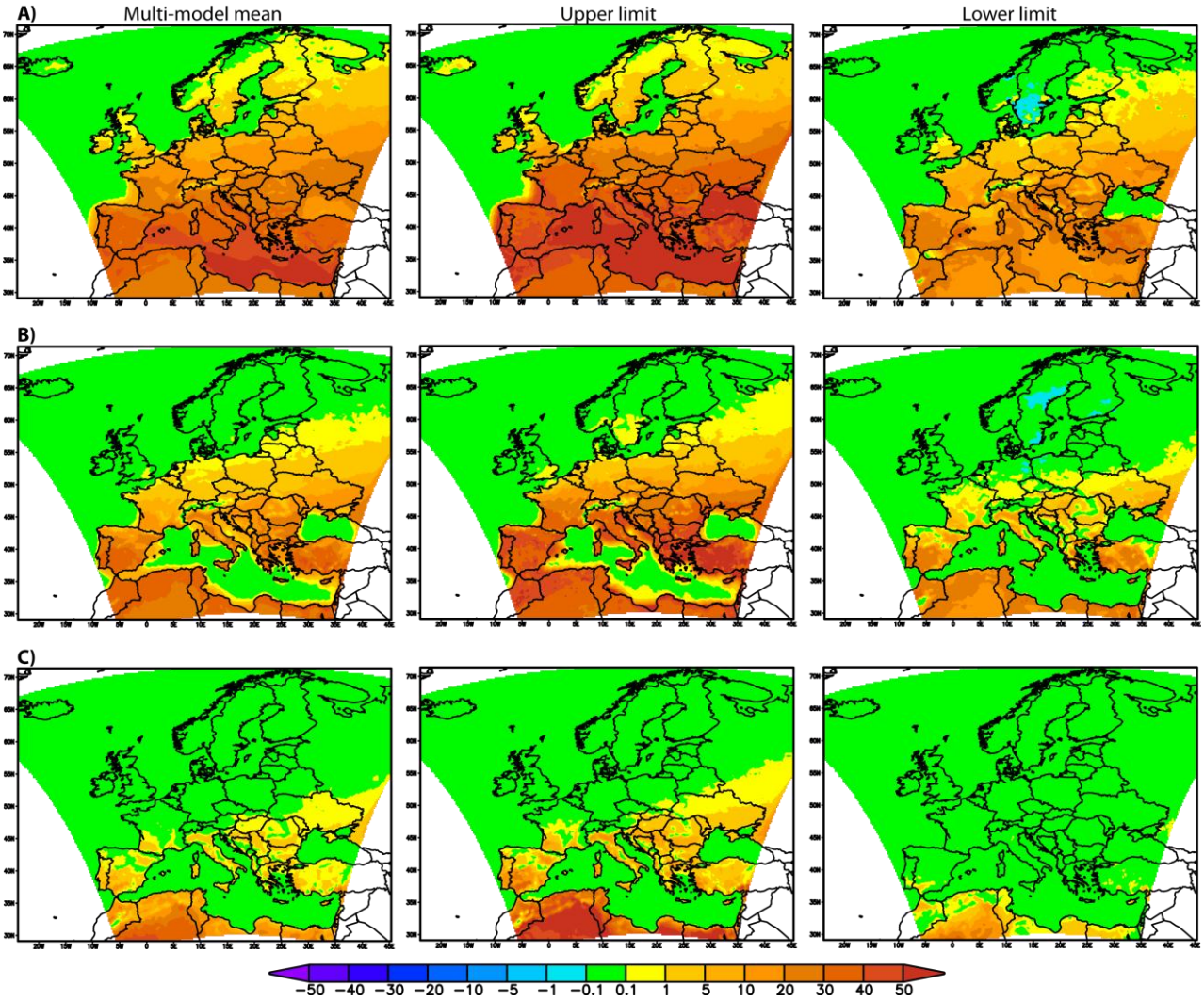

Figure 3.14. Multi-model mean, upper and lower limit of changes in annual heat-spells days from 1971-2000 to 2041-2070 exceeding (A) 25 °C, (B) 32 °C and (C) 45 °C based on six RCM simulations.

The projected increase in the duration and intensity of hot days will have a negative impact on transportation and infrastructure during the summer months, especially in those countries which already experience high temperatures.

3.5.6. Cold spells

The simulated cold extremes decline in occurrence substantially by 2070 over the whole continent (Fig. 3.15), and most strongly over Northern Europe. The decrease in the frequency of frost days (0 °C) varies between 20-30 days/year in Northern Europe and decreases gradually towards Southern Europe, with a decrease of 1-5 days/year. Most of the six models agree on the amplitude of change over land. This implies that Finland, Sweden and Norway are likely to experience as many frost days in the 2050s as some mid-latitude countries (such as the Baltic countries, Poland and Ukraine) do in the current climate.

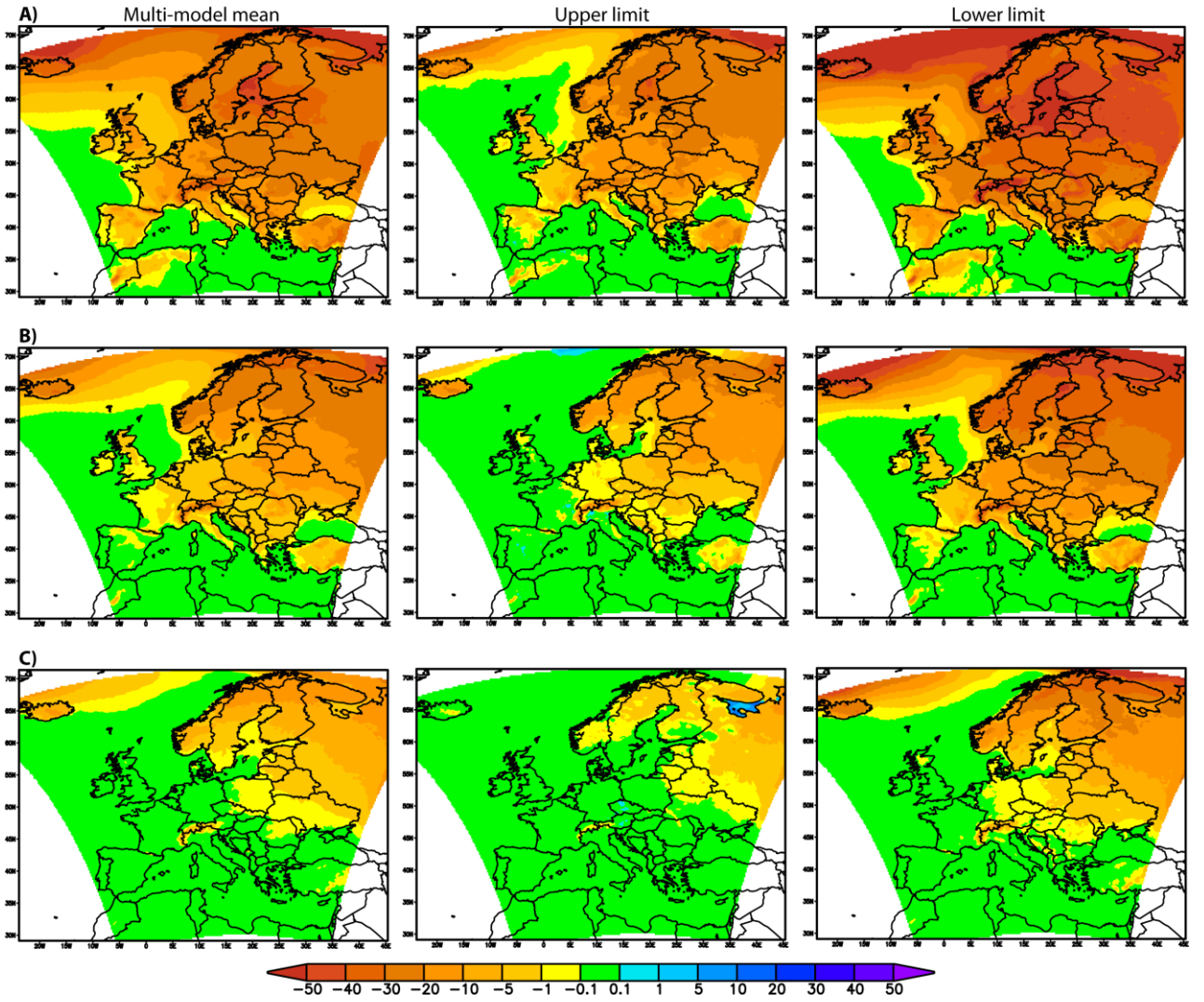

Figure 3.15. Multi-model mean, upper and lower limit of changes in annual cold-spell days from 1971-2000 to 2041-2070 exceeding (A) 0 °C, (B) -7 °C and (C) -20 °C based on six RCM simulations.

The spatial and temporal analysis of the extreme cold spells also indicates fewer days with temperatures < -20 °C for the affected areas, by 10-20 days/year in Scandinavia, Alps and the northeastern part of the continent. The RCMs agree on the variation of the upper and lower limits, the most negative change for the extreme cold spell is 1-5 days/year for Northern and Northeastern Europe. The largest differences from the current climate are 30-40 frost days/year in Scandinavia and the Alps, 50 days in the Arctic and Baltic Sea and 10-20 days in Southern Europe. The magnitude of change in the extreme cold spells (daily mean temperature < -20 °C) varies between 1-40 days/year according to the most negative projection (see Lower limit map), with the highest values at high latitudes.

3.6. Further scenarios for focused purposes

3.6.1. Events damaging infrastructure

Results for the fifty-year return values of those extreme weather events that are likely to cause damage to the transport infrastructure in Europe were given in Section 2.12. Here the projected changes of these variables from the present climate (1970-2000) to the period of 2041-2070 are provided based on the SMHIRCA-ECHAM5 simulations and the extreme analysis methods of Section 2.2.

Figure 3.16 shows an increase of several degrees in fifty-year return maximum air temperature in many parts of Europe, but the pattern is scattered and shows a decrease for some isolated regions, e.g. in England. There is a significant increase in many areas of Europe that are already hot (see Fig. 2.24).

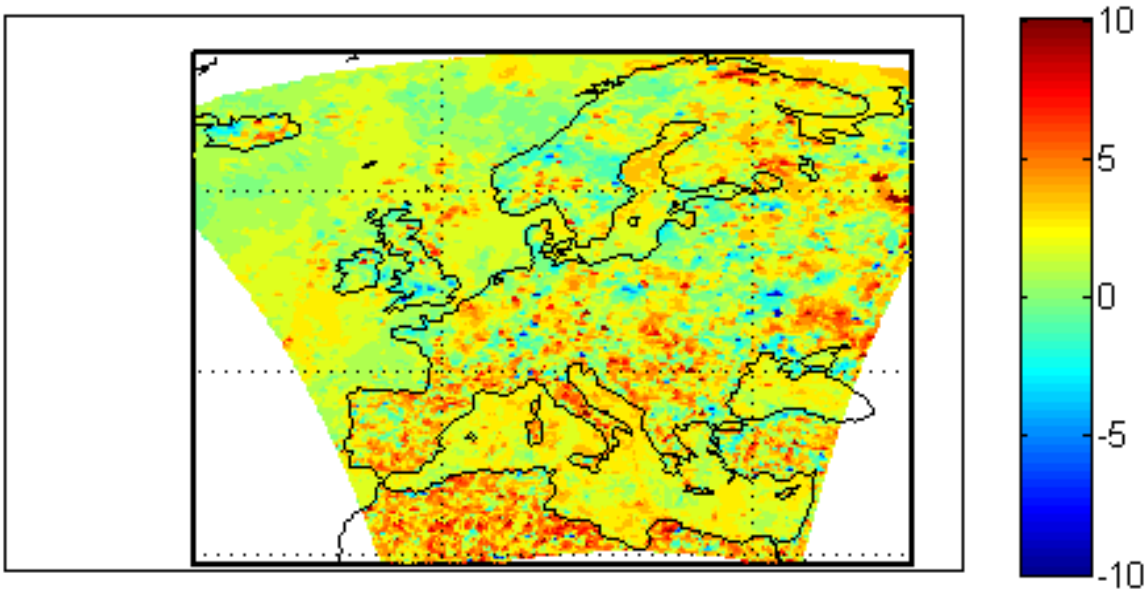

Figure 3.16. Simulated changes in the fifty-year return value of the annual maximum air temperature (in ^{o}C) based on SMHIRCA-ECHAM simulations.

The change in the fifty-year return value in the five-day precipitation total is shown in Fig. 3.17. These data include large stochastic variations and provide little evidence for regional variations. It appears, however, that, on average, there will be more severe flood-inducing precipitation events in

Europe, except perhaps in England, and the Mediterranean area. The most significant increase is likely to occur in Central Europe.

The change in the 50-year return wind speed is shown in Figure 3.18. These extreme wind speeds, potentially damaging the infrastructure of transport systems, appear to be changing little with climate change, except for the coastal regions of the North Sea and Baltic Sea. In some parts of these regions a remarkable increase, up to 50%, is projected by the simulations. However, data include large stochastic variation.

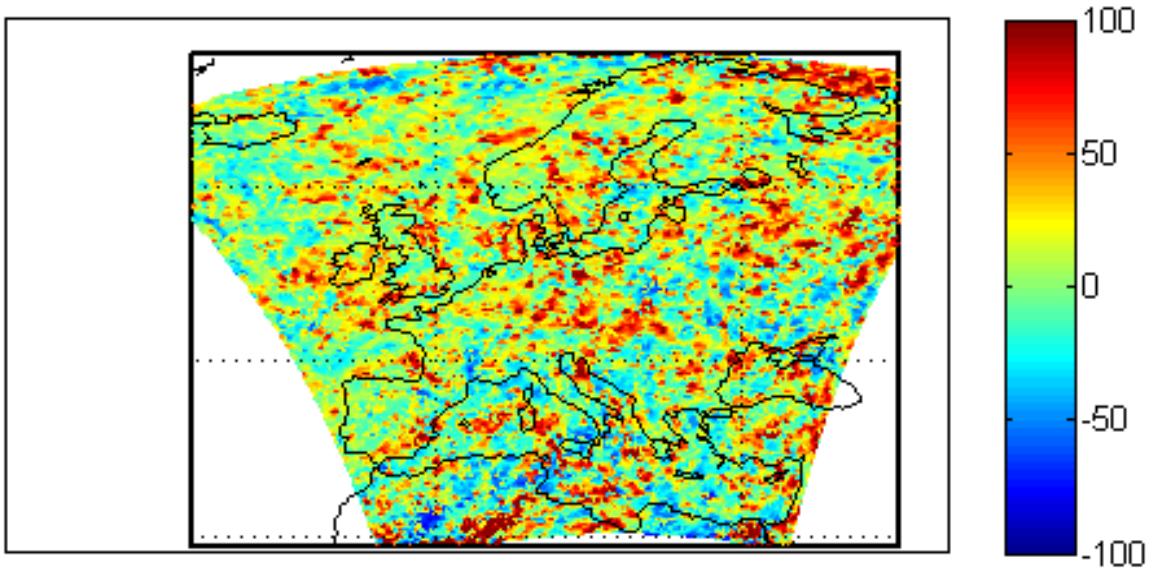

Figure 3.17. Simulated changes in the fifty-year return value of the annual five-day maximum precipitation total (in percent) based on SMHIRCA-ECHAM simulations.

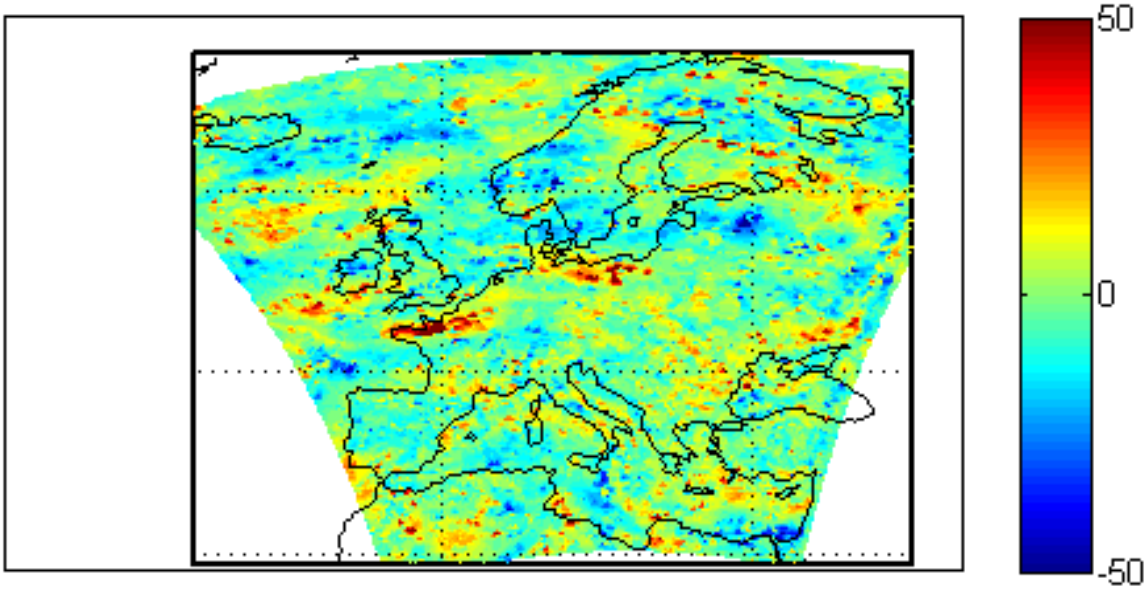

Figure 3.18. Simulated changes in the fifty-year return value of the 10-minute mean wind speed (in percent) based on SMHIRCA-ECHAM simulations.

3.6.2. Climate projections of thunderstorm-related hazards

The study of the connection between wind gusts, large hail, tornadoes and climate change is presently being pursued by only a few research groups worldwide. Here, we will describe briefly some of their work and results. Because of the small size, Brooks et al. (2003) have presented a concept taking reanalysis data to diagnose the global severe convective storm climatology by using so-called proxies. These proxies are developed through a statistical analysis of the "atmospheric environment" of severe convective storm events, as resolved by 4-dimensional atmospheric datasets. This approach has its foundations in studies of the storm environment that identified relevant physical quantities using radiosonde measurements in the proximity of extreme convective events (e.g. Rasmussen and Blanchard, 1998; Groenemeijer and van Delden, 2007; Brooks, 2009).

The most well-known proxy to characterize severe storm environments was developed by Brooks et al. (2003) that has since been used by other groups; a product of convective available potential energy (CAPE) and the vertical wind shear across the surface-to-6 km layer. Only two studies have used these methods on climate model data while addressing Europe, Marsh et al. (2009) and Sander (2011), see Figure 3.19.

These studies have split the problem into to two sub-questions:

1. What will be the climatic trend of thunderstorm occurrence?

2. What will be the climatic trend in the probability of thunderstorms to produce hazardous weather?

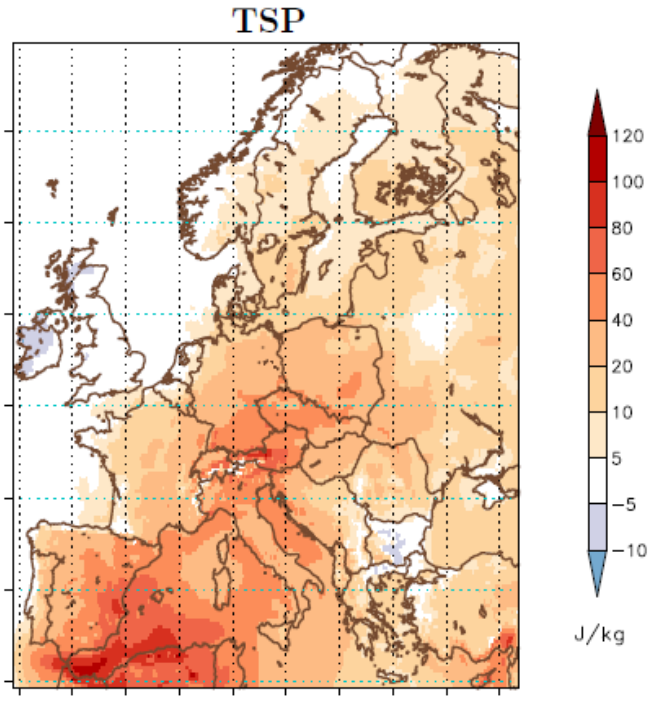

Figure 3.19. Increase in thunderstorm severity potential (TSP) as predicted by a regional climate model. From Sander (2011). Courtesy of Julia Sander.

The consensus of these two studies was that no indications of an increase in thunderstorm occurrence were found, and that it may even slightly decrease across most of Europe. However, the fraction of thunderstorms that may develop hazardous phenomena such as hail, severe wind gusts and

tornadoes, will likely increase. Whether this increase will compensate for the potentially reduced occurrence of storms is not clear, rendering these studies inconclusive in this respect.

3.6.3. Changes in the Baltic Sea ice cover by 2060

Climate change will have many consequences on society and nature in the Baltic Sea region. The Baltic Sea ice cover will face changes that affect transportation and ecosystems. Large scale atmospheric pressure systems strongly affect the climate in the Baltic Sea area. These include The Icelandic Low, the Azores High and the winter high and summer low over Russia. Humid and mild air flows with westerly winds into the Baltic Sea Basin. Because of warm ocean currents that bring heat through the Gulf Stream and the North Atlantic Drift, the mean air temperature in the Baltic Sea Basin is usually higher than in other areas at the same latitudes. Since the late 19th century, the annual mean temperature has increased by about 0.07-0.10°C per decade in the Baltic Sea area. The precipitation in wintertime has also increased (BACC, 2008).

Ice winters in the Baltic Sea have been classified into five different severity classes according to Seinä and Palosuo (1996). This classification is based on the observations of annual maximum sea ice cover for the period 1720-1995 (Table 4). In this classification the extreme categories (extremely mild and extremely severe) both contain about 10 % of the winters.

Table 4. Severity classification of ice winters according to Seinä and Palosuo (1996)

Severity	Ice cover extent (km^2)
Extremely mild	52000-81000
Mild	81001-139000
Average	139001-279000
Severe	279001-383000
Extremely average	383001-420000

The sea ice extent varies greatly from year to year (BACC, 2008). In extremely mild winters, only parts of the Gulf of Finland and Bothnian Sea and the Bothnian Bay are ice-covered, with maximum ice coverage of only about 12 % of the total Baltic Sea area. In extremely severe winters almost all of the Baltic Sea freezes. Since the late 19th century, the maximum sea ice extent has decreased. The frequency distribution of annual maximum Baltic Sea ice cover in 1951-2009 is shown in Fig. 3.20. The highest number of average ice winters occurred during this period, and mild and extremely mild ice winters were more common than severe and extremely severe ice winters.

According to BACC (2008), ice typically forms first in November and the freezing begins in the coastal areas of the northernmost Bothnian Bay. The ice cover usually reaches its maximum value in February or March. According to observations, the trend in the duration of the ice season shows a tendency towards milder conditions. The length of the ice season has decreased by about 14-44 days during the 20th century and is mainly due to the earlier break-up of ice.

In this study, future changes in the probability of annual maximum ice cover extent and average maximum sea ice thickness are assessed using observations of air temperature, sea ice cover in the Baltic Sea and climate model data. In winter 2011, the countries around the Baltic Sea agreed upon a new severity classification of ice winters in the Baltic Sea, because the old classification no longer

coincided with the situation in the changing climate. This new classification is based on observations from 1961-2010. However, in this study the old classification (Seinä and Palosuo, 1996) is still used.

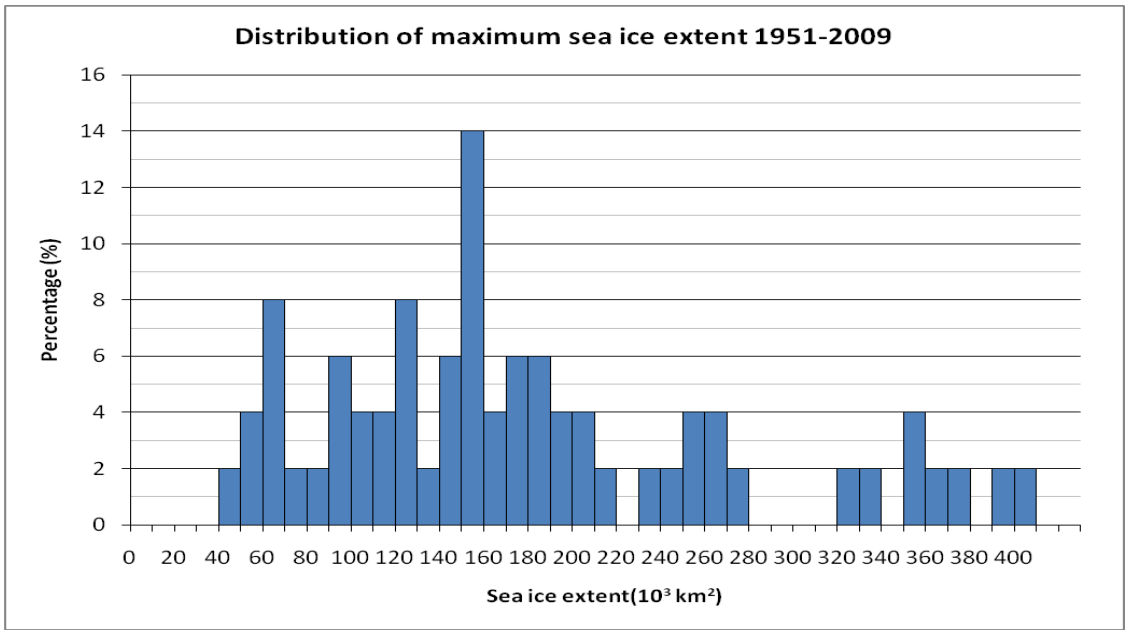

Figure 3.20. The frequency distribution of annual maximum ice cover extent in the Baltic Sea based on observations during 1951-2009.

Regression model for estimating the change in maximum ice cover extent

A regression model was fitted between the observed maximum ice cover extent and coastal November-March mean temperature for 1951-2009 (Fig. 3.21). The temperature observations were monthly mean values from E-OBS data set (Haylock et al., 2008). The regression model gives the resulting fit:

$$y = 81307e^{-0.2695x} \qquad (18)$$

where y is the maximum ice cover extent in km^2, and x is the November-March mean temperature in coastal grid points in degrees Celsius. The coefficient of determination is R2=0.8439 which means that the model can explain about 84 % of the observed variation. The RMS-error is 31964.15 km2. Using the regression model the future maximum ice cover extent was assessed for each decade until 2060.

The information on the future temperatures was obtained using the delta-change method. The estimate of the change in future temperature was obtained as a mean value of the output of 19 global climate models. The model data was originally downloaded from the World Climate Research Programme (WCRP) Coupled Model Intercomparison Project phase 3 (CMIP3) multimodel dataset (Meehl et al., 2007). After downloading, the model dataset (using emission scenario A1B) was interpolated onto the same 0.25 degrees grid as the observed temperature dataset.

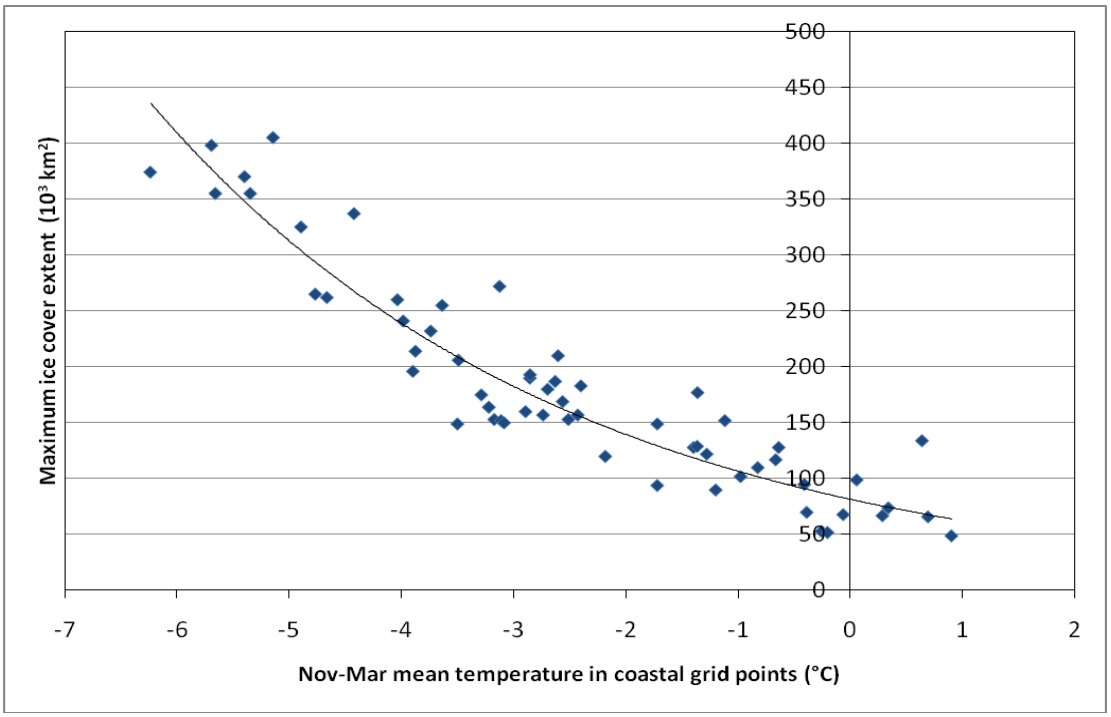

Figure 3.21. A regression model (black curve) fitted to the observed maximum ice cover extent and the coastal November-March temperatures (blue symbols) during 1951-2009.

The average temperature change from the output of the global climate models was calculated for five 30-year periods, so that the change in each period represented each of the five future decades: 2011-2020, 2021-2030, 2031-2040, 2041-2050, and 2051-2060. These values were added to the observed temperature of each winter in the period 1951-2000, so that the interannual variation remained for the future. This was done separately for each of the future decades. As a result a distribution of possible coastal winter temperatures was obtained for each decade. Using the regression model (18) and these temperature distributions the distribution of maximum ice cover extent for each decade was obtained.

Average maximum fast ice thickness using Stefan's law

The average maximum fast ice thickness was estimated using Stefan's law (Zubov, 1945):

$$h = \sqrt{a^2 S + d^2} - d \qquad (19)$$

where h is the average maximum fast ice thickness, S is frost sum, a=3 cm(°C·d)$^{-1/2}$ and d is the insulation efficiency of the surface layer of air over ice cover (about 10 cm). Stefan's law slightly overestimates the ice thickness because it does not take into account the insulating effect of any snow layer on top of the ice.

The frost sum for future decades required in equation (19) was obtained using the delta-change method. Mean temperature changes for each month, and each of the five future decades (2011-

2020, 2021-2030, 2031-2040, 2041-2050, 2051-2060) based on the output of 19 global climate models, was added to the observed 30-year mean temperature of each month in 1971-2000 to obtain a mean temperature for each month in each future decade. The frost sum was then calculated by multiplying the mean temperature of each month by the number of days in that month and then summing the negative values. Using this frost sum, and Stefan's law, an average maximum fast ice thickness was obtained for each decade. As the temperature observations were available for land areas only the results represent the average maximum fast ice thickness only in sea areas next to the coast line.

Maximum ice cover extent

As the warming proceeds the maximum sea ice extent will decrease in the coming decades. The cumulative probability distributions of the maximum sea ice extent for each decade until 2060 are shown in Figure 3.22, where it is assumed that the warming proceeds according to the average model results and emission scenario A1B. In the period 2011-2020 the probability for severe ice winters (ice cover extent more than 279 000 km^2) is less than 10 %, in the period 2021-2030 the probability is about 5 %. Finally in 2041-2050 and 2051-2060 the severe ice winters have practically disappeared.

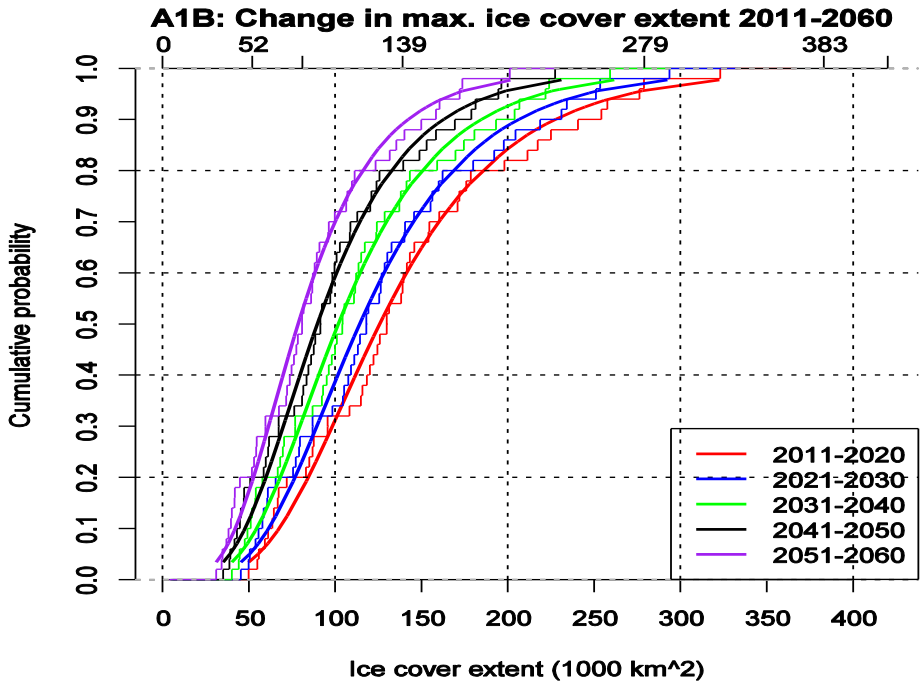

Figure 3.22. The change in the cumulative probability distribution of the maximum sea ice extent during five future decades. The curves with steps represent empirical cumulative probability distributions and the smooth curves represent theoretical cumulative distributions (generalized extreme value distribution, GEV) fitted to empirical distributions. On the upper x-axis the severity classification limits for ice winters are shown.

The probability curve in Figure 3.22 shifts towards the upper left corner which means that the portion of mild and extremely mild winters increases and the portion of severe winters decreases. For

example in 2011-2020 the probability that maximum sea ice extent reaches no more than $150 \cdot 10^3$ km^2 is about 65 %, and in 2021-2030 the probability is about 70 %. In 2031-2040 this probability is 80 %, in 2041-2050 it is almost 90 % and finally in 2051-2060 it is over 90 %. The winters when ice cover extent is more than $150 \cdot 10^3$ km^2 become increasingly rarer.

Average maximum fast ice thickness

As the temperature observations are only available in land areas, the fast ice thickness was assessed only in sea areas close to the coastline. The assessed average maximum fast ice thickness for each future decade according to the average model results is shown in Figure 3.23. In 2011-2020 the average maximum fast ice thickness in the Bay of Bothnia coast areas is about 90 cm, in the southern Baltic Sea the thickness is about 0-20 cm. In the Gulf of Finland the average maximum fast ice thickness varies mainly between 20 and 60 cm. In the next decade (2021-2030) the average maximum fast ice thickness is still over 80 cm in the coastal areas of the Bay of Bothnia, whereas in the southern Baltic Sea the coast areas remain partly ice-free. In the next two decades in the Bay of Bothnia the average maximum fast ice thickness will no longer reach values over 80 cm and in the Gulf of Finland the ice thickness is about 10-40 cm. The southern Baltic Sea and the west coast of the Northern Baltic will become ice-free in normal winters. In the final decade (2051-2060), the average maximum fast ice thickness is about 50-60 cm in the northern parts of the Bay of Bothnia and the southern areas are largely ice-free.

The ice thickness in future decades was compared to the average maximum fast ice thickness in 1971-2000 (not shown). The average maximum fast ice thickness for 1971-2000 was calculated in the same way as for the future decades; using Stefan's law and observed temperatures. In 2011-2020 the average maximum fast ice thickness was typically 10-15 cm thinner than in 1971-2000, in 2021-2030 the difference will be about 15-20cm, 20-25 cm by 2031-2040, and in 2041-2050 the average maximum fast ice thickness will be at least 25 cm thinner than in 1971-2000. Finally, by 2051-2060 the difference will reach about 30-40 cm.

Conclusions on the Baltic Sea ice cover

The Baltic Sea maximum ice cover extent and the average maximum fast ice thickness were assessed for the five future decades. Te results suggest that maximum ice cover extent and the probability of severe ice winters will decrease. Severe ice winters will become rare after 2030, with a corresponding increase in probability for mild and extremely mild ice winters.

The average maximum fast ice thickness was assessed only in the coastal sea areas and suggests that the average maximum fast ice thickness will become thinner everywhere, and in the southern region likely disappear completely. It is however important to remember that Stefan's law, used to estimate the average maximum fast ice thickness, does not take into account any snow layer on top of the fast ice. The results shown here are thus about 10-20 cm too high (Leppäranta, 1993), although it should also be noted that a warmer climate may also reduce the snow thickness.

Any change in the heat storage of the sea and its possible effect on the ice thickness has not been taken into account. Presumably, in the future, a warmer summer and autumn would increase the heat storage of the surface layer of the sea. This would delay the cooling of the sea in winter and

thus decrease the maximum fast ice thickness. Thus, any change in the heat storage is an important factor, especially in the open sea areas.

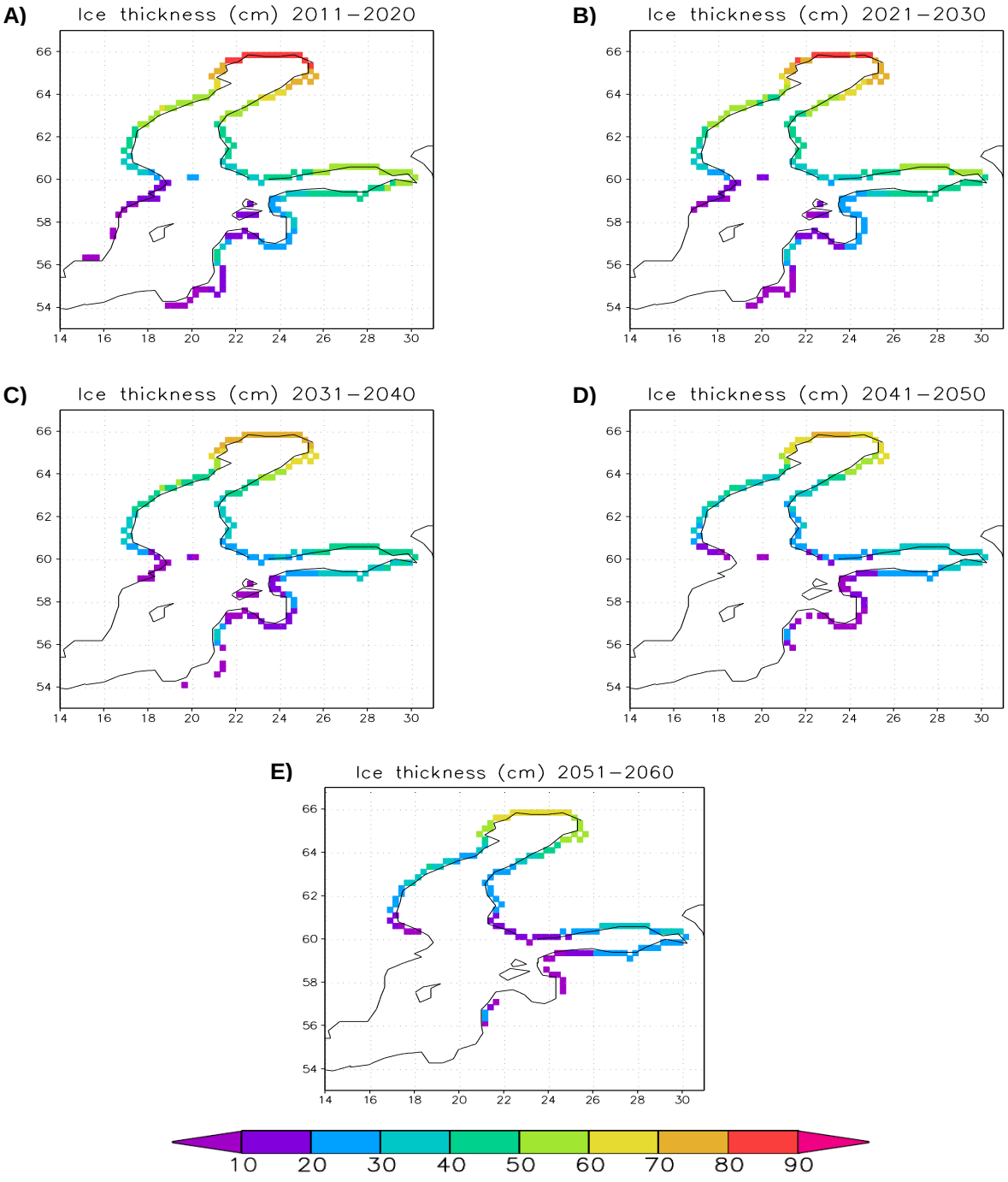

Figure 3.23. The average maximum fast ice thickness (cm) for each future decade. A) 2011-2020, B) 2021-2030, C) 2031-2040, D) 2041-2050, E) 2051-2060.

3.6.4. Scenarios on road networks: a Nordic view

Studies on impacts of climate change on roads have already been conducted around the world, e.g. Galbraith et al. (2005) in Scotland, Thordarson (2008) in Iceland, Youman (2007) in Australia, Natural Resources in Canada (2007) and most recently a comprehensive study in the USA by the National Science and Technology Council (2008). A feature common to all climate scenarios is that the changes will be most dramatic near the poles and during winter, due to the positive feedback effects of the shrinking snow and ice coverage.

The results of project IRWIN introduced in Chapter 3.3 indicated, however, that no dramatic changes are expected before 2050, according to established climate models. In northernmost Europe, mean air and road temperature will rise by 0.9-2.5 degrees by 2050, the rise being larger towards the north. Rainfall amounts display a positive trend in Northern Europe, but, correspondingly, accumulated snowfall amounts will be reduced. Results indicate an increase in extreme precipitation events. Average maximum wind will increase by 0.11-0.34 m/s, larger increases occurring in coastal areas or in the North. All these results are in good agreement with the results of this report.

Even though the expected average changes are relatively modest over the coming 30-40 decades, the need for road maintenance operations will change in different regions in response to the change in climate. As an example, in Northern or mountainous parts of Europe, warmer climate can both mean more requirements for salting due to more icy roads but at the same time less snow removal events when precipitation falls as rain instead of snow. The future will bring more rainy days on a cold surface in the north due to the milder climate and more rainy days in the north instead of precipitation falling as snow. The northern areas will also experience more slipperiness due to frost days when the surface temperature is low and the dew point is above the surface temperature. These frost days will occur less frequently in the future in more southerly areas, due to fewer days with temperatures below freezing.

Effects on road networks in Northern Europe

The effect of climate change on road networks are a matter of great concern to road owners, as many decisions, such as investments in infrastructure, may have implications over decades. A change in impacts may cause a need to modify road structures. Improvements in drainage, erosion control and raising road surface levels may be required. Other adaptation and proactive measures are the control of design criteria and improvement of current roads to assure they meet the service level. Services for road users may also require modification, in order to deliver appropriate warnings and other valid information through the most efficient channels.

Several results from climate models for road network have been shown in this report. Even though many of the trends seem to be slow and to not seriously affect the road network, some signals are alarming. This is true in particular for the predicted larger and heavier rainfall amounts. For example, according to the study by Saarelainen and Makkonen (2007) in Finland, risks for heavy rainfall showers and flash flooding will increase. The probability of very heavy showers may increase even by 25-50% in certain areas, most likely in parts of Central and Northern Europe. Even though there are no clear indications that the frequency of destructive storms will increase, trees will fall more easily during Northern wintertime storms because the layer of frost will be thinner Specifically a problem in the North, it will also become more and more difficult to maintain the present ice roads,

which provide temporary wintertime transport of goods and people to remote areas with no permanent road access.

It is also worth remembering that the progress of climate change depends crucially on the level of global greenhouse emissions, and most of the scenarios (also in this report) are based on a relatively modest and optimistic emission scenario, A1B. Some recent statistics indicate that the true anthropogenic emissions may be considerably larger and, if continued, will accelerate the warming relative to the A1B model results.

Even though the warming trend of European winters is evident, the large variability from year to year does not seem to disappear. We have recently experienced the risk inherent in long successions of warm winters, followed by a few colder "good old-time" winters. Road management resources and equipment have been optimized to a warmer climate minimum due to economic reasons, resulting in inadequate resources for dealing with harder winters. This has caused enormous economic losses for European transport during the winters of 2009-2010 and 2010-2011.

4. Discussion and summary

The present report provides an overview of changes in extreme and adverse weather events that are most likely to affect the European transport network, focusing on the present climate (1971-2000), and the possible future climate (2011-2070) under the SRES A1B emission scenario using a set of various threshold indices.

Present climate according to observational data

- The analysis of the observed changes in winter and summer temperature, precipitation and wind extremes revealed some common patterns on a European-wide level: high frequency of winter extremes (snowfall, cold spell and winter storms) in Northern Europe and Alpine regions, and a strong continental effect in the frequency of cold spells. Nevertheless, a decline has been observed in the probability of frost days and cold spells during the period studied, with a tendency towards wetter winters in Scandinavia and Eastern Europe.
- Extreme heat waves (25 °C and 32 °C) are most common in Southern Europe, although the frequency of very extreme heat waves (above 43 °C) has been reduced even in the south. The trend in heat waves indicates an increase, especially in the Mediterranean region.
- It is remarkable how dissimilar the degree of warming impacts on the number of cold and heat extremes, with heat waves being more accentuated. Similar asymmetric warming patterns of cold and warm tails were indicated in previous studies. Klein Tank and Können (2003) found a symmetric warming for the first half of their study period (1946-75) and an asymmetry for the 1976-99 subperiod. Moberg et al. (2006) reported a tendency for asymmetry in European warming for the entire century. However, the pattern broke down at a regional level, since regional differences were quite large.
- Although adverse rainfall events occur on a yearly basis over the entire continent, very extreme rain amounts are relatively rare and normally occur in the Alps and on the western coastline of the continent.
- Considering the trend of heavy precipitation events, moderate increases are seen over the Alps and sporadically over the western part of the continent, but no significant trend has been detected. This is, to some extent, in contrast with the findings from earlier studies that reported significant increase in the number of heavy precipitation days (Alexander et al., 2006, Groisman et al., 2005, Klein Tank and Können, 2003) for the second part of the twentieth century. It should be noted that, unlike our analyses, the studies mentioned did not consider the state of the precipitation events (snow and rain) separately. Moberg et al. (2006) found an average increase of winter precipitation and a weak increasing tendency for summer precipitation, but not an overall trend.
- Extreme wind events and blizzards are most common over the Atlantic and its shores and sea areas. Limited by the availability of data (22 years), no attempt was made to compute a trend.
- Low visibility due to fog at the main European airports is strongly related to the climate zone; the most affected airport being Milan due to its location in the fog-prone Po Valley. Other major airports with a high frequency of low visibility are Manchester, London Gatwick, Copenhagen, Brussels, Geneva, Zurich, Munich and St. Petersburg. According to observations the occurrence of low visibility events has strongly declined. Very dense fog conditions have diminished across all of Europe, and have even become non-existent at some of the airports in this study.

Future climate based on model projections

- On the basis of the multi-model mean climate projections, robust changes in temperature extremes but less coherent in precipitation extremes have, been detected.
- For wind extremes, any changes are fairly uncertain, with discrepancies among the models.
- Cold extremes are expected to become rarer, with a substantial decrease in the north and less accentuated over southern Europe in moderate cold extremes.
- Snow events in general tend to decrease over the continent. However, extreme snowfall events do not decrease with a similar pattern. Heavy snowfall events (> 10 cm/day) are projected to become more frequent over Scandinavia by 1-5 days by the 2050s.
- Extreme warm events intensify over the entire continent by 2070. The magnitude of this increase is larger in Southern Europe, by about 30-40 days/year for days with 32 °C, 10-20 days in Central Europe and 1-5 days in northern Europe for the same threshold. This implies a shift of the warm extremes northwards. The central European countries will experience as many cold spells by 2070 as the Mediterranean areas do in the current climate. Similar findings were reported by Nikulin et al. (2011) and Beniston et al. (2007) for changes in temperature extremes. Although we have not analysed the duration indices in this study, an increase in the intensity of heatwaves might be also expected. For example, Dankers and Hiederer (2008) indicated an increase in the 7-day heat wave duration index over most of the continent.
- Considering the magnitude of changes in precipitation extremes, we found a somewhat less clear change for the applied threshold indices than the earlier studies; an increase of 1-5 days/year over Europe except the Mediterranean, where no significant change or a sporadical decrease is expected. Nikulin et al. (2011) indicated an increase of 10-30% over Scandinavia, Poland and Baltic countries in 20-yr return levels and a significant decrease (10-40%) in the south-eastern part of the Iberian Peninsula for summer precipitation as well as an increase in winter precipitation over the whole continent. Beniston et al. (2007) found a tendency for winter precipitation to decrease in the south and to increase in central and northern Europe. Similar results were given by Frei et al. (2006) for winter precipitation, indicating an increase in extreme precipitation north, and a decrease south, of about 45 °N, but a change with a more complex character for summer precipitation. Nevertheless, the variance in patterns of changes in all studies relates to the number of regional models used as well as the different methods and indices applied.
- Changes in wind extremes are more difficult to assess, since the multi-mean indicates a clear decrease over the Atlantic and Mediterranean Sea but a slight decrease or no significant change in either direction over the continent. Additionally, there is a large variation in the results among the models.

Summary of regional characteristics

The nature and the extent of adverse and extreme weather events essentially depend on the climate region they eventuate in. The geographical location and topography of the location considerably determines the impact and consequences of the phenomena, e.g. a snowfall event resulting in a few cm of snow cover or daily mean temperature being around zero degrees can be either considered a common event in the northern Europe and in the mountainous regions, or very exceptional and extreme event in the Mediterranean. Different regions of Europe are impacted by different types of extreme weather phenomena. In order to provide an extensive climatology of adverse phenomena and extremes over Europe, a classification of regions affected by similar adverse and extreme events is a beneficial platform in the risk assessment for the European transport system. The regions described follow the classification used in the EWENT project, WP1 (Leviäkangas et al., 2011, Fig. 4) with a modification of dividing the temperate region into two parts.

Based on the frequency and probability maps of extremes, six climate regions with similarities in the most common phenomena were defined:

- Northern European (sub-arctic) region: NE
- Maritime (oceanic) region: O
- Mediterranean region: M
- Temperate Central European region: Tc
- Temperate Eastern European region: Te
- Alpine region: A

These regions are not strictly delimited from each other; rather they are connected through transitional sectors. Most of the European countries are characterised by several extreme climate regions (Table 5), thus when identifying extreme weather related hazards for a certain country, not only phenomena relevant to the representative geographical zones but preferably also those related to their adjacent zone should be considered.

Figure 5.1. Classification of climate regions based on adverse and extreme phenomena for European countries.

Table 5. European countries and their dominant climate regions

COUNTRY	CLIMATOLOGICAL REGION					
	NE	***O***	***Tc***	***Te***	***M***	***A***
Albania			*		*	
Andorra						*
Austria			*			*
Belarus				*		
Belgium		*				
Bosnia and Herzegovina			*			
Bulgaria				*		
Croatia			*		*	
Cyprus					*	
Czech Republic			*			
Denmark	*		*			
Estonia				*		
Finland	*					
Former Yug. Rep. of Macedonia			*			
France		*			*	*
Germany			*			*
Greece					*	
Hungary			*			
Iceland	*					
Ireland		*				
Italy					*	*
Latvia				*		
Lithuania				*		
Luxembourg		*				
Malta					*	
Moldova				*		
Monaco					*	
Montenegro					*	
Netherlands		*				
Norway	*					*
Poland			*	*		
Portugal					*	
Romania				*		*
Russia	*			*		
Serbia			*			
Slovakia			*			*
Slovenia			*		*	*
Spain		*			*	*
Sweden	*					*
Switzerland						*
Turkey				*	*	
Ukraine				*		
United Kingdom		*				

In the following we describe the characteristic phenomena of each climate region, focusing on their probabilities, intensities and spatial extensions in the present climate as well as changes in the projected future climate.

The **Northern European region (NE)**, primarily located in Fennoscandia, Russia - north of 55° latitude, Iceland and the northern part of Denmark (Fig. 5.1), is typically dominated by extreme winter phenomena. The frequency of cold spells, heavy snowfalls and blizzards is highest in this geographical zone. Within this zone the areas most impacted by winter extremes are located north of 65° latitude, e.g. Lapland and Iceland, recording the highest probability of extreme cold spells (20-35 days/year for daily mean temperature under -20 °C in Lapland), heavy snowfall (40-50 days/year with 10 cm/day on the western coast of Norway and Iceland), blizzards (locally over 140 cases between 1971-2000), and extreme wind (especially over Iceland). Heavy rainfalls are frequent over the fjord coast and westerly exposed mountain ranges of Norway. Conversely, the frequency of hot spells is the lowest within the Northern European zone (typically 5-15 days/year with maximum temperature over 25 °C).

In terms of projected future climate the winter extremes are predicted to moderate by 2050s in the Northern European zone compared to their present range, with a substantial decrease in the frequency of cold spells (with 20-30 days per year), blizzards and snowfall events, while heavy snowfalls (over 10 cm/24 hour) indicate a mixed behaviour marked by a reduction (5 days/24 hour) along the shore and a very slight increase over the land (up to 1 day). Maximum ice cover extent on the Baltic Sea and the probability for severe ice winters is expected to decrease. The average maximum fast ice thickness is likely to have decreased by 30-40 cm in 2060 relative to the control period 1971-2000, leaving the southern areas of Baltic Sea coast largely ice-free.

As anticipated in a warming climate, heat waves (> 25 °C) are expected to occur more frequently (ca. 5 days/year) in Scandinavia and northern Russia, however, the projected increase is not as robust as in Southern Europe. Precipitation extremes (> 30 mm/day) record a slight intensification (1-2 days). Wind gusts show a tendency of strengthening over the Baltic Sea and weakening over the land areas.

The **maritime (oceanic) region (O)**, located over the western part of the continent – British Isles, France, Spain, Belgium, Luxembourg and the Netherlands, features relatively moderate frequency of extreme winter phenomena, such as blizzards, extreme cold spells (on average less than 10 days/year with -7 °C and practically no cases with -20 °C) and heavy snowfall (in general 3% probability of 1 cm snow). On the other hand, as a consequence of the reduced probability of extreme winter events, most of the affected countries have a greatly reduced level of preparedness for these phenomena. This implies that once an extreme weather event eventuates, the severity of disruption and damages caused to transport systems are quite remarkable, such in the case of severe snowfall events during winter 2009 and 2010. The probability of heat waves is higher, especially over the mainland (5% for daily maximum temperature over 32 °C), while heavy rainfall and extreme wind gusts are more common over the British Isles (80 cases/year with 17m/s wind gust).

By the 2050s this climatic region is likely to become more impacted by warm extremes, with an increase of 5-10 days/year for the applied threshold indices, particularly over the land. Heavy precipitation events are expected to increase only slightly, on average by 1 day/year for the 30 mm threshold index. The intensity of cold temperatures, extreme snowfall and blizzard events are projected to

decrease significantly for all the threshold indices. In terms of wind extremes, the patterns of changes are mixed, with a slight decrease for 17 m/s gusts but an increase for 25 m/s.

The Mediterranean Sea and its coastal areas, the so called **Mediterranean zone (M),** is affected particularly by summer extreme phenomena, characterised by the highest frequency of heat waves in Europe (locally, a 25 % probability of daily maximum temperatures over 32 °C) and heavy rainfall (locally, more than 100 mm/24 h). However frost days and snowfalls may occur on an annual basis, while extreme winter events are uncharacteristic.

Dust events also impact the region occasionally, especially in the south-eastern Mediterranean. The trend analysis of synoptic classes with no-dust and dust deposition events indicates a tendency to decrease, however the classes with frequent dust deposition seem to become more frequent.

The multi-model mean indicates a robust intensification of warm extremes over the Mediterranean zone, with an increase of 30-40 days/year of daily maximum temperature above 32 °C and of 5-10 days of those above 43 °C. According to the RCM projections, the frequency and intensity of warm extremes increases more rapidly in this zone than over the rest of Europe. The spatial variation of changes in heavy rainfall events indicates mixed patterns, with no significant change over most of the Mediterranean basin, decreasing sporadically by 1 day/year. Cold temperatures and snowfalls decrease by 5-10 days, on average, over this region. Extreme winds tend to weaken, except in the eastern part of the region, where it locally alternates with strengthening.

The **temperate Central European region (Tc)** is less affected by very extreme weather events, however, adverse weather events might impact the area on yearly basis; there is a 5% probability of heat waves (Tmax ≥ 35 °C), 2% of heavy rainfall (30 mm/24 h) and on average 15-20 days/year with 17 m/s wind gusts. Winters might bring blizzards and sporadically severe snowfall (5 events/year), especially over the southern part of this region, together with cold spells (up to 20 days).

An intensification of warm extremes and decline in cold extremes are expected for this zone by the 2050s. The intensification is more robust heading southward, increasing by 20 days/year for days with 32 °C. Accordingly, by 2070, the central European region is expected to experience as many heat waves as the Mediterranean region currently does. Mixed patterns of changes are indicated for extreme wind gusts, with no general trend. Heavy rainfalls tend to increase by 1 day/year in frequency over most of the area, except locally over the Balkan Peninsula. Snowfalls are also expected to reduce in number by 5-10 days/year due mainly to a shift from snow to rain in the warming climate.

The **temperate Eastern European climate region (Te)** differs from the Central European one by the more pronounced effect of continentality. Accordingly, cold spells are more frequent and intense during winter, 30 days/year with -7 °C in the western part of the zone, increasing eastward to 70-80 days/year. Very extreme cold spells (under -20 °C) are frequent over the eastern part. Blizzards and heavy snowfall events (10 cm/24 h) impact the eastern European zone about 5 times/year; very heavy snowfall events may also occur sporadically. Days with 32 °C eventuate with a 5% probability every year, being more frequent over the southern part of the region (~10%). The spatial variation of heavy rainfalls does not differ from the general European patterns, although very heavy events (≥ 100 mm/24 h) may locally occur.

Regarding changes in extremes, a decrease in cold spells (by 5-10 days for -7 °C), snowfall (by 1-5 days for 10 cm/day snow) and blizzard events, is expected, and a significant increase in warm extremes (up to 20 days for 32 °C) by the 2050s. Wind gusts and heavy rainfall show mixed patterns over this region, with the frequency of heavy rainfall tending to increase over most of the region expect in the south.

In our regionalisation, the **Alpine region (A)** implies not only the Alps but also the Carpathians, the Pyrenees and in many aspects also the Scandinavian Mountains. These regions, due their topography, can have remarkably different extreme phenomena from their surroundings. The most characteristic extreme phenomena affecting the Alpine zone are cold spells (on average 50-60 days with -7 °C), heavy snowfall (40-45 days with 10 cm and 20 days with 20 cm of snow in 24 hours), blizzards, especially in the Scandinavian mountains (over 120 cases during 1989-2010) and Alps (20 cases), and heavy rainfall (about 20 cases/year with 100 mm/24 h), most significantly on the slopes. The frequency and intensity of these phenomena is somewhat moderated in the Pyrenees by its southern location.

By 2070 in the Alpine zone, extremes are predicted to abate especially cold spells (by 5-10 days/year, up to 20 days in the Scandes for -20 °C) and snow (by 5 days/year for 20 cm/24h snowfall) related phenomena, except in the Scandes where the frequency of heavy snowfall is likely to increase by 1-5 days/year. Heavy rainfall and warm-related extremes will become more intense.

The potential effect of changes in extremes on the transportation system is both positive and negative. A decrease in cold spells, extreme snowfalls and frozen precipitation have a positive impact on road, rail and air transportation, reducing the cost of maintenance and producing side benefits. However, even with a general decreasing trend in winter extremes, due to inter-annual variability winter extremes are still expected to have an impact on transportation, and would still need to be considered in maintenance and investment in preparedness for many European countries. Increases in warm extremes and heavy precipitation events are likely to have a negative impact on transportation and infrastructure. During summer, especially in countries which already experience high temperatures, further warming implies a need for improvements in the heat tolerance of the transport system.

All the changes anticipated in the RCM simulations applied follow the A1B emission scenario that lies in the central range of emission scenarios considered by IPCC. The present trends of greenhouse gas emissions, if continued in the future, would lead to larger changes according to recently modelled GCMs driven by hypothetical extremely high emission scenarios (Sanderson et al., 2011).

Acknowledgements

The study contributes to the EWENT project funded by the 7th Framework Programme of the European Union.

We acknowledge the E-OBS dataset from the EU FP6 project ENSEMBLES (http://ensembles-eu.metoffice.com) and the data providers in the ECA&D project (http://eca.knmi.nl). ERA-Interim data used in this study have been provided by ECMWF, and icing and visibility data by NOAA National Climatic Data Centre.

We acknowledge the climate modelling community. The ENSEMBLES and Coupled Model Intercomparision Project (CMIP3) multi-model data were widely used.

References

Agarwal M., Maze T.H. and Souleyrette R., 2005: Impacts of weather on urban freeway traffic flow characteristics and facility capacity, in: Proceedings of the 2005 Mid-Continent Transportation Research Symposium.

Alexander L.V. et al. (23 co-authors) 2006: Global observed changes in daily climate extremes of temperature and precipitation, J. Geophys. Res., 111, D05109, doi:10.1029/2005JD006290

Anon, 2001: CEN.prEN1990 - Eurocode: Basis of Structural Design, European Committee for Standardization, CEN

BACC Author team, 2008: Assessment of Climate Change for the Baltic Sea Basin Series, Regional Climate Studies, Springer, ISBN: 978-3-540-72785-9, 474p.

Beniston M., Stephenson D. B., Christensen O. B., Ferro C. A. T., Frei C., Goyette S., Halsnaes K., Holt T., Jylhä K., Koffi B., Palutikoff J., Schöll R., Semmler T. and Woth K., 2007: Future extreme events in European climate: An exploration of regional climate model projections, Climatic Change 81: 71-95.

Berrisford P., Dee D., Fielding K., Fuentes M., Kallberg P., Kobayashi S. and Uppala S., 2009: The ERA-Interim archive (Technical Report). European Centre for Medium-range Weather Forecasting, Reading.

Boberg F., Berg P., Thejll P., Gutowski W.J. and Christensen J.H., 2009: Improved confidence in climate change projections of precipitation evaluated using daily statistics from the PRUDENCE ensemble, Clim. Dyn. 32:1097–1106.

Brabson B.B. and Palutikof J.P., 2000: Tests of the generalized Pareto distribution for predicting extreme wind speeds, J. Appl. Meteorol. 39: 1627-1640.

Brooks H. E., 2009: Proximity soundings for severe convection for Europe and the United States from reanalysis data, Atmos. Res. 93: 546−553.

Brooks H. E., Lee J. W. and Craven J. P., 2003: The spatial distribution of severe thunderstorms and tornado environments from global reanalysis data, Atmos. Res. 67-68: 73−94.

Castillo E., 1988: Extreme Value Theory in Engineering. Academic Press, New York

Christensen J.H. and Christensen O.B., 2007: A summary of the PRUDENCE model projections of changes in European climate by the end of this century, Climatic Change 81 (Supplement 1): 7–30.

Cook N.J., 1982: Towards better estimation of extreme winds. J. Wind Eng. Ind. Aerodyn. 9: 295-323.

Cook N.J., Harris R.I. and Whiting R., 2003: Extreme wind speeds in mixed climates revisited, J. Wind Eng. Ind. Aerodyn. 91: 403-422.

Dotzek, N., Groenemeijer P., Feuerstein B. and. Holzer A. M, 2009: Overview of ESSL's severe convective storms research using the European Severe Weather Database, Atmos. Res. 93: 575-586.

Dankers R. and Hiederer R., 2008: Extreme temperatures and precipitation in Europe: analysis of a high-resolution climate change scenario, JRC Scientific and Technical Reports (EUR collection), JRC44124, 82 p.

Fisher, R.A., and Tippett L.H.C., 1928: Limiting forms of the frequency distributions of the largest or smallest members of a sample, Proc. Cambridge Phil. Soc. 24: 180-190.

Foley A.D., 2010: Quantifying sources of uncertainty in regional climate model scenarios for Ireland, PhD thesis, NUI Maynooth, http://eprints.nuim.ie/2438/

Frei, C., Schöll R., Fukutome S., Schmidli J., and Vidale P. L., 2006: Future change of precipitation extremes in Europe: Intercomparison of scenarios from regional climate models, J. Geophys. Res., 111, D06105, doi:10.1029/2005JD005965

Furrer, E.M. and Katz, R.W., 2008: Improving the simulation of extreme precipitation events by stochastic weather generators, Water Resources Res.: 44, W12439.

Galambos, J., and Macri, N., 1999: Classical extreme value model and prediction of extreme winds, J. Structural. Eng. 125: 792-794.

Galbraith, R.M., Price D. J. and Shackman L. (Eds.), 2005: Scottish road network climate change study, The Scottish Government, ISBN 0 7559 4652 9

Groenemeijer, P. and van Delden A. J., 2007: Sounding-derived parameters in the vicinity of large hail and tornadoes in the Netherlands, Atmos. Res. 67−68: 273−299.

Groisman P.Y., Knight R.W., Easterling D.R., Karl T.R., Hegerl G.C. and Razuvaev V.N., 2005: Trends in intense precipitation in the climate record, Journal of Climate 18: 1326-1350.

Gumbel E.J., 1958: Statistics of Extremes, Columbia University Press, New York.

Harris R.I., 2004: Extreme value analysis of eoch maxima – convergence, and choice of asymptote, J. Wind Eng. Ind. Aerodyn. 92: 897-918.

Harris R.I., 1996: Gumbel re-visited - a new look at extreme value statistics applied to wind speeds, J. Wind Eng. Ind. Aerodyn. 59: 1-22.

Haylock, M.R., Hofstra N., Klein Tank A.M.G., Klok E.J., Jones P.D., and New M., 2008: A European daily high-resolution gridded dataset of surface temperature and precipitation, J. Geophys. Res (Atmospheres), 113, D20119, doi:10.1029/2008JD10201.

Hawkins E. and Sutton R., 2009: The potential to narrow uncertainty in regional climate predictions, Bull. Amer. Met. Soc. 90: 1095-1107, doi:10.1175/2009BAMS2607.1.

Hofstra N., Haylock, M., New M. and Jones P.D., 2009: Testing E-OBS European high-resolution gridded data ser of daily precipitation and surface temperature, Geophys. Res., 114, D21101, doi:10.1029/2009JD011799.

Hosking J.R., 1985: Maximum-likelihood estimation of the parameters of the generalized extreme-value distribution, Appl. Stat. 34: 301-310.

Hosking J.R., Wallis J.R. and Wood E.F., 1985: Estimation of the generalized extreme value distribution by a method of probability weighted moments, Technometrics 27: 251-261.

IRWIN Improved local winter index to assess maintenance needs and adaptation costs in climate change scenarios. ERA-NET Road Final Report, February 2010, www.eranetroad.org

Kållberg P., 2008: Windstorm in ERA-40, Third WCRP International Conference on Reanalyses, Tokyo, 28 January - 1 February, 2008

Katz, R.W., Parlange, M.B. and Naveau, P., 2002: Statistics of extremes in hydrology, Adv. Water Resour. 25: 1287-1304.

Kjellström E., Nikulin G., Hansson U., Strandberg G and Ullerstig A., 2011: 21st century changes in the European climate: uncertainties derived from an ensemble of regional climate model simulations, Tellus A 63(1): 24-40.

Klein Tank A.M.G. and Können G.P., 2003: Trends in indices of daily temperature and precipitation extremes in Europe, 1946-99, Journal of Climate 16: 3665-3680.

Klok E.J. and Klein Tank A.M.G., 2008: Updated and extended European dataset of daily climate observations, Int. J. Climatol., doi:10.1002/joc.1779

Landwehr, J.M., Matalas, N.C. and Wallis, J.R., 1979: Probability weighed moments compared with some traditional techniques in estimating Gumbel parameters and quantiles, Water Resour. Res. 15: 1055-1064.

Leppäranta, M. 1993: A Review of Analytical Models of Sea-Ice Growth. Atmosphere-Ocean 31(1): 123-138.

Leviäkangas P. (ed.), Tuominen A. (ed.), Molarius R. (ed.), Kojo H. (ed.), Schabel J., Toivonen S., Keränen J., Ludvigsen J., Vajda A., Tuomenvirta H., Juga I., Nurmi P., RauhalaJ., RehmF., Gerz T., Muehlhausen T., Schweighofer J., Michaelides S., Papadakis M., Dotzek N.(†) and Groenemeijer P., 2011: Extreme weather impacts on transport systems-EWENT Project deliverable D1, VTT Working Paper 168, 133p.

Lieblein J., 1974: Efficient methods of extreme-value methodology, Natl. Bur. Stand. (US), 1974: Rep. NBSIR 74-602.

Lott J.N., 2000: NOAA National data centre climate data online for use in research and atmospheric icing studies. Proceedings, 9th International Workshop on Atmospheric Icing of Structures, 5-8 June 2000, Chester, U.K., EA Technology Ltd. (proceedings had no page numbers).

Makkonen L., 2006: Plotting positions in extreme value analysis, J. Appl. Meteorol. Climatol. 45: 334-340.

Makkonen L., 2008a: Problems in the extreme value analysis, Structural Safety 30: 405-419.

Makkonen L., 2008b: Bringing closure to the plotting position controversy, Commun. Stat.–Theory Methods 37: 460-467.

Makkonen L., 2011: Reply to Comments by N. Cook on "Plotting positions in extreme value analysis", J. Appl. Meteorol. Climatol. 50: 267-270.

Makkonen L., Ruokolainen L., Räisänen J. and Tikanmäki M., 2007: Regional climate model estimates for changes in Nordic extreme events, Geophysica 43:19–42.

Marsh P., Brooks H. E. and Karoly D. J., 2009: Preliminary investigation into the severe thunderstorm environment of Europe simulated by the Community Climate System Model 3, Atmos. Res. 93: 607–618.

Martins E.S. and Stedinger J.R., 2000: Generalized maximum likelihood generalized extreme-value quantile estimators for hydrological data, Water Resour. Res. 36: 737-744.

Meehl G. A., Covey C., Delworth T., Latif M., McAvaney B., Mitchell J. F. B., Stouffer R. J. and Taylor K. E., 2007: The WCRP CMIP3 Multimodel Dataset: A New Era in Climate Change Research, Bull. Amer. Meteor. Soc. 88: 1383–1394.

Michaelides S.C., Pattichis C.S.and Kleovoulou G., 2001: Classification of rainfall variability by using artificial neural networks, International Journal of Climatology 21: 1401–1414.

Michaelides S., Tymvios F., Paronis D. and Retalis A., 2011: Artificial Neural Networks for the diagnosis and prediction of desert dust transport episodes. In: Soft Computing in Green and Renewable Energy System. Gopalakrishnan, K., Khaitan, S.K., Kalogirou, S. (editors), Springer-Verlag, Berlin, Heidelberg, p. 285-304.

Moberg A. et al. (39 co-authors), 2006: Indices for daily temperature and precipitation extremes in Europe analyzed for the period 1901–2000, J. Geophys. Res. 111, D22106, doi:10.1029/2006JD007103.

National Science and Technology Council, 2008: Scientific Assessment of the Effects of Global Change on the United States, A report of the Committee on Environment and Natural Resources, 271 p.

Natural Resources Canada, 2007: Climate Change Impacts and Adaptation: A Canadian Perspective, Adaptation in the Transportation Sector.
http://adaptation.rncan.gc.ca/perspective/transport_5_e.php

Nikulin G., Kjellström E., Hansson U., Strandberg G. and Ullerstig A., 2011: Evaluation and future projections of temperature, precipitation and wind extremes over Europe in an ensemble of regional climate simulations, Tellus 63A: 41-55.

Peterson T.C., McGuirk M., Houston T.G., Horvitz A.H., and Wehner M.F., 2008: Climate variability and change with implications for transportation, 90 p.
http://onlinepubs.trb.org/onlinepubs/sr/sr290Many.pdf

Prezerakos N.G., Michaelides S.C., and Vlassi A.S., 1991: Atmospheric synoptic conditionsassociated with the initiation of north-west African depressions, International Journal of Climatology 10: 711-729.

Rasmussen E. N. and Blanchard D. O., 1998: A baseline climatology of sounding-derived super cell and tornado forecast parameters, Wea. Forecasting 13: 1148−1164.

Rasmussen P.F. and Gautam N., 2003: Alternative PMW-estimators of the Gumbel distribution, J. Hydrol. 280: 265-271.

Roach W.T. and Findlater J., 1983: An aircraft encounter with a tornado, The Meteorological Magazine 112: 29-49.

Rummukainen M., 2010: State-of-the-art with regional climate models, WIREs Climate Change 1(1): 82-96.

Saarelainen S. and Makkonen L., 2007: Adaptation to climate change in the road management (In Finnish). Prestudy. Finnish Road Administration, FinnRA reports 4/2007, Helsinki. 53 p.

Sander J. 2011: Extremwetterereignisse im Klimawandel: Bewertung der derzeitigen und zukünftigen Gefährdung. Ph. D. Thesis, University of Munich, 125 p.

Sanderson B.M., O'Neill C.O., Kiehl J.T., Meehl G.A., Knutti R. and Washington W.M., 2011: The response of the climate system to very high greenhouse gas emission scenarios. Environmental Research Letters 6:034005 doi:10.1088/1748-9326/6/3/034005.

Seinä A. and E. Palosuo, 1996: The classification of the maximum annual extent of ice cover in the Baltic Sea 1720-1995, Meri, Report Series of the Finnish Inst. Of Marine Res. 20: 79-910.

Simmons A., Uppala S., Dee D. and Kobayashi S., 2006: ERA-Interim: New ECMWF reanalysis products from 1989 onwards. ECMWF Newsletter 110: 26–35.

Thordarson S., 2008: Climate change and winter road service, COST 353 Final Seminar, Bad Schandau, Germany May 26-28 2008, 7 p.

Uppala S.M., Kållberg P.W., Simmons A.J., Andrae U., da Costa Bechtold V., Fiorino M., Gibson J.K., Haseler J., Hernandez,A., Kelly G.A., Li X., Onogi K., Saarinen S., Sokka N., Allan R.P., Andersson E., Arpe K., Balmaseda M.A., Beljaars A.C.M., van de Berg L., Bidlot J., Bormann N., Caires S., Chevallier F., Dethof A., Dragosavac M., Fisher M., Fuentes M., Hagemann S., Hólm E., Hoskins B.J., Isaksen L., Janssen P.A.E.M., Jenne R., McNally A.P., Mahfouf J.-F., Morcrette J.-J., Rayner N.A., Saunders R.W., Simon P., Sterl A., Trenberth K.E., Untch A., Vasiljevic D., Viterbo P., and Woollen J., 2005: The ERA-40 re-analysis, Quart. J. R. Meteorol. Soc. 131: 2961-3012, doi:10.1256/qj.04.176

van der Linden P. and J.F.B. Mitchell (eds.) 2009: ENSEMBLES: Climate Change and its Impacts: Summary of research and results from the ENSEMBLES project. Met Office Hadley Centre, Fitz-Roy Road, Exeter EX1 3PB, UK. 160 p.

van Oldenborgh G.J., Yiou P. and Vautard R., 2010: On the roles of circulation and aerosols in the decline of mist and dense fog in Europe over the last 30 years, Atmos. Chem. Phys. 10: 4597-4609.

Vautard R., Yiou P., and van Oldenborgh G. J., 2009: Decline of fog, mist and haze in Europe over the past 30 years, Nature Geoscience 2: 115-119.

Wang Q.J., 1991: The POT model described by the generalized Pareto distribution with Poisson arrival rate, J. Hydrol. 129: 263-280.

Youman P., 2007: The implications of climate change on road infrastructure planning, design and management, Proceedings, 16th NSW Coastal Conference, 10 p.

Zubov N. N., 1945: L'dy Arktiki [Arctic Ice]. Izdatel'stvo Glavsermorputi, Moscow. EngI. Transi. 1963 by U.S. Naval Oceanogr. Off. and Am. Meteorol. Soc., San Diego, Calif.

RAPORTTEJA — RAPPORTER — REPORTS

1986: 1. Savolainen, Anna Liisa et al., 1986. Radioaktiivisten aineiden kulkeutuminen Tshernobylin ydinvoimalaonnettomuuden aikana. Väliaikainen raportti. 39 s.

2. Savolainen, Anna Liisa et al., 1986. Dispersion of radioactive release following the Chernobyl nuclear power plant accident. Interim report. 44 p.

3. Ahti, Kari, 1986. Rakennussääpalvelukokeilu 1985-1986. Väliraportti Helsingin ympäristön talvikokeilusta 18.11.-13.3.1986. 26 s.

4. Korhonen, Ossi, 1986. Pintatuulen vertailumittauksia lentoasemilla. 38 s.

1987: 1. Karppinen, Ari et al., 1987. Description and application of a system for calculating radiation doses due to long range transport of radioactive releases. 50 p.

2. Venäläinen, Ari, 1987. Ilmastohavaintoihin perustuva arvio jyrsinturpeen tuotantoedellytyksistä Suomessa. 35 s.

3. Kukkonen, Jaakko ja Savolainen, Anna Liisa, 1987. Myrkyllisten kaasujen päästöt ja leviäminen onnettomuustilanteissa. 172 s.

4. Nordlund, Göran ja Rantakrans, Erkki, 1987. Matemaattisfysikaalisten ilmanlaadun arviointimallien luotettavuus. 29 s.

5. Ahti, Kari, 1987. Rakennussäätutkimuksen loppuraportti. 45 s.

6. Hakola, Hannele et al., 1987. Otsonin vaihteluista Suomessa yhden vuoden havaintoaineiston valossa. 64 s.

7. Tammelin, Bengt ja Erkiö, Eero, 1987. Energialaskennan säätiedot – suomalainen testivuosi. 108 s.

1988: 1. Eerola, Kalle, 1988. Havaintojen merkityksestä numeerisessa säänennustuksessa. 36 s.

2. Fredrikson, Liisa, 1988. Tunturisääprojekti 1986-1987. Loppuraportti. 31 s.

3. Salmi, Timo and Joffre, Sylvain, 1988. Airborne pollutant measurements over the Baltic Sea: meteorological interpretation. 55 p.

4. Hongisto, Marke, Wallin, Markku ja Kaila, Juhani, 1988. Rikkipäästöjen vähentämistoimenpiteiden taloudellisesti tehokas valinta. 80 s.

5. Elomaa, Esko et al., 1988. Ilmatieteen laitoksen automaattisten merisääasemien käyttövarmuuden parantaminen. 55 s.

6. Venäläinen, Ari ja Nordlund, Anneli, 1988. Kasvukauden ilmastotiedotteen sisältö ja käyttö. 63 s.

7. Nieminen, Rauno, 1988. Numeeristen paine- ja ja korkeuskenttäennusteiden objektiivinen verifiointisysteemi sekä sen antamia tuloksia vuosilta 1985 ja 1986. 35 s.

1989: 1. Ilvessalo, Pekko, 1989. Yksittäisestä piipusta ilmaan pääsevien epäpuhtauksien suurimpien tuntipitoisuuksien arviointimenetelmä. 21 s.

1992: 1. Mhita, M.S. and Venäläinen, Ari, 1991. The variability of rainfall in Tanzania. 32 p.

2. Anttila, Pia (toim.), 1992. Rikki- ja typpilaskeuman kehitys Suomessa 1980-1990. 28 s.

1993: 1. Hongisto, Marke ja Valtanen Kalevi, 1993. Rikin ja typen yhdisteiden kaukokulkeutumismallin kehittäminen HIRLAM-sääennustemallin yhteyteen. 49 s.

2. Karlsson, Vuokko, 1993. Kansalliset rikkidioksidin analyysivertailut 1979 - 1991. 27 s.

1994: 1. Komulainen, Marja-Leena, 1995. Myrsky Itämerellä 28.9.1994. Säätilan kehitys Pohjois-Itämerellä M/S Estonian onnettomuusyönä. 42 s.

2. Komulainen, Marja-Leena, 1995. The Baltic Sea Storm on 28.9.1994. An investigation into the weather situation which developed in the northern Baltic at the time of the accident to m/s Estonia. 42 p.

1995: 1. Aurela, Mika, 1995. Mikrometeorologiset vuomittausmenetelmät - sovelluksena otsonin mittaaminen suoralla menetelmällä. 88 s.

2. Valkonen, Esko, Mäkelä, Kari ja Rantakrans, Erkki, 1995. Liikenteen päästöjen leviäminen katukuilussa - AIG-mallin soveltuvuus maamme oloihin. 25 s.

3. Virkkula, Aki, Lättilä, Heikki ja Koskinen, Timo, 1995. Otsonin maanpintapitoisuuden mittaaminen UV-säteilyn absorbtiolla: DOAS-menetelmän vertailu suljettua näytteenottotilaa käyttävään menetelmään. 29 s.

4. Bremer, Pia, Ilvessalo, Pekko, Pohjola, Veijo, Saari, Helena ja Valtanen, Kalevi, 1995. Ilmanlaatuennusteiden ja -indeksin kehittäminen Helsingin Käpylässä suoritettujen mittausten perusteella. 81 s.

1996: 1. Saari, Helena, Salmi, Timo ja Kartastenpää, Raimo, 1996. Taajamien ilmanlaatu suhteessa uusiin ohjearvoihin. 98 s.

1997: 1. Solantie, Reijo, 1997. Keväthallojen alueellisista piirteistä ja vähän talvipakkastenkin. 28 s.

1998: 1 Paatero, Jussi, Hatakka, Juha and Viisanen, Yrjö, 1998. Concurrent measurements of airborne radon-222, lead-210 and beryllium-7 at the Pallas-Sodankylä GAW station, Northern Finland. 26 p.

2 Venäläinen, Ari ja Helminen, Jaakko, 1998. Maanteiden talvikunnossapidon sääindeksi. 47 s.

3 Kallio, Esa, Koskinen, Hannu ja Mälkki, Anssi, 1998. VII Suomen avaruustutkijoiden COSPAR-kokous, Tiivistelmät. 40 s.

4 Koskinen, H. and Pulkkinen, T., 1998. State of the art of space weather modelling and proposed ESA strategy. 66 p.

5 Venäläinen, Ari ja Tuomenvirta Heikki, 1998. Arvio ilmaston läm- penemisen vaikutuksesta teiden talvikunnossapidon kustannuksiin. 19 s.

1999: 1 Mälkki, Anssi, 1999. Near earth electron environment modelling tool user/software requirements document. 43 p.

2 Pulkkinen, Antti, 1999. Geomagneettisesti indusoituvat virrat Suomen maakaasuverkostossa. 46 s.

3 Venäläinen, Ari, 1999. Talven lämpötilan ja maanteiden suolauksen välinen riippuvuus Suomessa.16 s.

4 Koskinen, H., Eliasson, L., Holback, B., Andersson, L., Eriksson, A., Mälkki, A., Nordberg, O., Pulkkinen, T., Viljanen, A., Wahlund, J.-E., Wu, J.-G., 1999. Space weather and interactions with scacecraft : spee final report. 191 p.

2000: 1 Solantie, Reijo ja Drebs, Achim, 2000. Kauden 1961 - 1990 lämpöoloista kasvukautena alustan vaikutus huomioiden, 38 s.

2 Pulkkinen, Antti, Viljanen, Ari, Pirjola, Risto, and Bear working group, 2000. Large geomagnetically induced currents in the Finnish high-voltage power system. 99 p.

3 Solantie, R. ja Uusitalo, K., 2000. Patoturvallisuuden mitoitussadannat: Suomen suurimpien 1, 5 ja 14 vrk:n piste- ja aluesadantojen analysointi vuodet 1959 - 1998 kattavasta aineistosta. 77 s.

4 Tuomenvirta, Heikki, Uusitalo, Kimmo, Vehviläinen, Bertel, Carter, Timothy, 2000. Ilmastonmuutos, mitoitussadanta ja patoturvallisuus: arvio sadannan ja sen ääriarvojen sekä lämpötilan muutoksista Suomessa vuoteen 2100. 65 s.

5 Viljanen, Ari, Pirjola, Risto and Tuomi, Tapio, 2000. Abstracts of the URSI XXV national convention on radio science. 108 p.

6 Solantie, Reijo ja Drebs, Achim, 2000. Keskimääräinen vuoden ylin ja alin lämpötila Suomessa 1961 - 90. 31 s.

7 Korhonen, Kimmo, 2000. Geomagneettiset mallit ja IGRF-appletti. 85 s.

2001: 1 Koskinen, H., Tanskanen, E., Pirjola, R., Pulkkinen, A., Dyer, C., Rodgers, D., Cannon, P., Mandeville, J.-C. and Boscher, D., 2001. Space weather effects catalogue. 41 p.

2 Koskinen, H., Tanskanen, E., Pirjola, R., Pulkkinen, A., Dyer, C., Rodgers, D., Cannon, P., Mandeville, J.-C. and Boscher, D., 2001. Rationale for a european space weather programme. 53 p.

3 Paatero, J., Valkama, I., Makkonen, U., Laurén, M., Salminen, K., Raittila, J. and Viisanen, Y., 2001. Inorganic components of the ground-level air and meteorological parameters at Hyytiälä, Finland during the BIOFOR project 1998-1999. 48 p.

4 Solantie, Reijo, Drebs, Achim, 2001. Maps of daily and monthly minimum temperatures in Finland for June, July, and August 1961-1990, considering the effect of the underlying surface. 28 p.

5 Sahlgren, Vesa, 2001. Tuulikentän alueellisesta vaihtelusta Längelmävesi-Roine -järvialueella. 33 s.

6 Tammelin, Bengt, Heimo, Alain, Leroy, Michel, Rast, Jacques and Säntti, Kristiina, 2001. Meteorological measurements under icing conditions : EUMETNET SWS II project. 52 p.

2002: 1 Solantie, Reijo, Drebs, Achim, Kaukoranta, Juho-Pekka, 2002. Lämpötiloja eri vuodenaikoina ja eri maastotyypeissä Alajärven Möksyssä. 57 s.

2. Tammelin, Bengt, Forsius, John, Jylhä, Kirsti, Järvinen, Pekka, Koskela, Jaakko, Tuomenvirta, Heikki, Turunen, Merja A., Vehviläinen, Bertel, Venäläinen, Ari, 2002. Ilmastonmuutoksen vaikutuksia energiantuotantoon ja lämmitysenergian tarpeeseen. 121 s.

2003: 1. Vajda, Andrea and Venäläinen, Ari, 2003. Small-scale spatial variation of climate in northern Finland. 34 p.

2. Solantie, Reijo, 2003. On definition of ecoclimatic zones in Finland. 44 p.

3. Pulkkinen, T.I., 2003. Chapman conference on physics and modelling of the inner magnetosphere Helsinki, Finland, August 25 -29, 2003. Book of abstracts. 110 p.

4. Pulkkinen, T. I., 2003. Chapman conference on physics and modelling of the inner magnetosphere Helsinki, Finland, August 25 -29, 2003. Conference program. 16 p.

5. Merikallio, Sini, 2003. Available solar energy on the dusty Martian atmosphere and surface. 84 p.

6. Solantie, Reijo, 2003. Regular diurnal temperature variation in the Southern and Middle boreal zones in Finland in relation to the production of sensible heat. 63 p.

2004: 1. Solantie, Reijo, Drebs, Achim and Kaukoranta, Juho-Pekka, 2004. Regular diurnal temperature variation in various landtypes in the Möksy experimental field in summer 2002, in relation to the production of sensible heat. 69 p.

2. Toivanen, Petri, Janhunen, Pekka and Koskinen, Hannu, 2004. Magnetospheric propulsion (eMPii). Final report issue 1.3. 78 p.

3. Tammelin, Bengt et al., 2004. Improvements of severe weather measurements and sensors – EUMETNET SWS II project. 101 p.

4. Nevanlinna, Heikki, 2004. Auringon aktiivisuus ja maapallon lämpötilan vaihtelut 1856 - 2003. 43 s.

5. Ganushkina, Natalia and Pulkkinen, Tuija, 2004. Substorms-7: Proceedings of the 7th International Confrence on Substorms. 235 p.

6. Venäläinen, Ari, Sarkkula, Seppo, Wiljander, Mats, Heikkinen, Jyrki, Ervasto, Erkki, Poussu, Teemu ja Storås, Roger, 2004. Espoon kaupungin talvikunnossapidon sääindeksi. 17 s.

7. Paatero, Jussi and Holmen, Kim (eds.), 2004. The First Ny-Ålesund - Pallas-Sodankylä atmospheric research workshop, Pallas, Finland 1 - 3 March 2004 - Extended abstracts. 61 p.

8. Holopainen, Jari, 2004. Turun varhainen ilmastollinen havaintosarja. 59 s.

2005: 1. Ruuhela, Reija, Ruotsalainen, Johanna, Kangas, Markku, Aschan, Carita, Rajamäki, Erkki, Hirvonen, Mikko ja Mannelin, Tarmo, 2005. Kelimallin kehittäminen talvijalankulun turvallisuuden parantamiseksi. 47 s.

2. Laurila, Tuomas, Lohila, Annalea, Tuovinen, Juha-Pekka, Hatakka, Juha, Aurela, Mika, Thum, Tea, Walden, Jari, Kuronen, Pirjo, Talka, Markus, Pesonen, Risto, Pihlatie, Mari, Rinne, Janne, Vesala, Timo, Ettala, Matti, 2005. Kaatopaikkojen kaasupäästöjen ja haihdunnan mikrometeorologisten mittausmenetelmien kehittäminen (MIKROMETKAA). Tekesin Streams – ohjelman hankken loppuraportti. 34 s. (Ei julkaistu – Not published)

3. Siili, Tero, Huttunen, Emilia, Koskinen, Hannu ja Toivanen, Petri (toim.), 2005. Kymmenes Suomen avaruustutkijoiden kokous (FinCospar) Kokousjulkaisu. 57 s.

4. Solantie, Reijo and Pirinen, Pentti, 2005. Diurnal temperature variation in inversion situations. 34 s.

5. Venäläinen, Ari, Tuomenvirta, Heikki, Pirinen, Pentti and Drebs, Achim, 2005. A basic Finnish climate data set 1961 – 2000 – description and illustrations. 24 p.

6. Tammelin, Bengt, Säntti, Kristiina, Dobech, Hartwig, Durstewich, Michel, Ganander, Hans, Kury, Georg, Laakso, Timo, Peltola, Esa, Ronsten, Göran, 2005. Wind turbines in icing environment: improvement of tools for siting, certification and operation – NEW ICETOOLS. 127 p.

2006: 1. Mälkki, Anssi, Kauristie, Kirsti and Viljanen Ari, 2006. Auroras Now! Final Report, Volume I. 73 p.

2. Pajunpää, K. and Nevanlinna, H. (eds), 2006. Nurmijärvi Geophysical Observatory : Magnetic results 2003. 47 p.

3. Pajunpää, K. and Nevanlinna, H. (eds), 2006. Nurmijärvi Geophysical Observatory : Magnetic results 2004. 47 p.

4. Pajunpää, K. and Nevanlinna, H. (eds), 2006. Nurmijärvi Geophysical Observatory : Magnetic results 2005. 49 p.

5. Viljanen, A. (toim.), 2006. Sähkömagnetiikka 2006. Tiivistelmät – Abstracts. 30 s.

6. Tuomi, Tapio J. & Mäkelä, Antti, 2006. Salamahavainnot 2006 - Lightning observations in Finland, 2006. 39 p.

7. Merikallio, Sini, 2006. Preliminary report of the analysis and visualisation software for SMART-1 SPEDE and EPDP instruments. 70 p.

8. Solantie, Reijo, Pirinen, Pentti, 2006. Orografian huomioiminen loka- huhtikuun sademäärien alueellisissa analyyseissä. 34 s.

9. Ruosteenoja, Kimmo, Jylhä, Kirsti, Räisänen, Petri, 2006. Climate projections for the Nordic CE project – an analysis of an extended set of global regional climate model runs. 28 p.

10. Merikallio, Sini, 2006. Analysis and visualisation software for DEMETER Langmuir Probe instrument. 31 p.

2007: 1. Solantie, Reijo, Järvenoja, Simo, Pirinen, Pentti, 2007. Keskimääräisten kuukauden minimilämpötilojen alueellinen jakauma kautena 1992 – 2005 Suomessa sekä muutos kaudesta 1961 – 1990. 59 s.

2. Pulkkinen, Tuija, Hari, Ari-Matti, Haukka, Harri, Leinonen, Jussi, Toivanen, Petri, Koskinen, Hannu, André, Mats, Balasis, Georgios, Boscher, Daniel, Dandouras, Iannis, Grande, Mauel, De Keyser, John, Glassmeier, Karl-Heinz, Hapgood, Mike, Horne, Richard, Ivchenko, Nikolay, Santolik, Ondrej, Torkar, Klaus; Trotignon, Jean Gabriel, Vennerstrøm, Susanne, 2007. Waves and acceleration of relativistic particles (WARP). 36 p.

3. Harri, A-M., Leinonen, J., Merikallio, S., Paton, M., Haukka, H., Polkko, J., Linkin, V., Lipatov, V., Pichkadze, K., Polyakov, A., Uspensky, M., Vasquez, L., Guerrero, H., Crisp, D., Haberle, R., Calcutt, S., Wilson, C., Taylor, P., Lange, C., Daly, M., Richter, L., Jaumann, R., Pommereau, J-P., Forget, F., Lognonne, Ph., Zarnecki, J., 2007. MetNet – In situ observational network and orbital platform to investigate the Martian environment. 35 p.

4. Venäläinen, Ari, Saku, Seppo, Kilpeläinen, Tiina, Jylhä, Kirsti, Tuomenvirta, Heikki, Vajda, Andrea, Räisänen, Jouni, Ruosteenoja, Kimmo, 2007. Sään ääri-ilmiöistä Suomessa. 81 s.

5. Tuomi, Tapio J. & Mäkelä, Antti, 2007. Salamahavainnot 2007 - Lightning observations in Finland, 2007. 47 p.

6. Pajunpää, K. and Nevanlinna, H. (eds), 2007. Nurmijärvi Geophysical Observatory : Magnetic results 2006. 49 p.

2008: 1. Pajunpää, K. and Nevanlinna, H. (eds), 2008. Nurmijärvi Geophysical Observatory : Magnetic results 2007. 49 p.

2. Verronen, Pekka T. (ed), 2008. 1st international HEPPA workshop 2008, Book of abstracts. 81 p.

3. Gregow, Hilppa, Venäläinen, Ari, Laine, Mikko, Niinimäki, Niina, Seitola, Teija, Tuomenvirta, Heikki, Jylhä, Kirsti, Tuomi, Tapio ja Mäkelä, Antti, 2008. Vaaraa aiheuttavista sääilmiöistä Suomen muuttuvassa ilmastossa. 99 s.

4. Tuomi, Tapio J. & Mäkelä, Antti, 2008. Salamahavainnot 2008 – Lightning observations in Finland, 2008. 49 p.

5. Heino, Raino and Tolonen-Kivimäki, Outi (eds), 2008. Finnish national report

on systematic observations for climate – 2008. 27 p.

6. Paatero, Jussi et al., 2008. Effects of Kola air pollution on the environment in the western part of the Kola peninsula and Finnish Lapland : final report. 26 p.

2009:

1. Nevanlinna, H., 2009. Geomagnetismin ABC-kirja. 204 s.

2. Nevanlinna, H. (toim.), 2009. Ilmatieteen laitos 170 vuotta, 1838 - 2008. 69 s.

3. Nevanlinna, Heikki, 2009. Revontulihavainnot Suomessa 1748 – 2009. 88 s.

4. Jylhä, K., Ruosteenoja, K., Räisänen, J., Venäläinen, A., Tuomenvirta, H., Ruokolainen, L., Saku, S. ja Seitola, T., 2009. Arvioita Suomen muuttuvasta ilmastosta sopeutumistutkimuksia varten. ACCLIM-hankkeen raportti 2009. 102 p.

5. Mäkelä, Antti & Tuomi, Tapio, J., 2009. Salamahavainnot 2009 – Lightning observations in Finland, 2009. 51 p.

6. Verronen, Pekka (ed.), 2009. 5th International Atmospheric Limb Conference and Workshop : Book of abstracts. 92 p.

7. Pajunpää, K. and Nevanlinna, H. (eds), 2009. Nurmijärvi Geophysical Observatory : Magnetic results 2008. 48 p.

8. Kersalo, Juha and Pirinen, Pentti (eds), 2009. Suomen maakuntien ilmasto. 185 s.

2010:

1. Rauhala, Jenni & Mäntyniemi, Päivi, 2010. Luonnononnettomuuksien vaikutus ja niihin vaikuttaminen. (valmisteilla).

2. Pilli-Sihvola, K. Löwendahl, E., Ollikainen, M., van Oort, B., Rummukainen, M. & Tuomenvirta, H., 2010. Survey on the use of climate scenarios and climate change research information in decision making in Finland, Sweden and Norway. Report for the project Climate change adaption in Norway, Sweden and Finland – do research, policy and practice meet? (CARePol). 57 p.

3. Pajunpää, K. and Nevanlinna, H. (eds), 2010. Nurmijärvi Geophysical Observatory : Magnetic results 2009. 48 p.

4. Luomaranta, A., Haapala, J., Gregow, H., Ruosteenoja, K., Jylhä, K. and Laaksonen, A. 2010. Itämeren jääpeitteen muutokset vuoteen 2050 mennessä. 23 s.

5. Mäkelä, Antti, 2010. Salamahavainnot 2010 – Lightning observations in Finland, 2010. 50 p.

2011:

1. Saku, Seppo et al., 2011. Äärilämpötilojen alueellinen vaihtelu Suomessa. (valmisteilla)

2. Pajunpää, K. and Nevanlinna, H. (eds), 2011. Nurmijärvi Geophysical Observatory : Magnetic results 2010. 49 p.

3. Virta, Hanna et al., 2011. Ilmastonmuutoksen ääri-ilmiöihin liittyvän riskienhallinnan kustannushyötyanalyysi osana julkista päätöksentekoa (IRTORISKI). 97 s.

4. Nevanlinna, H. 2011. Magneettiset havainnot Helsingin magneettis-meteorologisessa observatoriossa, 1844-1910. 54 s.

5. Hilppa Gregow, Kimmo Ruosteenoja, Ilkka Juga, Sigbritt Näsman, Miika Mäkelä, Mikko Laapas, Kirsti Jylhä, 2011. Lumettoman maan routaolojen mallintaminen ja ennustettavuus muuttuvassa ilmastossa. 45 s.

6. Jylhä, Kirsti et al. (valmisteilla)

7. Mäkelä, Antti, 2011. Salamahavainnot 2011 – Lightning observations in Finland, 2011.

8. Riihelä. Aku, Lahtinen, Panu, Hakala, Teemu, 2011. Radiation, snow characteristics and albedo at Summit (RASCALS) expedition report. 48 p.

9. Vajda, Andrea, Tuomenvirta, Heikki, Jokinen, Pauli, Luomaranta, Anna, Makkonen, Lasse, Tikanmäki, Maria, Groenemeijer, Pieter, Saarikivi, Pirkko, Michaelides, Silas, Papadakis, Matheos, Tymvios, Filippos and Athanasatos, Spyros, 2011. Probabilities of adverse weather affecting transport in Europe: climatology and scenarios up to the 2050s. 94 p.